Hydrogen Production via Thermocatalytic Decomposition of Methane Using Carbon Supported Materials

by

Khalida Binte Harun

A thesis submitted to the Graduate Faculty of
Auburn University
in partial fulfillment of the
requirements for the Degree of
Master of Science

Auburn, Alabama
May 5, 2018

Key words*:* Thermocatalytic decomposition (TCD), Douglas fir, activated carbon, biochar

Approved by

Sushil Adhikari, Chair, Professor of Biosystems Engineering
Carlos Carrero Marquez, Assistant Professor of Chemical Engineering
Brian Via, Professor of Forestry and Wildlife Sciences
Brendan Higgins, Assistant Professor of Biosystems Engineering

Abstract

Convectional hydrogen (H_2) production process such as steam methane reforming process (SMR) produces massive amounts of CO_2 (i.e., 13.7 kg CO_2 per kg H_2 production). Because of the large amount of CO_2 production during the process, it is questionable whether H_2 can be considered as a clean fuel. Besides, H_2 is the main ingredient of ammonia production process, and ammonia is the second highest chemical all over the world based on quantity production per year. In order to solve this issue, hydrogen either needs to be produced from water electrolysis or CO_2 needs to be captured without releasing to the atmosphere. Water electrolysis process requires a large amount of energy for the water splitting process and CO_2 capturing could be capital intensive. However, the most promising process, thermocatalytic decomposition (TCD) of methane, provides several benefits those include but not limited to i) provide a more straightforward path for hydrogen production, ii) eliminate COx production, and iii) reduce production costs.

In the present study, six catalysts (Zeolite Socony Mobil-5 (ZSM-5), 3% Ruthenium (Ru) doped ZSM-5 (Ru-ZSM-5), activated carbon (AC) (commercial), 3% Ru doped AC (Ru-AC), and biochars (chemically activated (KOH) biochar and heat treated biochar) were used for TCD of methane at 800 ^oC and atmospheric pressure in a fixed bed reactor. Two different feed flow rates (0.1 and 0.4 WHSV (weight hourly space velocity: total mass flow rate of reactants divided by total mass of catalyst in the reactor)) were used to examine catalytic behavior in this thesis. XRD (Powder X-ray Diffraction) analysis, TPR (Temperature Programmed Reduction) analysis, surface area, pore volume and pore size distributions analysis, chemisorption, elemental analysis, TGA

(Thermogravimetric Analysis), SEM and EDS (Scanning Electron Microscope and Energy Dispersive X-ray spectroscopy) analysis were performed to characterize these catalysts. From the reaction results, it is evident that 3% Ru enhanced the activity of ZSM-5 and AC. Pure ZSM-5 exhibited 20% and 10% conversion at 0.1 and 0.4 WHSV, respectively. These conversions increased to 40% and 26% at 0.1 and 0.4 WHSV, respectively when Ru-ZSM-5 catalyst was used. AC exhibited 51% and 35% conversion at 0.1 and 0.4 WHSV, respectively, whereas Ru-AC exhibited 73% and 61% conversion for the same flow rates. HB (heat-treated biochar) exhibited 41% and 29% conversion for 0.1 and 0.4 WHSV, respectively. On the other hand, AB (activated biochar) exhibited 69% and 59% conversion for the same flow rates. Among six different catalysts, Ru-AC and AB displayed highest conversions. Therefore, both of catalysts were tested for the catalytic stability over the long run (60 h) at 800 ^{o}C and 0.1 WHSV. Ru-AC achieved 21% conversion, whereas AB displayed 51% conversion after 60 h of reaction time. Carbon produced in reactions were analyzed using scanning and transmission electron microscope. All of the catalysts showed production of carbon nano-tubes (CNTs) except with the use of AC. From all of the results, it can be concluded that Douglas fir biomass-derived catalysts have great potentials to be used as catalysts for thermocatalytic decomposition of methane to produce CO_x-free hydrogen.

Key words: Thermocatalytic decomposition (TCD), methane, Douglas fir, activated carbon, Ru, biochar, catalyst.

Acknowledgments

I would like to express my deepest appreciation to all of the persons to those who made this thesis become a reality. I am grateful to the Department of Biosystems Engineering of Auburn University to give me a chance to pursue my M.S. degree. The last two and half years that I have spent at Auburn University were the one of the most memorable years of my life. I am grateful to my Professor, Dr. Sushil Adhikari, for giving me a chance to complete my M.S. thesis under his supervision. His continuous guidance, support, and motivation gave me the strength to finish my work in an organized way. He taught me how to solve a problem in an organized and scientific manner. He also gave me a chance to attend a summer internship, which significantly enriched my career. I would like to thank my committee member, Dr. Carlos Carrero Marquez, for his comments and advices on my thesis work, especially on how I can make my thesis more presentable. I also would like to thank my committee member, Dr. Brain Via, for his continuous support while I was working in the Forest Products Lab. I am grateful to Dr. Brendan Higgins for his comments and advices throughout my thesis work. I am thankful to Dr. Michael Miller, Dr. Mehmet Zeki Billor, and Dr. Jeffrey Fergus for giving me a chance to use their lab instruments throughout my thesis work.

I want to thank Dawayne “Doc” Flynn for his continuous help and support throughout my experiments. Without him, it would not have been possible to run all of these experiments. He babysat my reactor system for me while I was running another experiment in a different lab. He

helped me to disassemble and assemble my reactor system. He solved reactor-related problems for me. I am grateful to my friend, Haixin Peng, who was always there for me when I was running my reactions, especially at night. She even was with me at 11 p.m. when I was running my 60 h reaction. She always has believed in me even when I was frustrated with myself. I would like to thank Dr. Zhouhong Wang for teaching me to use most of the lab equipment. I want to thank Dr. Saravanan Ramiah Shanmugam and Dr. Nam Hyungseok for helping me while I was running pyrolysis reactions and giving me suggestions and correcting grammar in my draft thesis manuscript. I am grateful to all of my lab members and colleagues for their continuous help and support. I am lucky to have them as my friends.

I am obliged to thank my parents, younger brother, and elder sisters. Without their motivation and support, I could not have completed my M.S. Finally, I am grateful to my husband for his support and unconditional love.

Table of Contents

Lists of Figures

Lists of Tables

List of Abbreviations

Abbreviation	Explanation
%	Percentage
AB	Chemically activated (KOH) biochar
AC	Activated Carbon
atm	Atmospheric pressure
BET	Brunauer Emmett Teller
BJH	Barrett Joyner Halenda
CB	Carbon black
CDNG	Catalytic decomposition of natural gas
CNF	Carbon nano-fiber
CNT	Carbon nano-tube
COx	CO and CO_2
DFT	Density Functional Theory
EDS	Energy Dispersive Spectroscopy
ft	foot
GC	Gas Chromatograph
h	Hour
HB	Heat-treated biochar
H_2S	Hydrogen sulfide
kg	Kilogram
KOH	Potassium hydroxide

NG	Natural gas
NH_3	Ammonia
NOx	Nitrogen oxides
POX	Partial oxidation
Ru-AC	3 wt% Ru doped AC
Ru-ZSM-5	3 wt% Ru doped ZSM-5
S	Sulfur
SMR	Steam reforming reaction
TCD	Thermocatalytic decomposition
TEM	Transmission Electron Microscope
TGA	Thermogravimetric Analysis
TPR	Temperature Programmed Reductions
SEM	Scanning Electron Microscope
VOC	Volatile organic compounds
WHSV	Weight hourly space velocity

CHAPTER ONE: INTRODUCTION

1.1 Background

To fulfill the increasing energy demand, people utilize fossil fuels such as coal, natural gas for their essential needs (electricity, transportation, and industrial purpose). As a result, acid rain becomes more common; ocean's surface water becomes acidic and global temperature increases day-by-day [1-5]. One of the major challenges of today's world is to minimize anthropogenic greenhouse gas emissions with increasing world's population. Coal emits 41 % CO_2 of total global CO_2 emission, natural gas (NG) emits 20 % and oil accounts remaining [1]. To solve the energy crisis of today's world, hydrogen can be a green alternative to fossil fuel. Hydrogen produces only water during its controlled oxidation in a fuel cell or in its direct combustion. It is the most abundant element in the whole universe, but unfortunately, it is not found in its purest form on earth. Hence, it is the secondary energy source produced mainly from methane using various processes. Besides energy sector, hydrogen has several uses in electrical industries, glass industries, pharmaceutical industries, and fertilizer industries [1-5].

For example, ammonia is one of the well-known fertilizers throughout the world, and also one of the primary raw materials used in urea production. Ammonia plays a vital role as a fertilizer to increase global crop production, which, in turn could provide food to humans. Ammonia is also used as raw material for several types of chemical production such as day-to-day cleaning agent to detergent, pre-harvest defoliant agent to food preservatives [3,6].

Hydrogen is used in electrical industry to reduce silicon tetrachloride to silicon for epitaxial growth of polysilicon. Hydrogen is also used in metal and glass industry. Hydrogen has the lowest viscosity of all known fluids. Because of this property, it is widely used in friction reduction process of rotating armature in electricity generation industry. One of the new uses of hydrogen is to crack molten plastic to recycle it to keep environment plastic free [1,4].

Hydrogen can be produced from several sources and among them, major sources include natural gas, biomass, fossil fuel, and water [4]. Water electrolysis is normally used to produce high purity hydrogen. However, this process is uneconomical for industrial use [5]. Biomass gasification can be an industrial source of hydrogen but in most of the time, this process is used to produce syngas. Syngas is used to produce wax, higher hydrocarbon, and methanol but not for pure hydrogen production [6]. In the commercial production of hydrogen from fossil fuel, a combination of steam reforming reaction and partial oxidation of hydrocarbon is used. Large amount of COx (CO, CO_2) production is responsible for costly purification steps, which increases hydrogen production cost [7]. Methane (CH_4) is the main component of natural gas. Since methane has the highest hydrogen carbon ratio (4:1), it gives lowest COx while producing hydrogen in steam reforming and partial oxidation processes [5]. This is one of the main reasons that methane or natural gas is mainly used for hydrogen production in industry. Around 48% of world's total hydrogen production is coming from natural gas [5]. For this reason, methane was used as feedstock in this research.

Steam reforming is the most common way to produce hydrogen from methane. Partial oxidation of methane and methanol are also well-known procedure for hydrogen production. But all of these processes emit COx with hydrogen, which is bad not only for the environment but also increase production cost by including separation steps. To avoid the vast amount of COx

production, thermocatalytic decomposition (TCD) of methane has attracted the attention of researchers in recent years [1,5,7].

Thermocatalytic decompositions (TCD) of methane is the most straightforward green process for the production of hydrogen. As no COx separations are need from hydrogen, this process reduces the hydrogen production cost too. Moreover expensive filamentous carbon (carbon nanotubes or nanofiber) is produced as the byproduct if metals are present in catalyst [1,4,5]. However, this process needs a good and long lasting catalyst. Carbon deposition on the active surface area of catalyst causes quick deactivation of catalyst and makes this process unsuitable for commercial applications. Recently, research efforts were diverted towards figuring out a long lasting catalyst for this process. In this research, thermocatalytic decomposition of methane was used to produce hydrogen in a green way using novel catalysts.

Zeolite has a microporous crystalline structure with silicon, aluminum, and oxygen in its structure and cation, water, and other molecules in its pores. Presence of weak and strong acid sites together with large surface area and thermal stability make zeolite a perfect support for high-temperature reaction. ZSM-5 (Zeolite Scony Mobil-5) was used in non-oxidative methane conversion by several researchers [8,9,10]. Nahreen et al. [8] used 3% Ru-ZSM-5 in a non-oxidative conversion of methane and achieved 44% conversion. Activated carbon (AC) has a high surface area with irregularity and free valences. It shows stable catalytical behavior at high-temperature methane decomposition. Moreover, it can absorb feed impurities (such as sulfur (S) compounds) present in natural gas. On the other hand, Ru shows the highest S resistance among group 8-10 metal [9] and Ru addition increases S resistance of catalyst [10]. By considering all these advantages, ZSM-5 and AC before and after being doped with Ru were used as catalyst in this study.

Douglas fir is one of the widely harvested biomass in Northern part of the USA [11]. It has the highest strength among all softwoods available in the USA. Hence, this biomass is widely used by wood industries. In the past, different types of char, especially char made from charcoal was used in TCD of methane (as a catalyst for stable conversion). However, biochar (byproduct) produced during pyrolysis process has not been investigated in this regard. Since activated biochar produced from Douglas fir has a large surface area, it could be used as a potential catalyst or catalyst support. Presence of different types of metal oxides (K_2O, Na_2O, CaO, MgO, etc.) [11] makes this biochar an excellent catalyst for decomposition of a stable compound. Considering all these reasons, heat-treated biochar and activated biochar produced from Douglas fir biomass were investigated as catalysts in this research.

Filamentous carbon has unique thermodynamic properties than graphite, which could be exploited for a variety of applications in different fields ranging from drug delivery systems to constructions materials. Major applications can be divided into four major areas, as catalyst support, as polymer additives, for gas storage and in electronic devices [7].

1.2 Research Objectives

The main disadvantage of thermocatalytic decomposition of methane is the catalyst deactivation. Carbon formed in this reaction covers the active surface area of catalysts and eventually catalysts deactivate very quickly. Biomass is one of the most abundant resources that can be exploited in different ways. Recently, research on utilization of biochar for different value added applications is gaining popularity. However, very few studies in the past have investigated biochar as a catalyst/catalyst support. Hence, the main objective of this study was to use biomass-derived catalyst (biochar) for thermocatalytic decomposition of methane.

The specific objectives were to

I. Investigate the catalytic behavior of ZSM-5 and activated carbon (commercial) before and after being doped with Ru.

II. Investigate the catalytic behavior of Douglas fir biochar following two different types of pre-treatments (heat-treatment and chemical (KOH) activation).

1.1.1. Investigate the catalytic behavior of ZSM-5 and activated carbon (commercial) before and after being doped with Ru

ZSM-5 is one of the widely used catalysts in different industrial applications. Its networking structure makes it unique to perform as a catalyst. On the other hand, activated carbon is disordered and has surface defects, dislocations and irregular array of carbon bond. These types of abnormality create high-energy sites for the reactant. A small amount of metal doping on these two catalysts creates high-energy sites for methane molecule [12]. Hence, in this objective, the catalytic behavior of ZSM-5 and activated carbon before and after being doped with Ru were investigated for the thermocatalytic decomposition of methane.

1.1.2. Investigate the catalytic behavior of Douglas fir biochar following two different types of pre-treatments (heat-treatment and chemical (KOH) activation)

Recently, biochar has been exploited for its use in different value-added applications. However, biochar from Douglas fir was never investigated as the catalyst for methane decomposition or hydrogen productions. Biochar has the abnormality, free valences, surface defects in its structure. Moreover, activated biochar has large surface area available for reactant molecule [2,12]. Hence, in this research, Douglas fir biochar was used as a catalyst following two

types of pre-treatment (such as chemical activation (KOH) and heat treatment) to decompose methane.

To summarize, this study is focused on catalytic behavior of ZSM-5, AC (before and after being doped with Ru), and biochar (Heat-treated and activated) to produce hydrogen from thermocatalytic decomposition of methane. On Chapter 1, background and motivation of research are discussed. On Chapter 2, hydrogen use, different hydrogen production methods, different types of catalyst used on the thermocatalytic decomposition of methane are described. Catalyst preparation method, experimental set-up, and experimental procedure are discussed in Chapter 3. Chapter 4 talks about results and discussion. Chapter 5 covers conclusion of the overall study, key findings, and future work guidelines.

1.3 References

1. H. F. Abbas and W. W. Daud, "Hydrogen production by methane decomposition: a review," *International Journal of Hydrogen Energy*, vol. 35(3), 1160-1190, 2010.
2. J. D. Holladay, J. Hu, D. L. King, and Y. Wang, "An overview of hydrogen production technologies," *Catalysis Today*, vol. 139(4), 244-260 2009.
3. R. Ramachandran and R. K. Menon, "An overview of industrial uses of hydrogen," *International Journal of Hydrogen Energy*, vol. 23(7), 593-598, 1998.
4. U. P. M. Ashik, W. W. Daud, and H. F. Abbas, "Production of greenhouse gas free hydrogen by thermocatalytic decomposition of methane–a review." *Renewable and Sustainable Energy Reviews*, vol. 44, 221-256, 2015.
5. Y. Li, D. Li, and G. Wang, "Methane decomposition to COx-free hydrogen and nano-carbon material on group 8–10 base metal catalysts: a review," *Catalysis Today*, vol. *162*(1), 1-48, 2011.
6. R. Lan, J. T. Irvine, and S. Tao, "Ammonia and related chemicals as potential indirect hydrogen storage materials," *International Journal of Hydrogen Energy*, vol. 37(2), 1482-1494, 2012.
7. R. M. Navarro, M. A. Pena, and J. L. G. Fierro, "Hydrogen production reactions from carbon feedstocks: fossil fuels and biomass," *Chemical Reviews*, vol. 107(10), 3952-3991, 2007.
8. S. Nahreen, S. Praserthdam, S. Perez Beltran, P. B. Balbuena, S. Adhikari, and R. B. Gupta, "Catalytic upgrading of methane to higher hydrocarbon in a non-oxidative chemical conversion," *Energy & Fuels*, vol. 30(4), 2584-2593, 2016.
9. A. Arcoya, X. L. Seoane, N. S. Figoli, and P. C. L'Argentiere, "Relationship between sulfur resistance and electronic state of the metal on supported palladium catalysts," *Applied Catalysis*, vol. 62(1), 35-45, 1990.
10. C. K. Ryu, M. W. Ryoo, I. S. Ryu, and S. K. Kang, "Catalytic combustion of methane over supported bimetallic Pd catalysts: Effects of Ru or Rh addition," *Catalysis Today*, vol. 47(1), 141-147, 1999.
11. S. Link, S. Arvelakis, M. Hupa, P. Yrjas, , I. Külaot, and A. Paist, "Reactivity of the biomass chars originating from reed, Douglas fir, and pine," *Energy & Fuels*, vol. 24(12), 6533-6539, 2010.
12. N. Shah, D. Panjala, and G. P. Huffman, "Hydrogen production by catalytic decomposition of methane," *Energy & Fuels*, vol. 15(6), 1528-1534, 2001.

CHAPTER TWO: LITERATURE REVIEW

2.1. Hydrogen Applications

Hydrogen is the first member of the periodic table. Its simple structure makes it so reactive that it cannot be found in pure form in the mother earth although it is the most known abundant element in the whole universe. This reactive character makes hydrogen eligible to be used for different purposes in the modern industrial world. Because of having highest combustion energy releasing capacity among any known materials, hydrogen is used as a rocket fuel. It can also be used in automobile directly as fuel using the fuel cell. In recent days, hydrogen has attracted researchers' attention as a green alternative to fossil fuel. One of the primary reasons for increasing greenhouse gas emissions is due to the production of COx, NOx, and VOC (volatile organic compound) during the combustion of ever increasing demand of fossil fuels. Only in the USA, 225 million light vehicles are traveling 7 billion miles and consuming 8 million barrels oil per day [1]. Combustion of this massive amount of oil not only causes environmental damage but also creates the vast demand for fossil fuels. It is expected that the amount of imported oil in the USA will increase about 60% by 2025 [1]. Therefore, fuel cell technology can be an alternative solution. Toyota showed their bus ran by fuel cell during 2005 Car Expo at Nagoya, Japan. There were 85 hydrogen refueling stations established in the USA in 2010. Most of the fueling station uses water splitting process for hydrogen production, which was not a cost-effective process. As a result, a number of hydrogen refueling stations were closed by 2013 due to the unavailability as well as the low demand of hydrogen. German and Italian army have already started using hydrogen as a

submarine fuel, which is safer than nuclear fuel. U.K. and France declared that they would band sales of new fossil fuels car by 2040 to prevent greenhouse gas emission [1-6].

In present days, highest hydrogen consumption industry is ammonia. About 50 % of hydrogen production all over the world is consumed in ammonia production industry (Figure-2.1). To feed the massive population with a limited amount of farming land, no one can imagine agriculture sector without fertilizer. Ammonia is one of the well-known fertilizers throughout the world. It is also one of the primary raw materials for urea and other fertilizer production [7,8].

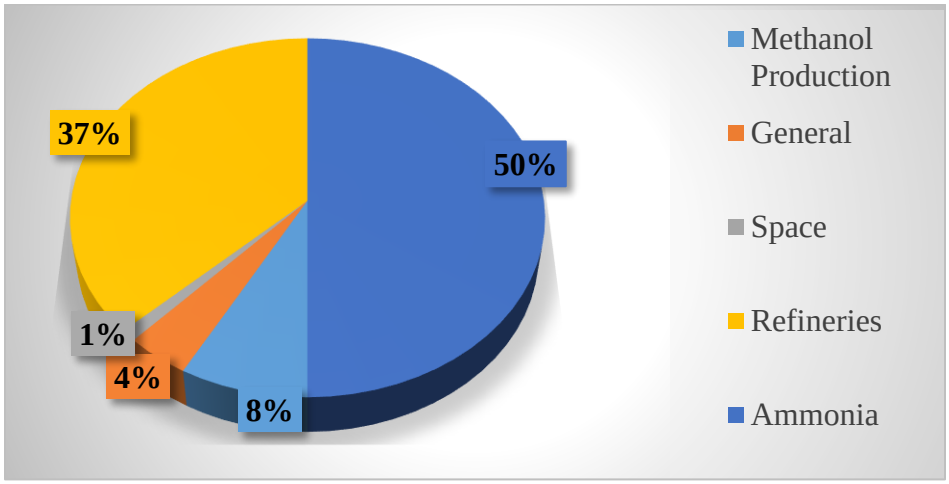

Figure 2.1: World's hydrogen consumption redrawn from ref [7]

Ammonia is a potential indirect hydrogen storage materials. Ammonia and ammonia related chemicals like hydrazine and urea can be used as fuel in fuel cells. It is the second large chemical based on the production all over the world. About 80 % of the total ammonia production is used as fertilizer (Figure-2.2). Ammonium sulfate, urea, ammonium hydrogen phosphate, and ammonium nitrate are well-known fertilizer. Ammonia has a broad application in different areas including cleaning agent preparation industries, dye industries, plastic industries, and food preservative industries. Besides, ammonia is an excellent refrigerant gas and used in purification of water supply [7,8].

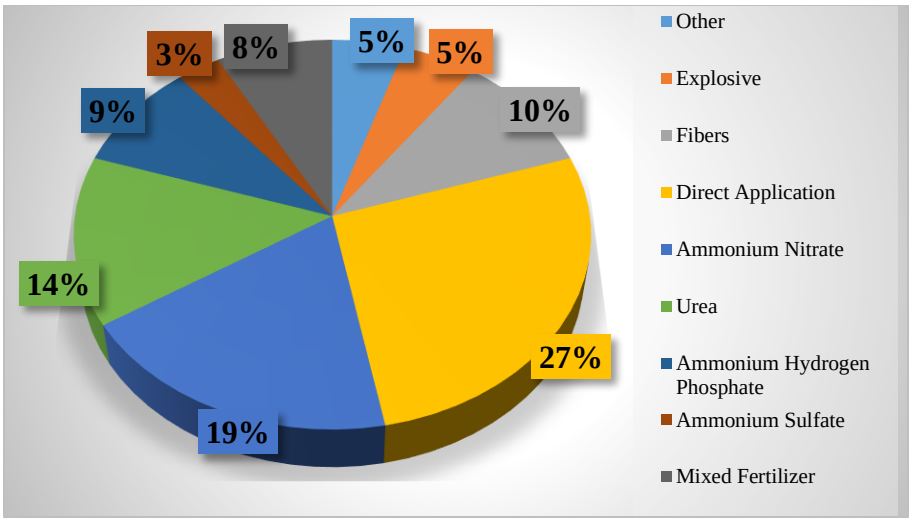

Figure 2.2: World's ammonia consumption redrawn from ref [7]

In the petroleum industry, hydrogen is widely used in hydrocracking and hydroprocessing of crude oil to produce refined oil. Hydroprocessing removes sulfur and nitrogen compounds (H_2S, NH_3). On the other hand, hydrocracking breaks down higher hydrocarbon to lower hydrocarbon.

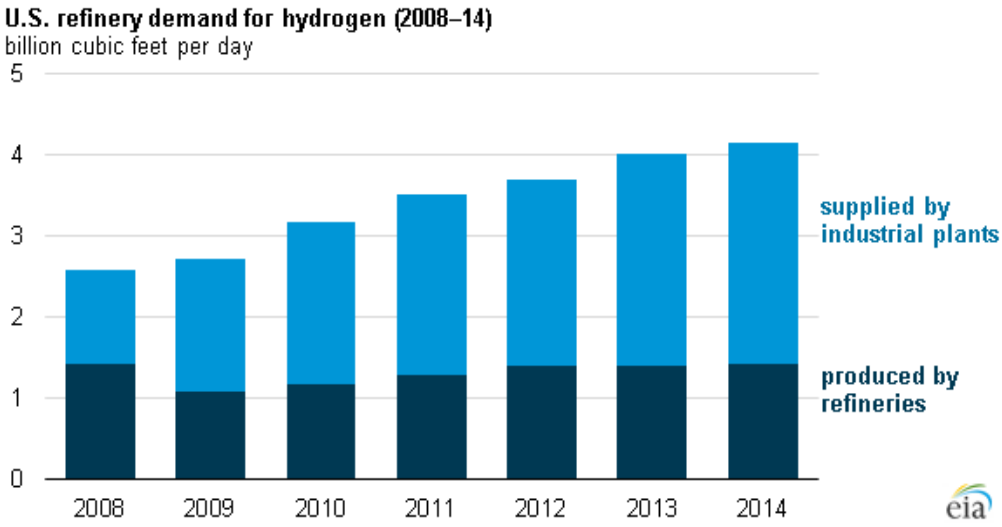

Figure 2.3: U.S refineries demand for hydrogen [9]

Figure 2.3 represents U.S. refinery demand for hydrogen. It shows that demand for hydrogen became double from 2008 to 2014. Since environmental regulations are becoming stringent day

by day, the demand for lighter hydrocarbon, hydrogen rich product as such gasoline is also increasing [3].

2.2 Hydrogen Sources

Four primary sources including natural gas (NG), biomass, water, and fossil fuel are mainly used for the production of hydrogen in the industrial scale. Above 80 % of ammonia production industries use natural gas as hydrogen feedstock. Almost every hydrogen production plants in the USA uses steam reforming reaction of methane. The main reason for using natural gas is its availability and proven reserves. Figure 2.4 represents the percentage of hydrogen produced from different sources [2-6].

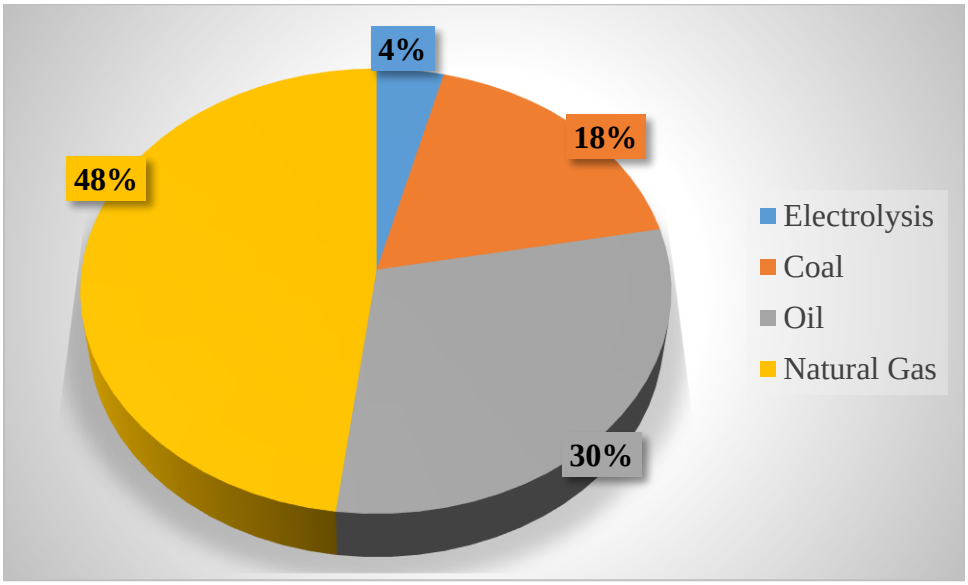

Figure 2.4: Sources of hydrogen redrawn from ref [7]

Steam reforming reaction, which is about 90 % efficient, is used in the industrial hydrogen production process. Biomass gasification is mainly used for syngas production but not for pure hydrogen productions. Water splitting process is not industrially economic process and still in

research level. In refineries, hydrogen is also produced by steam reforming reactions. In few industries, hydrogen is produced as a by-product. For example, in petrochemical industries, hydrogen is a byproduct of olefins production. In the same way, hydrogen is a byproduct of chlorine production in chloro-alkali industry [1-7].

Methane is the first member of hydrocarbon family. It has very stable structure, carbon atom bonded to four hydrogen atoms. Methane is a famous greenhouse gas and a major component of natural gas. Figure 2.5 shows the amount of natural gas production, import and proven reserves. The proven reserve of NG is increasing day by day. If somehow this abundant amount of NG release in the atmosphere, this will cause severe damage to the environment because methane traps 24 times heat compared to CO_2. Methane can found not only as a main component of NG but also as methane clathrates. Methane clathrate is ice of methane trapped on the ocean floor. Methane is also produced in landfill, wetlands or from waste materials by anaerobic bacterial decomposition. By considering all the facts, methane was considered as a feedstock for hydrogen production in this research [1-7].

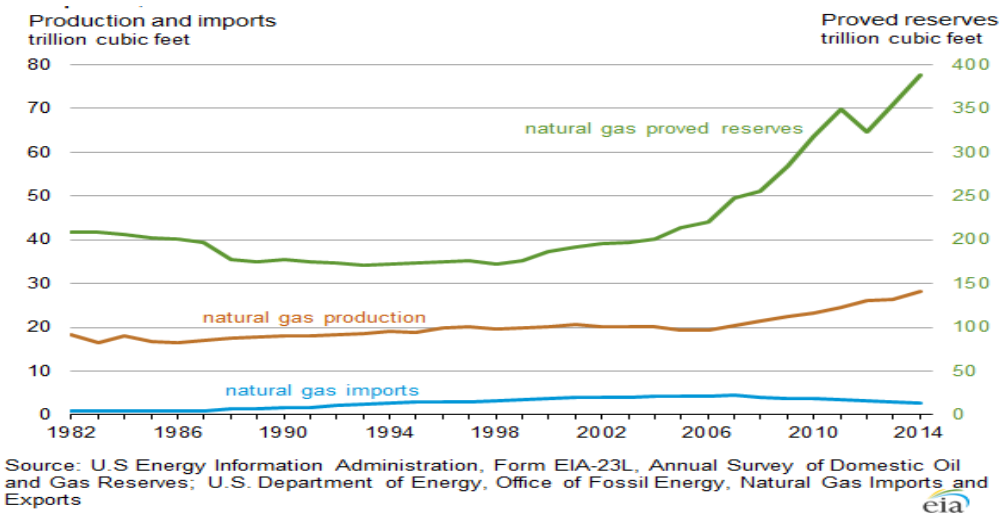

Figure 2.5: US natural gas production from 1982 to 2014 [9]

2.3 Hydrogen Production Process

2.3.1 Steam Reforming Reaction

Steam reforming reaction is the most well-known industrial procedure to produce hydrogen from natural gas. Different hydrocarbon, such as ethane, acetone, methanol, ethanol and higher hydrocarbon can be used as feedstock for this process. But only methane gives favorable byproduct (carbon) compared to other feedstocks. Almost 80 % ammonia production industries all over the world use this process and 95 % hydrogen is produced by this process in the USA. In this process, natural gas is heated at 750-1450 ^{o}C and 5-25 atm with steam in the presence of Ni, Zn, Al, Ce catalyst. Because of coke formation, two series reactors are used to achieve higher conversion [4-8,10]. Steam reforming reaction is given below [10].

$CH_4 + H_2O \rightarrow CO + 3H_2$ ……..(1)

Then, water gas shift reaction is carried out to increase the amount of hydrogen and to convert CO to CO_2 [10].

$CO + H_2O \rightarrow CO_2 + H_2$ …….....(2)

After that, this mixture of CO_x and H_2 is passed through several units to separate CO_x. But it is not possible to completely separate CO_x and H_2 so in most of the cases, methanation reaction is carried out to convert all the remaining CO_x to CH_4 [10].

$CO + 3H_2 \rightarrow CH_4 + H_2O$ …….....(3)

$CO_2 + 4H_2 \rightarrow CH_4 + 2H_2O$ ……...(4)

So, this process requires multiple stages and units to get pure hydrogen. The process train is represented in Figure-2.6. This method supplies 50 % hydrogen production throughout the world.

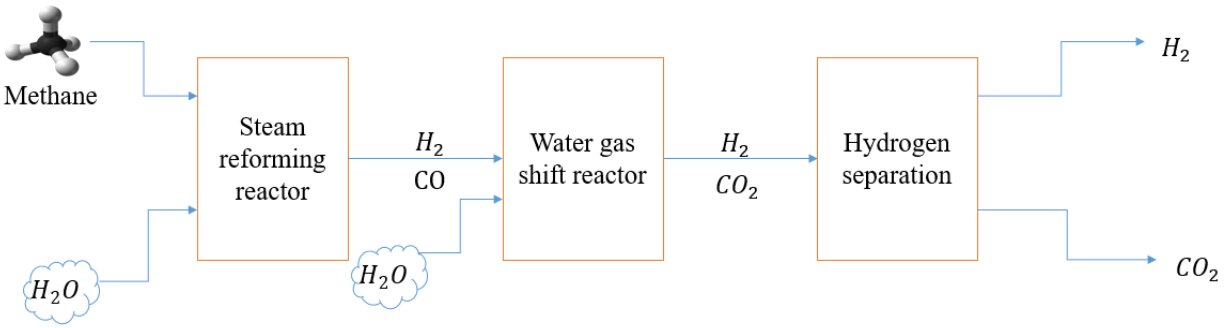

Figure 2.6: Multiple stages for production of hydrogen with steam reforming reaction redrawn from ref [10]

The following are the disadvantages of steam reforming reaction:

- Massive amount of COx is produced during the process. From a study, 13.7 kg of CO_2 is produced while producing only 1 kg H_2 [11].
- Hydrogen produced in this method cannot be used directly in the fuel cell. CO presents even in ppm level can damage membrane of proton exchange membrane fuel cell. Also, CO_2 damage alkaline fuel cell even in ppm level [12].
- To separate COx from hydrogen, several high-pressure washing units, adsorption units, and catalytic steps are used which increase the plant installation cost and as well as production cost [13].
- In ammonia industry, if COx presents with H_2 feedstock then it will react with ammonia and will produce ammonium carbamate (NH_2COONH_4). Ammonium carbamate is corrosive and will damage product line, and the whole plant will be collapsed with time [8].

2.3.2 Partial Oxidation Reaction

Partial oxidation (POX) of hydrocarbon is another known method to produce hydrogen. Hydrocarbon is decomposed in the presence of control amount of oxygen in this process. For non-catalytic oxidation, 1300-1500 ^{o}C temperature is required. Catalyst can reduce required temperature to 450-1000 ^{o}C. Ni, Fe, Co are commonly used catalysts in this process [10].

$$CH_4 + \frac{1}{2}O_2 \rightarrow CO + 2H_2 \quad (5)$$

It is tough to maintain a uniform temperature in the reactor system because of coke formation and hot spots (due to exothermic nature of the reaction). Usually, POX reactors have 60-70 % thermal efficiency with methane or natural gas [14]. Another fact that makes this process uneconomical is the lack of a suitable catalyst. Typically, catalysts based on Ni and Rh are used in this process for methane decomposition. Ni cannot work above 650 ^{o}C and tends to produce coke, and Rh is a costly metal. Krummenacher et al. [15] have suggested and used this method for higher hydrocarbon like decane, hexadecane and diesel fuel.

The following are the disadvantages with regards to partial oxidation reaction [2]:

- This process is not efficient with methane or natural gas.
- Produce large amount of CO, even more than steam reforming reaction.
- Needs high installation and operation costs to remove CO from hydrogen.
- Requires below 50 ppm of sulfur to avoid catalyst poisoning.
- Mainly used for syngas production.

2.3.3 Autothermal Reforming

Autothermal reforming combines steam reforming and partial oxidation reactions. This reaction creates a thermal zone for partial oxidation or catalytic partial oxidation to generate heat

and use this heat to carry steam reforming reaction [16-18]. By eliminating the need for an external heat source, this reaction reduces start-up time. Most important advantages for this reaction over steam reforming and partial oxidation is that this reaction can be maintained easily and can be started and stopped rapidly in case of large scale hydrogen production. The main disadvantage of this process is huge COx production. Hence, this particular process is typically used for syngas production for Fisher-Tropsch synthesis. Another operational disadvantage is that oxygen to fuel and steam to carbon ratios need to be controlled all the time to maintain temperature and continuous reaction as well as final product composition [16-19]. Based on the higher heating value, this reaction has thermal efficiency around 60-75 % [14].

2.3.4 Thermocatalytic Decomposition of Methane

Thermocatalytic decomposition (TCD) of methane has been attracted researchers' attention since 1960 [5,20-21]. This is the most economic hydrogen production method and also eliminates greenhouse gas production. Hydrogen produced in this process can be directly used in hydrogen fuel cell and ammonia production industries without further purifications. Moreover, carbon produced by this method can be used for different purposes. Fibrous carbon can be used in construction industries and polymer additives industries. According to Lane and Spath [22], the selling price of hydrogen would be $7-21 /GJ (1 GJ= 1.05461 MMBTU) based on the price of natural gas and byproduct carbon. Steinberg et al. [13] made an estimation and showed that selling price of hydrogen produced by TCD reaction would be $58/1000 m^3 whereas selling price with steam reforming reaction is $67/1000 m^3. They compared TCD and SMR reaction for hydrogen production and showed that TCD gives more advantages with stable solid carbon production and easy separation of hydrogen. Duford et al. [23] studied different hydrogen production process with

life cycle assessment tools and reported that thermocatalytic decomposition is the most environmentally friendly procedure. The energy requirement for TCD reaction is 37.8 kJ/mol H_2 production whereas 63 kJ/mol H_2 needs for steam reforming reaction [1]. For the aforementioned reasons, it was decided to use thermocatalytic decomposition of methane in this study.

2.3.4.1 Mechanisms

Methane has the most stable molecular structure among hydrocarbons with four C-H bonds (440 kJ/mol) [4]. This stable structure makes its decomposition very difficult, and it only takes place above 1200 ^oC without the catalyst. Different metal and carbonaceous materials have been studied to reduce this temperature. Methane decomposition process can be divided into five steps [24].

1. Chemisorption of methane molecule on the surface of the catalyst.
2. Progressive breakdown of four C-H bonds and detachment of methane molecule from the catalyst surface.

$(CH_4)_g \rightarrow (CH_3)_a + (H)_a$ ……...(6)

A series of surface stepwise dissociation follows above reaction to form elemental carbon and hydrogen.

$(CH_{3-x})_a \rightarrow (CH_{2-x})_a + (H)_a$ ……...(7)

where, $0<x<2$

3. Two adsorbed atomic hydrogen aggregate into hydrogen molecule and emit as gaseous hydrogen molecule.

$2(H)_a \rightarrow (H_2)_g$ ……..(8)

4. Aggregation of atomic carbon into encapsulated carbon cause progressive catalyst deactivation or because of existing pronounced concentration gradient, atomic carbon diffuse through the bulk catalyst's leading face to trailing face.
5. Fibrous carbon formation and growth from carbon nucleation in the trailing face of catalyst.

$(C)_a \rightarrow 1/n\ (C_n)_c$ ……(9)

Here, a, c and g represent adsorbed, crystalline and gaseous phase, respectively. Activation energy and reaction order for each intermediate steps are unknown [24].

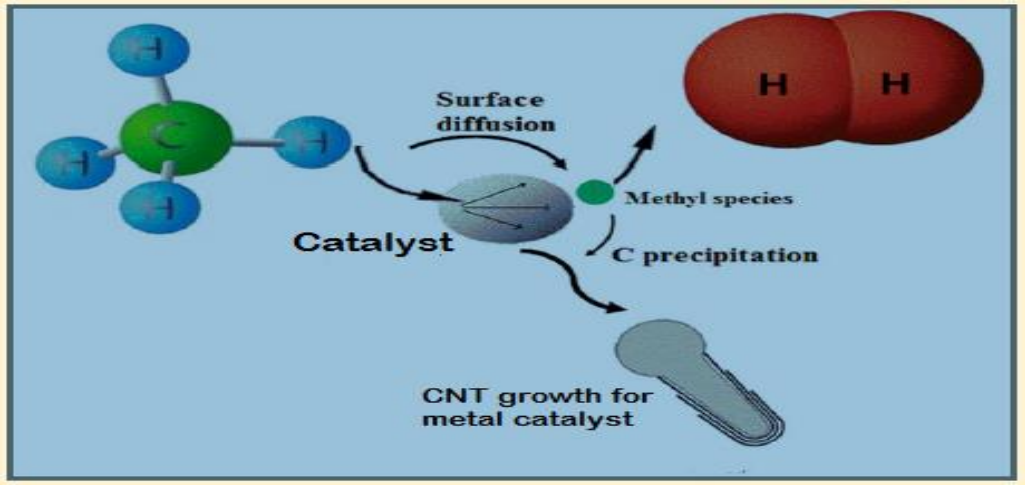

Figure 2.7: Thermocatalytic decomposition of methane [15]

As a growing technology, thermocatalytic decomposition has several critical challenges which are giving below [1]:

- No suitable catalyst has been found yet;
- Fast catalyst deactivation because of carbon formation;
- Presence of unreacted methane in the product stream;
- Regeneration of deactivated catalysts; and
- The possibility of COx production in case of co-feed and during the regeneration of the deactivated catalyst.

2.4 Ammonia Production in Industrial Scale with Steam Reforming Reaction

Ammonia is colorless alkaline liquid and has very pungent as well as penetrating odor. The boiling point for ammonia is -33^{o}C at ambient pressure and can be in the liquid state even at 9-10 bar pressure at ambient temperature. Ammonia is lighter than air and because of this characteristics, it can spread very quickly, causing a death threat if there is any leak in ammonia production industry. The Haber-Bosch process is the most famous and widely used process for ammonia production in industrial scale. This process is named after two scientist Fritz Haber and Carl Bosch. Both of them won the noble prize for inventing this process [25,26].

In Haber Bosch process, nitrogen and hydrogen combine at 400-500 ^{o}C at 200 atm in the presence of iron catalyst. Ammonia production reaction is an exothermic and reversible reaction [26].

$N_2 + 3H_2 \rightarrow 2NH_3$ ……..(10)

But, conducting this reaction in the industrial scale is not an easy task. Several units need pure hydrogen production. In industry, Haber Bosch process uses steam reforming reaction and water gas shift reaction to produce hydrogen from natural gas. A schematic diagram of industrial ammonia synthesis process from natural gas is described in Figure 2.8. The steps involve in the ammonia production process are described below.

2.4.1 Primary Reformer

After desulfurization, natural gas is mixed with process steam. Then, the gas mixture is heated up to 500-600 ^{o}C before entering primary reformer. Primary reformer contains a large number of nickel-chromium alloy tubes which are filled with catalysts. Nickel-containing catalyst

is used in this unit. Only 30-40 % natural gas is converted in primary reformer. The flue gas leaving primary reformer has about 780-830 ^{o}C temperature [25].

$$CH_4 + H_2O \rightarrow CO + 3H_2 \quad \text{.....(11)}$$

$$CO + H_2O \rightarrow CO_2 + H_2 \quad \text{.....(12)}$$

2.4.2 Secondary Reformer

Processed air is compressed and heated to 600 ^{o}C. Heated air is mixed with process gas from the primary reformer and passed through secondary reformer which contains a nickel-rich catalyst. Almost 99 % conversion is achieved in this reformer, and product gas temperature is around 1000 ^{o}C. The process gas is cooled down to 350-400 ^{o}C [25].

2.4.3 Shift Converter

Two shift converters (high and low temperature shift reactor) are used to convert CO present in product gas from the secondary reformer to CO_2. In high-temperature shift reactor, product gas is mixed with steam and passed through iron/chromium oxide bed at 400 ^{o}C. Product gas from secondary reformer contains 12-15 % CO. After high-temperature shift reactor, product gas contains 3 % CO on the dry basis. On the other hand, in low-temperature shift reactor, product gas is passed through copper/zinc oxide catalyst at 200-220 ^{o}C. In Figure 2.8, high-temperature shift reactor is denoted by first shift reactor and low-temperature reactor is denoted by second shift reactor [25].

$$CO + H_2O \rightarrow CO_2 + H_2 \quad \text{.....(13)}$$

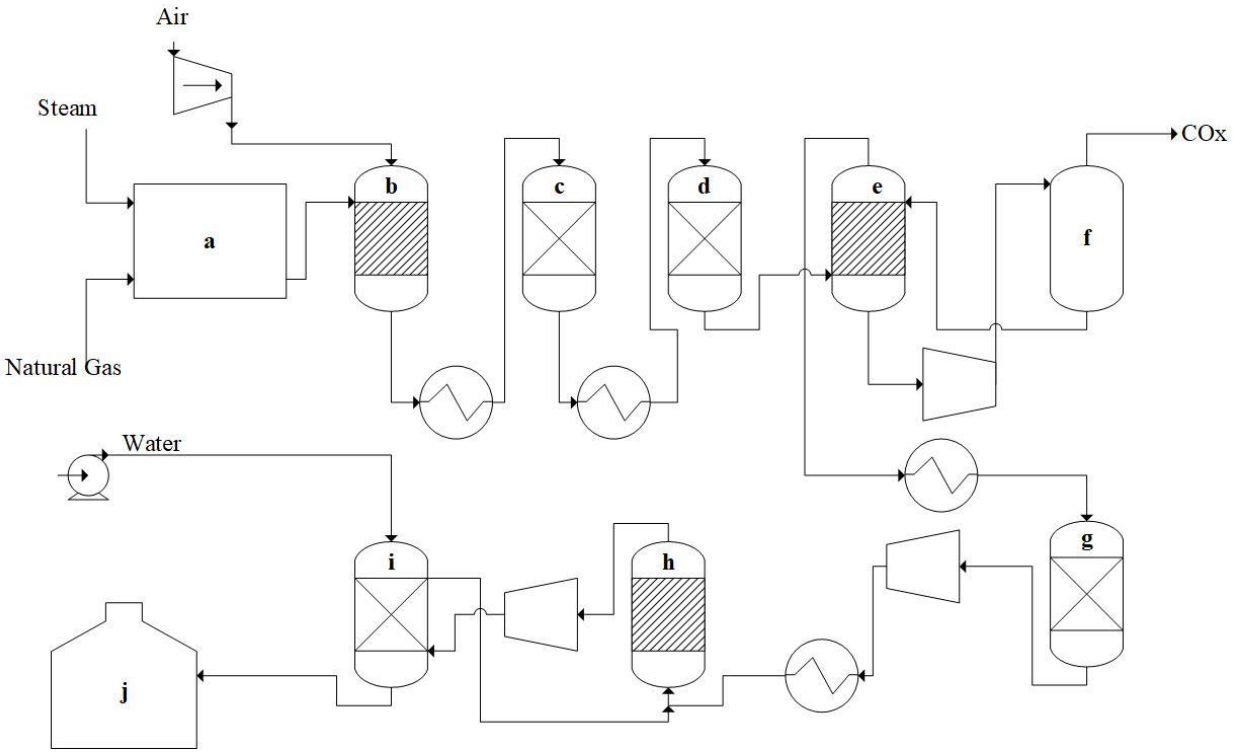

Figure 2.8: Schematic diagram of ammonia production plant with steam reforming reaction: a) Primary reformer, b) Secondary reformer, c) First shift converter, d) Second shift converter, e) Absorber, f) CO_2- stripper, g) Methanation reactor, h) Ammonia synthesis reactor, i) Ammonia separator, j) Ammonia storage tank, redrawn from ref [25]

2.4.4 Absorber and Stripper

Stream absorber and stripper are used in industries to separate COx from H_2 and N_2. Absorber used for CO_2 removal is either physical or chemical absorber. Physical absorber contains such as glycol dimethyl ethers, and propylene carbonate; whereas, chemical absorber contains aqueous amine solutions. Even after using all these separation units, it is not possible to completely separate COx from H_2 and N_2 stream. Therefore, one methanation reactor is used in the industrial process to eliminate COx completely [25].

2.4.5 Methanation Reactor

A portion of produced hydrogen is used to convert residual COx to methane in a methanation reactor. The reactor temperature is 300 ºC, and a nickel-containing catalyst is used inside the reactor. As methane is very stable gas, it remains inert in ammonia synthesis reaction [25].

$CO + 3H_2 \rightarrow CH_4 + H_2O$ …….....(14)

$CO_2 + 4H_2 \rightarrow CH_4 + 2H_2O$ ….……..…..(15)

2.4.6 Ammonia Synthesis Reactor

The product stream from methanation reactor and nitrogen from air react with each other at 400-550 ºC and 200 atm in the presence of an iron catalyst. Because of unfavorable equilibrium conditions, reaction conversion is only 20-30 % [25].

$N_2 + 3H_2 \leftrightarrow 2NH_3$ …….(16)

Although ammonia synthesis reaction is a one-step reaction, it requires several units because of the hydrogen purification process. If thermocatalytic decomposition of methane process is used in ammonia synthesis, then whole purification system would be eliminated. Figure 2.9 describes ammonia synthesis process with the thermocatalytic decomposition of methane. In Figure 2.9, reactor 1 and reactor 2 will be used for hydrogen production from methane by thermocatalytic decomposition of methane. Then, no purification step is required. Product gas from the reactor can be directly used in ammonia synthesis process.

A small amount of COx even in ppm level is poisonous to ammonia synthesis catalyst. Moreover, residual COx reacts with ammonia and cause the production of ammonium carbamate (NH_2COONH_4). Ammonium carbamate is very corrosive. It corrodes product line and causes

ammonia spillage. As ammonia is lighter than air, ammonia spillage to outside environment will spread quickly and cause the death of thousand people [25-28].

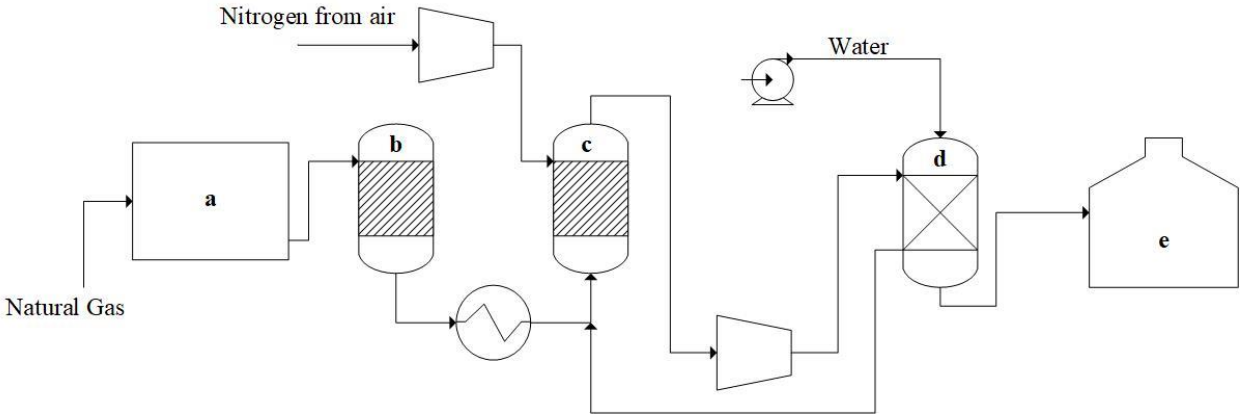

Figure 2.9: Proposed ammonia synthesis plant with thermocatalytic decomposition of methane: a) Reactor 1, b) Reactor 2, c) Ammonia synthesis reactor, d) Ammonia separator, e) Ammonia storage tank

Thermocatalytic decomposition of methane (TCD) will eliminate extra purification steps as well as will reduce hydrogen production cost. Moreover, this process will eliminate the risk of ammonia spillage. Considering all these advantages, this research chose thermocatalytic decomposition of methane as hydrogen production method.

2.5 Application of Carbon Produced in TCD Reaction

The selling price of carbon, produced as a byproduct during the TCD reaction, can help to reduce H_2 production cost. Two types of carbon is produced during the TCD of methane: a) fibrous carbon, and b) amorphous carbon. Fibrous carbon (carbon nanotube and carbon nanofiber) has comparatively higher price than amorphous carbon [29,30]. It was estimated that carbon produced by steam reforming reaction has a credit of $92/ton [13]. However, amorphous carbon produced in the TCD of methane or natural gas is ash and sulfur-free [29]. So, this carbon has a market value

greater than $300/ton. This carbon will be an excellent substitute for petroleum coke. Price of high-quality petroleum coke is $310-$460/ton [31]. Filamentous carbon has higher market value. Carbon nanofiber has a market value from $100-$500/lb, and carbon nanotube has a market value of around $100/lb [29].

Carbon nanotube and nanofiber are a well-known component in building and construction industries. Traditional construction materials have already been substituted by carbon-based materials. Carbon-carbon composite and manufactured graphite are well accepted in automobile, aerospace and construction industries. Carbon composites have several advantages over steel and other construction material. Carbon composites are 5 times lighter than steel and do not need any heavy equipment to install and most importantly, they do not corrode [29,30]. A 40-story building with carbon composite has already been designed [32].

Carbon can also be used as a catalyst. Because of its structure, fibrous carbon can be an excellent support and accommodate active component in its networking structure. Multi-walled carbon nanotube is mainly used as electrically conducting components in the polymer composite. Semiconductor industries are becoming a major consumer of carbon nanotubes. Carbon nanotubes have high electronic conductivity and high electrochemically accessible surface area with mechanical strength. All of these characteristics make it attractive electrode for devices that have double layer charge injection including the super capacitor [29,30]. Figure 2.11 represents nano-electronic device manufactured with carbon nanotube.

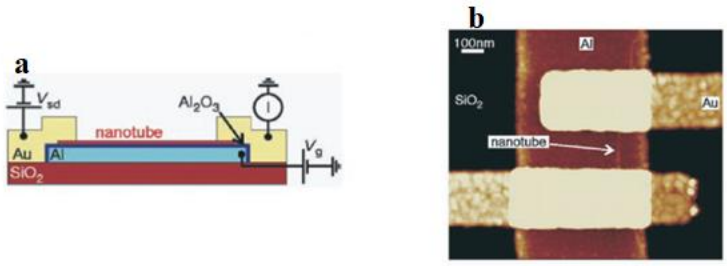

Figure 2.10: Nanoelectronic devices: a) Schematic illustration of a carbon NT-FET (the semiconducting nanotube), b) Scanning tunneling microscope (STM) image of a SWNT field-effect transistor manufactured with the design of (a) [30,34]

Amorphous carbon produced in TCD reaction will be a great source for cathode material in Li-Na ion batteries. Legrain et al. [35] used amorphous carbon as anode material for Na+ batteries. Noh et al. [36] used amorphous carbon coated Tin anode for Li batteries. This type of carbon is also a good alternative of petroleum coke. 85 % of petroleum coke is used as anode in alumina smelting industries via the Hall-Herroult process. But petroleum coke has sulfur and other impurities in it. So extra expense is needed to purify the carbon. TCD amorphous carbon has no sulfur or impurities. This quality makes it perfect for this use. This type of carbon can also be used in carbon fuel cell to generate electricity [29,37].

Soil amendment is also an attractive use of amorphous carbon. Studies has shown that soil amendment increases the soil nutrition and water retention capacity, activates root activity, and supports microbial communities. As a result, seed germinations, plant growth, and crops yield increase up-to 200 % [38]. Figure 2.12 represents hydrogen applications area in energy sector produced from catalytic decomposition of natural gas (CDNG). This diagram also indicates different application areas for by-product carbon.

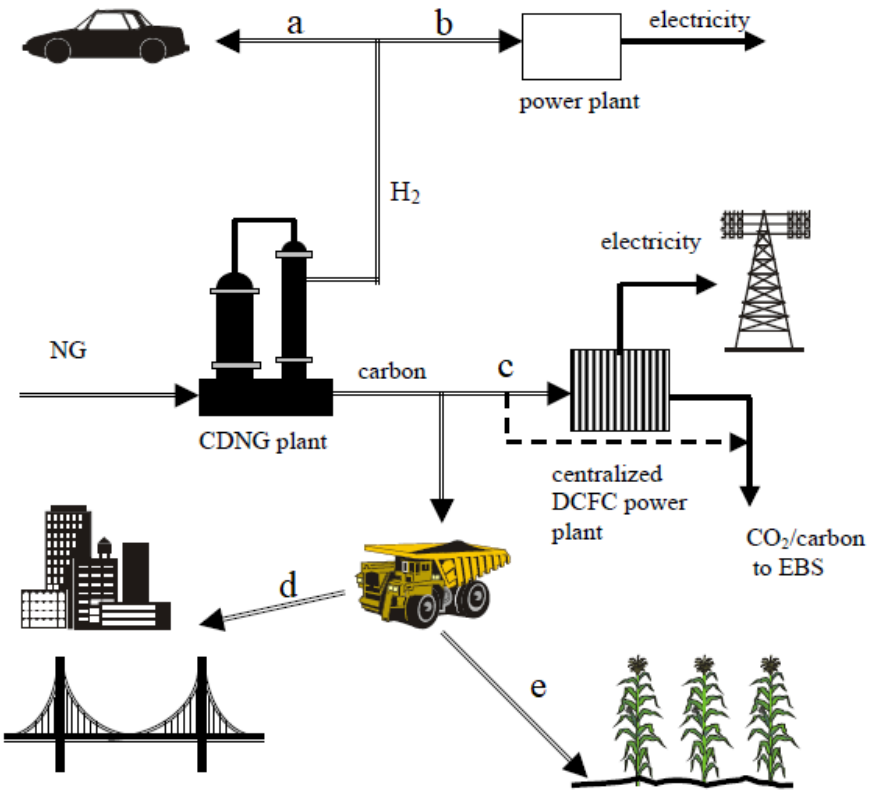

Figure 2.11: Hydrogen application areas: a) transportation, b) power generation, carbon application areas: c) Direct Carbon Fuel Cell (DCFC), d) Building and construction, e) Soil Amendment [28]

2.6 Catalyst

Catalyst is a chemical substance that increases or decreases the rate of chemical reactions without undergoing any permanent change. From gasoline to fertilizer, most of the chemical production processes involve catalysts during the production steps. Normally, catalysts consist of three major components: active phase, promoter, and support materials. The active phase is only part of a catalyst which actively controls the rate of reaction. Promoters just enhance the activity of catalyst. Finally, support materials ensure the uniform distribution of active components on its

surface, gives stability, high surface area and easy accessibility to reactant to increase catalyst activity [39,40].

Promoter can be divided into two groups, textural and structural. Textural promoter enhances, and stabilizes the catalyst activity and prevents agglomeration on support. On the other hand, structural promoter changes the chemical or electronics properties or state of organizations of active phase [39,40].

Support should have porous, inert body with its shape, dimensions, and chemical integrity throughout the chemical reactions. Depending on the reactor and process, catalyst support can be in different form and in different size. The advantages of using support in industrial process are given below [39,40]:

1. Provides hardness and resistance to crushing and erosions.
2. Gives mechanical strength and properties for a longer period of operations.
3. Ensures better and uniform dispersions of active phase.
4. Gives higher stability against sintering.
5. Maximize the exposed surface area for easy access of reactants.
6. Reduces the cost of catalyst as well as catalytic process.
7. Provides easy separation of active components from reaction product.
8. Improves the selectivity of product and regenerability of catalyst.

2.6.1 Catalyst Support Selection Criteria

Porosity and surface area are primary selection criteria for support material. If catalyst's active phase is super active and there is a probability of side reaction, then low surface area with nonporous support is used to reduce catalyst activity and prevent side reactions. Because of

nonporous structure, reactant residence time become low to decrease catalyst activity. But the problem of these type of catalyst is to ensure adhesion between active phase and support materials. Porous structure with low surface area catalysts are used for moderately active catalyst where there is no possibility of side reaction but reactant need to convert for a specific portion. On the other hand, high porosity and high surface area must be needed when reactant is in pretty stable conditions, and it is required to break down the bonds between the reactant molecules. Since methane is a very stable compound and hard to crack, catalyst with a higher surface area will be a suitable choice for the TCD reaction [39,40].

2.6.2 Role of Catalyst Support in Catalyst Preparations

The goal of catalyst preparation methods is to disperse active component uniformly in catalyst support. The characteristics of finished catalyst depend on the interaction between support and precursors of the active component. In precipitation and co-precipitations methods, active component and support precipitate in solid phase continuously. Post-precipitation treatment (hydrothermal treatment, washing, filtrations, drying, grinding, mixing, calcinations etc.) controls the characteristics of the catalyst. Longer calcination time and higher temperature decrease the surface area of final catalysts. Catalyst preparation methods are straightforward in case of wet impregnations method. In this method, solid catalyst support is mixed with required amount of precursor solutions of active component to get the desired amount of active phase. Commonly, powder support is doped with active component's precursor to ensure homogeneous contact between support and precursor solution. After deposition of active phase on the support, further steps should be designed in a way so that there will be no change in distributions and macroscopic structure of catalysts. Commonly, impregnated supports are thermally treated to get active phase

in final form and to enhance better dispersion. Finally, in-situ reduction step gives active metal phase (in case of metallic catalyst) on the catalyst surface [39,40,41]. Figure 2.13 represents drying mechanism of active precursor solution on support. When metal solution gets contact with solid support, metal particles adsorb or trap inside the pore of support due to diffusion and capillary flow. Precursor solution dries with time and the metal phase remains on the surface of support.

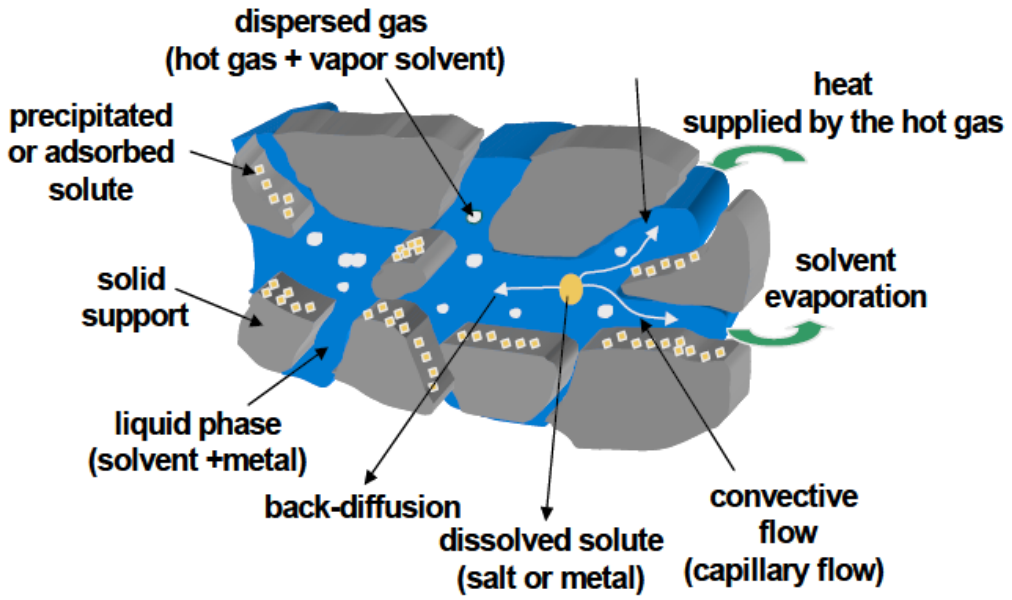

Figure 2.12: Drying mechanism of active precursor solution in support material [42]

2.6.2.1 Metal –Support Interactions during Impregnations or Evaporation

Surface chemistry of support-precursor solution performs a significant role to determine support-active component interaction in impregnation methods. Three tentative mechanisms are given below [39,40]:

1. In evaporation of precursor solution step, support materials behave as a micro recipient for crystallizations and the pores are filled by active component. In this case, an active phase is doped on the support by crystallizations in evaporations steps. The amount of active

component can be controlled by the concentration of precursor solution and the pore volume of the support. At the same time, the solubility of the precursor solution limits the amount of active component. Because of weak support interactions, active phase may redistribute in drying period [39,40].

2. If support surface has charged ions, then that portion of support attract opposite ions of precursor solutions. Finally charged ions of precursor solution attached with surface ions by ion exchanged or adsorbed on the solid support. In ion exchange process, electrically charged ions are brought into the contact with charged support for impregnation. In case of electrostatic adsorption, there is a strong bond between support and active component. So usually, there is no redistribution in the drying process. Precursor solution concentrations, pH and concentration of competitive ions plays the vital role to control this type adsorption [39,40].
3. In new chemical compound produced mechanism, support and precursor solutions react with each other to produce a new chemical compound. Initially, advanced level of dispersion happens at low concentration. In drying and calcination steps, a strong interaction develops to improve the degree of organizations. There is a small region at support (oxide support)-active component interphase. In this region, oxygen content of two components bonded with each other to give resistance against surface migrations and sintering of small metal particles [39,40].

2.6.2.2 Metal Support Interactions during Catalyst Activation Steps

Calcination and reduction steps mainly control the active component and support interaction among all preparations steps. Usually, support and active components are bonded by

van der Waals forces only. Several techniques can be applied to understand the catalyst-support interactions. From the different studies, it is evident that support provides surface area for high dispersion of active component and has a significant effect on reaction rate. Chemical glue produced in support-metal interface prevents sintering of reduced metal particles. The nature of catalyst support controls the strength of support-metal interactions. Depending on all these phenomenon, metal-support interactions can be classified as below [39,40]:

Weak Metal-Support Interactions

The equilibrium contact angle between the active metal component and the support is modified because of compromised interfacial effect. As a result, the support will not be wetted by the metal solution in a vacuum or inert atmosphere. Hence, when the catalyst is reduced by hydrogen, the surface energy diminishes and cause sintering and coalesce. On the other hand, if the oxidation is performed by oxygen then the reverse effect will take place and will cause a good spreading and redistribution of metal on a support [39].

Medium Strength Metal-Support Interactions

Active metal supported in zeolite has this type interaction. From different spectroscopic data analysis, it is evident that small metal particles give electrons to zeolite surface sites. So, zeolite channels confined with small particles are electron deficient. This electrophilic character enhances the activity of the zeolite supported catalyst [39].

Strong Metal Support Interactions

The nature of this type catalyst-support interactions is still debated. There are several explanations for this type of catalyst. One of the explanation is that the support gives the electrons to the active component which creates the negatively charged metal particle. Therefore, this type

of catalyst remains unchanged in oxygen chemisorption. Sometimes intermetallic compound (for metal oxide support) is produced at an elevated temperature in the hydrogen environment. This causes low activity in hydrogenolysis, isomerizations, and hydrogenation but better performance for methane cracking [39].

2.7 Catalyst Used in Thermocatalytic Decomposition of Methane

Catalyst used in TCD reaction can be divided into two major group. Metal catalyst and carbonaceous catalyst. Figure-2.14 shows the classification of catalyst [4].

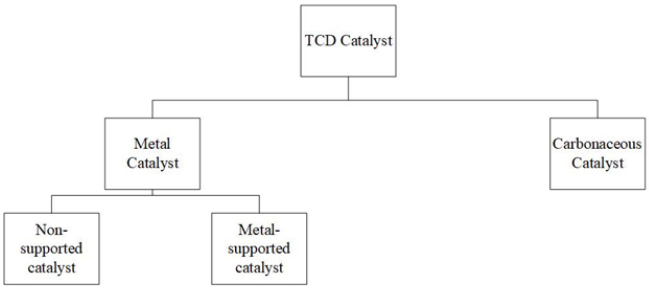

Figure 2.13: Classification of TCD catalyst

2.7.1 Metal Catalysts

Metal catalysts in TCD reaction have been studied over past few decades to find out suitable catalysts with a moderate condition. The reaction mechanism is similar on different metal catalysts. But structure and morphology of formed carbon depend on catalyst structure, promoter activity, catalysts composition and preparation methods. Metal catalysts can be divided into two major groups, non-supported and supported metal catalysts [4-6].

2.7.1.1 Non-supported Metal Catalysts

The order of methane decomposition rate in different non-supported metals are as follows, Ni, Co, Ru, Rh > Pt, Re, Ir > Pd, Cu, W, Fe, Mo [33]. Because of the low cost, better activity and stability, Ni, Co and Fe have attracted a significant attention. Among them, Ni is an excellent catalyst for its sulfur resistance compared to the other metals. But Ni catalyst deactivates rapidly because of rapid aggregation and carbon encapsulation above 600 ^{o}C temperature [44]. At the same time, theoretical thermodynamic equilibrium studies were revealed that methane conversion at that temperature is thermodynamically inadequate [45,46]. As a result, amount of hydrogen produced is very low [47]. But Ni alloy shows good conversion above 600 ^{o}C. Fe and Co work well at the higher temperature (700-1000 ^{o}C) [48]. Invaluable thin wall carbon nanotubes produce with Fe catalysts [49]. Therefore, Fe is mainly used to produce carbon nanotube as the main product not hydrogen. Ni, Fe and Co have partially filled 3d orbitals. Therefore, dissociation of methane molecule can be easily done by partially accepting electrons in 3d orbital. Because of this interaction, electronic structure of absorbed methane is changed and methane molecule dissociates easily in those catalysts [50]. Main advantages of non-supported metal catalyst is its magnetic property. Because of this property, catalyst can be easily recovered after reaction [51].

2.7.1.2 Supported Metal Catalyst

The heterogeneous catalyst is the most common catalyst form used in industry. In this type of catalyst, strong metal-support interaction increases the dispersion of metal. The intensity of interaction also changes the crystallography and electronic state of active metal [52]. There are several factors which control the activity of the final catalyst. Those factors are dispersion of the metal particle [53], crystalline size [53], pore geometry of support, textural properties, electronic

state of the metal particle, catalyst preparation method, catalyst composition, and catalyst rinsing solvent, etc. [54].

For TCD reaction, several types of metal-support combination were used such as Ni-Cu [20, 55], Ni-Zn [56], Fe-Ni [57], Fe-Pd [57], Ni/Cu/Al [58], Ni-Cu/Al_2O_3 [54]. Cu promoted Ni produces octopus and porous carbon nanofiber (CNF) [56]. Cu-doped Fe gives better catalyst lifespan and conversion (51 %) than only Fe [59]. Fe gives better conversion when it makes the coupling with Mg, Pd, Co, Mo or Ni at 700-800 ^oC [57, 60-61]. Chen et al. used a micro tubular reactor and got 55 % initial conversion with 3Ni-3Cu-2Al catalyst. But catalyst deactivated completely after 5 h [62]. Carillo et al. achieved 30 % initial conversion at 975 ^oC with 30 % Mn/YSZ (Y_2O_3 :ZrO_2 =5) [63]. Avdeeva et al. used vibrating flow reactor and compared conversion achieved between 90 Fe-Al_2O_3, 85 FeCo-Al_2O_3, 75 Co-Al_2O_3, 90 Ni-Al_2O_3. According to them, 90 Ni-Al_2O_3 gives 14 % stable conversion for 14 h at 550 ^oC [64]. Saraswat et al. [65] used Ni-Cu-Zu/Al_2O_3 catalyst and achieved stable conversion with initial conversion 61 % and final conversion was 50 % after 20 h at 750 ^oC. They produced carbon nanotube as a byproduct. Ni-based catalyst gives better performance than Fe-based catalyst, but it shows bad performance at higher temperature [65].

The following are the advantages of metal catalysts [4]:

1. Recovery of catalyst is very easy.
2. C produced in reaction is expensive fibrous carbon (carbon nanotube or nanofiber).
3. Higher methane conversion is achieved.
4. Catalyst preparation process is less sophisticated.

The following are the disadvantages of metal catalysts [4]:

1. Comparatively expensive.

2. Deactivate very quickly.
3. Produce metal carbide.
4. Difficult to remove the produced CNTs without harming metal catalyst.

2.7.2 Carbonaceous Catalyst

Though metal catalysts give very high initial conversion for TCD reaction, they deactivate very fast with time. Formation of metal carbide is a major challenge for metal or metal-based catalysts. Carbonaceous catalyst overcame this problem and has attracted researchers' attention for better stability [1,4]. The primary challenge with methane decomposition is sulfur content. Almost every reservoir of NG contains a small portion of the sulfur compounds. These sulfur compounds are poisonous to metal-based catalysts. Carbonaceous catalysts are resistant to sulfur compound and can absorb sulfur compound from the feedstock. Activated carbon (AC), carbon black (CB), coal chars, glossy carbon, multi-walled nanotube (MWNT), graphite, fullerenes, etc. have been used as catalyst in TCD reaction [66,67]. Because of higher activity and better stability, AC and CB attracted researchers' attention the most. Murdov et al. [68] studied thirty different carbonaceous materials and found AC and CB are more active than the ordered one. The carbon catalysts activity has following order: amorphous> turbostractic>graphite [69]. Amorphous carbon (AC and Activated Biochar) is not well-ordered. Irregular array of carbon bond creates free valences, surface defects, and dislocations. These types energetic abnormality increases high energy active sites for the reactant. So these types catalyst will give better performance in TCD reaction [70]. For all of these reasons, activated carbon (commercial), activated biochar (AB) (Douglas fir) and heat-treated biochar (derived from Douglas fir) were used as catalyst for methane decomposition.

The following are the advantages of carbonaceous catalysts [1,4]:

1. Cheap material.
2. Resistant to high temperature.
3. Resistant to sulfur and other harmful impurities in feed gas.
4. No metal carbide formation.
5. Produced carbon can catalyzed further reaction. So external supply of expensive catalysts can be avoided.
6. No need to separate produced carbon from catalysts.

The following are the disadvantages of carbonaceous catalysts [1,4]

1. Carbon produced in reaction has less economic value.
2. Catalyst recovery procedure is complicated.
3. Catalyst synthesis procedure is complicated.

2.7.3 Carbon Catalytic Activity Boost by Metal Doping

To utilize the advantages of both metal and carbonaceous catalysts, recently researchers are trying to add a small amount of metals on carbon materials. Carbon can be reduced at high temperatures. This ability helps metal oxide for in-situ reduction during pre-treatment step [45]. Carbon catalyst with a small amount of metal on it (doped or genuinely present) increases its activity to a great extent [69]. Small metal addition on amorphous carbon create active high energy sites, which attract stable methane molecule and increase conversion. Jin et al.[45] used commercial coconut shell activated carbon and doped it with Fe-Al_2O_3 by impregnation method. At 750 ^oC methane conversion was very low (5.7 %) despite metal loadings, because Fe works well as a catalyst above 800 ^oC. Just Al_2O_3 loading (0Fe-40Al/AC) gave 28.6 % initial conversion,

but conversion decreased to 2 % by 100 min. While only Fe loading (40Fe-0Al/AC) gave very sharp declined trend for first 60 min, conversion reduced from 21. 3% to 12.7 % and next 140 min conversion increased to 26.7 %. Finally, conversion steadily decreased to 13.1 % after 360 min. Prasad et al. [71] doped 5 % and 10 % Pd on AC. AC-Pd10 gave 50 % conversion after 4 h of reaction time whereas AC-Pd5 gave 30 % conversion after 4 h of reaction time. Zhang et al. [72] doped Ni on coal and CLR (carbon-loaded rubber) based carbon and got stable and consistent conversion than only metal, coal and CLR based carbon at 850 ^{o}C. Ni/Al_2O_3, Ni/SiO_2, and CLR gave 40 %, 50 % and 20 % initial conversion which decreased to 10 % after 3 h of reaction at 850 ^{o}C. However, Ni-doped on carbon gave 30 % initial conversion, which increased to 80 % after 8 h of reaction at 850 ^{o}C [73]. Hierarchical porous carbon (HPC) with Al_2O_3 gave 27% initial conversion and this conversion increased to 61% after 10 h of reaction time at 850 ^{o}C. Fibrous carbon produced as by-product in this study [73]. The following are the advantages of metal boosted carbon catalysts [1,4]:

1. Comparatively cheaper than pure metal catalyst.
2. Carbon materials help metal oxide to reduce easily in pre-treatment because of high temperature reducibility of carbon.
3. Metal enhances the activity of carbon material and increase the catalyst life.
4. Metal causes production of high energy sites in carbon material.

2.8 Catalyst Choice for This Research

2.8.1 ZSM-5 as Catalyst

Zeolite is a synthetic aluminosilicate with virtually unlimited SiO_4 and AlO_4 tetrahedra linking together to create pores, channels, and cavities in a wide variety of shape and size. Zeolite

has a high surface area and channeled structure with a well-defined aperture which controls pore size in molecular level [74]. In case of ZSM-5 (Zeolite Scony Mobile-5), the formula can be written as $Na_nAl_nSi_{96-n}O_{192}.16H_2O$ ($0<n<27$). ZSM-5 is a very well-known catalyst used in the different industrial processes. ZSM-5 is extensively used in the non-oxidative conversion of methane for higher hydrocarbon production with different metals. Different transition metals can be used with ZSM-5 to achieve good conversion as well as good selectivity of higher hydrocarbon [74,75]. Wang et al. [76] first used Mo/HZSM-5 catalyst to produce benzene from methane in a non-oxidative condition. Nahreen et al. [77] achieved 44 % conversion by using 3 wt% Ru-ZSM-5 catalyst for 60 h at 800 ^oC in a non-oxidative conversion of methane. Tang et al. [78] used 2 wt.% Mo/HZSM-5 in methane aromatization and observed that after beginning the reaction only CO_2, CO, H_2O, and H_2 are produced, but no benzene or hydrocarbon was detected. Choudary et al. [79] used two different zeolites for methane decomposition. They got 33 % initial conversion and filamentous carbon as a by-product. After 14 h, this conversion lowered to 10 %. Since ZSM-5 used in non-oxidative methane conversion with a very low selectivity of higher hydrocarbon and very few research works were found on the TCD of methane, ZSM-5 was used as a catalyst for hydrogen production from methane in the present study

2.8.2 Activated Carbon as Catalyst

According to Murdov et al. [68], AC and CB show better activity than ordered carbon material. Activated carbon has a higher surface area and catalytic activity comparatively CB [1, 80]. Amorphous structure of AC has different abnormality, free valences, and various surface functional group (R-COOH, R-OCO, R-OH, R=O) [1]. According to Murdov et al. [69], these surface functional group may play the vital role in the high initial conversion of methane. Moliner

et al. [81] and Suelves et al. [82] found a good correlation between the concentration of reduced functional group and reaction rate. Lie et al. [83] used commercial AC for methane decomposition and got initial 60 % conversion at 800 ^{o}C and this conversion decreased to 40 % after 6 h of reaction. Abbas et al. [84] used a fixed bed reaction to determine kinetics of methane decomposition over AC, and they got 67 % initial conversion at 850 ^{o}C. Lee et al. [85] used coconut shell and coal-derived activated carbon and found that coconut shell derived activated carbon gave 20 % conversion after 4 h of reaction whereas coal-derived activated carbon gave 14 % conversion after same time of reaction at 850 ^{o}C. The main advantage with activated carbon is that it can absorb sulfur compound from methane feedstock. So considering all the benefits, activated carbon was also used as a catalyst in this research.

2.8.3 Ru in Methane Decomposition

Ni and Fe based catalyst attracted researcher attention in recent days because of their capability to the production of CNT and CNF. But sulfur compound is very poisonous to Fe as well as Co catalysts. In case of sulfur poisoning, Ru and Ni show more noble behavior compared to Co and Fe. Carbon deactivation and sulfur poisoning cannot change the electronic properties of Ru and Ni, but those can change electronic properties of active sites of Co and Fe. Sulfur poisoning damage geometry of active sites and block them for the reactant [86]. According to Arcoya et al. [87], group 8-10 metal catalysts show following order for sulfur resistance, Pt< Pd< Ni<<Rh<Ru. According to Ryu et al. [88], addition of Ru increase the catalyst resistance against sulfur poisoning. Stanley et al. [89] used Pt-Ru alloy to improve sulfur resistance for hydrogenation catalyst. Nahreen et al. [77] used 3 %Ru-ZSM-5 catalyst for non-oxidative methane conversion and got 44 % conversion even after 60 h of reaction at 800 ^{o}C. Yasyerli et al. [90] used Ru to

promote Ni-MCM-41 mesoporous catalyst for dry reforming of methane. 1% Ru incorporated Ni-MCM-41 catalyst gave 35 % conversion of methane even after 4 h of reaction. Wang et al. [91] used Fe-Ru bimetallic catalyst to produce single-wall nanotubes by chemical vapor deposition method. They got 200 % more nanotubes when used Fe-Ru bimetallic catalysts than only Fe catalysts. Though Ru catalysts are used in two steps methane activation, non-oxidative methane decomposition, dry reforming of methane, and single-walled nanotube production, there is no significant research work found on the TCD of methane. So in this research 3% Ru was doped with ZSM-5 and AC to investigate their catalytic behavior in the TCD of methane.

The reasons behind selecting Ru as active component are given below [1,4],

1. Non-supported Ni catalyst cannot go above 600 ^{o}C, but methane conversion is very low at this temperature.
2. Fe deactivates very quickly in presence of sulfur compound. It is very efficient above 700 ^{o}C but loose activity after repeated cycles. Co is also not good with feed gas impurities.
3. Lots of study carried out for Ni, Co and Fe. But there is no study with Ru doped in different supports.
4. Group 8-10 metal catalysts show following order for sulfur resistance: Pt< Pd< Ni<<Rh<Ru [84].
5. Addition of Ru increases the catalyst resistance against sulfur poisoning [88-90].

2.8.4 Activated Biochar and Heat-Treated Biochar from Douglas Fir Biomass

Douglas fir is famously known as Christmas tree. *Pseudotsuga menziesii* (Douglas fir) is an evergreen tree and grow in the moist northern part of USA. Figure 2.15 is shows the growing region of Douglas fir biomass. It can grow up to 40-250 ft tall. It can self-prune its lower branch.

Therefore, long straight consistent fiber makes it very valuable for wood industry. It has highest strength and modulus of elasticity among North American softwood. Douglas fir biomass is widely used for the wood panel, floor and wall panel [92-94].

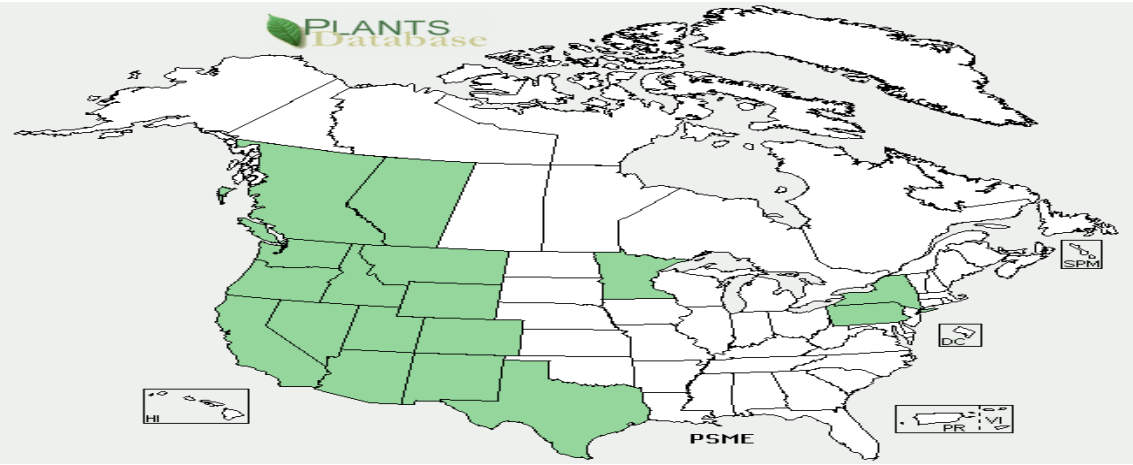

Figure 2.14: Growing region of Douglas fir biomass [95]

A vast amount of wood chips waste from wood industries can be used for biochar production. Douglas fir biomass contains alkali and alkaline earth metallic species as ash content. Table 2.1 represents alkali and alkaline content of Douglas fir biomass.

Table 2.1: Ash chemical analysis of Douglas fir biomass samples (wt%) [92]

Ash Content (wt%)							
K_2O	Na_2O	CaO	MgO	SiO_2	Al_2O_3	Fe_2O_3	Cl
4.13	1.48	10.90	4.90	55.50	11.60	7.24	0.73

Biochar can be produced from biomass by two main ways, gasification and pyrolysis. In gasification process, biomass is heated at elevated temperature (>700 ^oC) in the presence of a limited amount of oxygen, air or steam. Mainly gaseous products are produced in this process. It is mainly used for syngas production [96]. Biochar is mainly produced by pyrolysis process. Pyrolysis process can be categorized into two groups: fast pyrolysis and slow pyrolysis. In slow

pyrolysis, biomass is treated in the oxygen-free environment at 300-500 ^{o}C with a lower heating rate and longer residence time. Lower heating rate and longer residence time help the vapor and aerosol compound to decompose and produce consistent char. Fast pyrolysis is industry-friendly process to produce biochar because it is a continuous process. In fast pyrolysis process, dried biomass is heated at a higher heating rate (200 ^{o}C/min) with a shorter residence time (0.5-5 s). The reaction temperature is maintained around 500 ^{o}C in the absence of oxygen [97-99]. The reaction products are 60-70 % bio-oil, 15-25 % biochar and 10-20 % gaseous product [96]. Presence of alkali and alkaline earth metals increase the production of biochar [96]. Surface area of final activated carbon depends on source and activation process. Azargohar et al. [100] used fast pyrolysis biochar and activated that with KOH to produce activated biochar. According to them, activated carbon which is produced by fast pyrolysis and goes through KOH activation has the surface area 50 times higher than the starting material.

Char from different types of coal was also used as a catalyst in the TCD of methane. Bai et al. [101] used three different types coal to produce char and used in TCD reaction. Since the char produced from the coal has very low surface area, they got very low conversion in TCD reaction. At 950 ^{o}C, initial conversion was around 26 % but catalyst deactivated after 70 min. Several researchers used different lignocellulosic precursor (coconut shell, plum, almond, cherry, peach) to produce activated carbon [1]. But very few investigation were done on biochar derived carbon for TCD reaction as catalyst. Abbas et al. [102] used palm shell based activated carbon to figure out reaction order on activated carbon and found 0.5 order with 210 kJ/mol activation energy. But most of the researchers used commercial activated carbon or coal derived carbon as catalysts on TCD reaction. Wood chips waste of Douglas fir biomass from wood industry can be

an ideal source of biochar production by fast pyrolysis process. Since there was no research found on Douglas fir biomass derived catalyst for TCD reaction and considering all advantages of fast pyrolysis with KOH activation, two carbonaceous catalysts derived from Douglas fir biomass were used as catalysts in this research. One is activated carbon which was activated by KOH and another one is heat-treated biochar.

2.8.5. Activation with KOH

KOH activation is a well-known process to produce activated carbon. The mechanism for activated carbon production is still not well understood because of lots of variables (experimental variables and the reactivity of different precursors) that would influence the activation process. In general, the solid-solid reaction starts between carbon and KOH. Then solid-liquid reaction proceeds including the production of metallic K from the reduction of potassium compounds. At the same time, the oxidation of carbon to carbon oxide / dioxide and carbonate occurs, and other reactions among various active intermediates proceed simultaneously [103,104].

According to Otowa et al. [103], H_2, H_2O, CO, CO_2, potassium oxide (K_2O), and potassium carbonate (K_2CO_3) are the main products in KOH activation of petroleum coke below 700 ^oC. This procedure contains several simultaneous/consecutive reactions (eqn. (17)–(20)). At 400 ^oC, KOH transforms into K_2O (eqn. (17)). Then carbon reacts with water and produced H_2 (eqn. (18) and eqn. (19)). K_2O and CO_2 react with each other to form K_2CO_3 (eqn. (20)).

$$2KOH \rightarrow K_2O + H_2O \quad \text{.....(17)}$$

$$C + H_2O \rightarrow CO + H_2 \quad \text{.....(18)}$$

$$CO + H_2O \rightarrow CO_2 + H_2 \quad \text{.....(19)}$$

$CO_2 + K_2O \rightarrow K_2CO_3$…….(20)

At about 400 ^oC, K_2O react with CO_2 to produce K_2CO_3 (eqn. (20)). Around 600 ^oC, KOH is consumed completely (eqn. (21)). K_2CO_3 is decomposed to K_2O and CO_2 above 700 ^oC and completely disappear at 800 ^oC. CO_2 is converted to CO by C (eqn. (22)). Finally, metallic K is produced above 700 ^oC (eqn. (23) and (24)) [103-105].

$K_2CO_3 \rightarrow CO_2 + K_2O$……..(21)

$CO_2 + C \rightarrow 2CO$……...(22)

$K_2CO_3 + C \rightarrow 2K + 3CO$…….(23)

$K_2O + C \rightarrow 2K + CO$……(24)

From above discussion, three activation mechanism can be concluded [103-108],

- The redox reactions between different potassium compounds and carbon (eqn. (23) and (24)) cause etching in the carbon framework. This process is called chemical activation which is responsible for generating the pore network.
- The formation of H_2O (eqn. (17)) and CO_2 (eqn. (19) and (21)) in the activation process cause further growth of porosity through the gasification of carbon.
- The expansion of carbon lattices results from intercalating of metallic K into carbon lattices of the carbon matrix. In washing step, intercalated metallic K and other potassium compound removed but the expanded carbon lattices cannot return to non-porous structure.

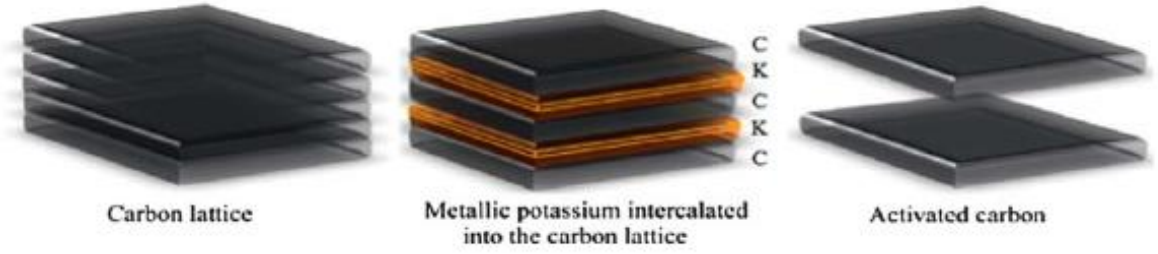

Figure 2.15 : KOH activation mechanism to produce activated carbon: metallic K penetrate into carbon lattice and result the expansion. After removal of metallic K, porous carbon cannot back to non-porous structure [108]

Before activation process, char is produced from different carbon precursors. Then this char is mixed with KOH by physically, or impregnation process (solution of KOH) based on mass ratio ranges from 2.5 to 3.5. In case of impregnation process, an extra evaporation step is conducted to remove excess water. Then the mixture of KOH and biochar is placed in two steps heat-treatments. At first, heat-treatment at 370-400 ^{o}C for 0.5 to 1.5 h for dehydration of KOH and production of K_2CO_3 (eqn. (17)-(20)). The second step consists of the production of metallic K (eqn. (21) to (24)) at 750-900 ^{o}C for 0.5 h to 2.0 h. Finally, the mixture of heat-treated biochar and KOH wash thoroughly to remove remaining KOH, salt, and metallic K [103].

Table 2.2: Summary of literature review

References	Catalyst	Reactor	%Conversion reduction per h	Reaction T (ºC)	Reaction Time (h)	Ref.
Chen et al. 2004	2Ni-1Cu-1Al (atomic ratio)	Horizontal micro tubular reactor	3.53 (55%-2%)	740	15	62
Sarswat et al. 2016	Ni-Cu-Zn/Al_2O_3	Fixed bed	0.35 (62%-55%)	800	20	65
Liu et al. 2016	AC	Fixed bed	4.17 (65%-40%) (920)	800	6	83
Carillo et al. 2016	Mn/YSZ 10 (Y_2O_3 :ZrO_2 =5)	Tubular quartz fixed bed	3.13 (30%-25%) (7.9)[a]	975	1.6	63
Takenaka et al. 2003	Pd-Ni-SiO_2	Conventional gas flow system	1.00 (12%-2%)	600	10	48
Avdeeva et al. 2002	90% Ni-Al_2O_3	Vibrating flow reactor	0.37 (14%-8%)	625	16	64
Lee et al. 2004	AC from coal	Fluidized bed reactor	8.8(79%-35%)	850	5	85
Konieczny et al. 2007	FeO	Fixed bed reactor	98%	800	72	109

Reshetenko et al. 2005	15%Ni-Catalytic Filamentous Carbon(CFC)	Vibrating flow reactor	0.36 (8%-0%) (125)a	525	22	110
Bai et al. 2007	6.7%Ni/AC (from coal)	Quartz tube fixed bed (TPD)	8.33 (27%-2%)	850	3	111
Zhang et al. 2013	10%Ni doped on direct liquefaction residue of coal	Fixed bed	+4.44 (15%-55%) (589)a	850	9	72
Jin et al. 2013	AC supported 40%Fe-0%Al	Fixed bed	0.71 (22%-15%) (518)a	850	4	43
Prasad et al. 2010	10%Pd/AC	Fixed bed	+5.00 (35%-55%) (752)a	850	4	71
Zhang et al. 2013	0.1% Al-RC	Fixed bed	+3 (25%-61%) (1507)a	850	10	73
Cunha et al. 2009	Cu50-Al	Tubular reactor	+24, 3.46(10%-50%-35%)(17)[a]	600	6	59
Cunha et al. 2009	Ni30-Cu50 Alloy Raney type catalyst	Tubular reactor	0.83(65%-60%)(23.9)[a]	600	6	112
Saraswat et al. 2009	50%Ni-5%Cu-5%Zn/MCM-22	Fixed bed	1.44 (82%-10%)	750	50	20
Figueiredo et al. 2009	NiCuLa (Hydrogen pretreatment)	Tubular reactor	(80%-80%) (27)[a]	700	22	113

2.9 References

1. H. F. Abbas and W. W. Daud, "Hydrogen production by methane decomposition: a review," *International Journal of Hydrogen Energy*, vol. 35(3), 1160-1190, 2010.
2. J. D. Holladay, J. Hu, D. L. King, and Y. Wang, "An overview of hydrogen production technologies," *Catalysis today*, vol. 139(4), 244-260 2009.
3. R. Ramachandran and R. K. Menon, "An overview of industrial uses of hydrogen," *International Journal of Hydrogen Energy*, vol. 23(7), 593-598, 1998.
4. U. P. M. Ashik, W. W. Daud, and H. F. Abbas, "Production of greenhouse gas free hydrogen by thermocatalytic decomposition of methane–a review." *Renewable and Sustainable Energy Reviews*, vol. 44, 221-256, 2015.
5. Y. Li, D. Li, and G. Wang, "Methane decomposition to COx-free hydrogen and nano-carbon material on group 8–10 base metal catalysts: a review," *Catalysis Today*, vol. *162*(1), 1-48, 2011.
6. Z. Wei, J. Sun, Y. Li, A. K. Datye, and Y. Wang, "Bimetallic catalysts for hydrogen generation," *Chemical Society Reviews*, vol. 41(24), 7994-8008, 2012.
7. R. Lan, J. T. Irvine, and S. Tao, "Ammonia and related chemicals as potential indirect hydrogen storage materials," *International Journal of Hydrogen Energy*, vol. 37(2), 1482-1494, 2012.
8. M. Appl, "Ammonia: principles and industrial practice," (pp. 137-138). Weinheim, Germany: Wiley-VCH, 1999.
9. EIA, (09/01/2017), Available: https://www.eia.gov/todayinenergy/detail.php?id=24612
10. T. L. LeValley, A. R. Richard, and M. Fan, "The progress in water gas shift and steam reforming hydrogen production technologies–a review," *International Journal of Hydrogen Energy*, vol. 39(30), 16983-17000, 2014.
11. P. L. Spath and M. K. Mann, "Life cycle assessment of hydrogen production via natural gas steam reforming (No. NREL/TP-570-27637)". National Renewable Energy Lab., Golden, CO (US), 2000.
12. J. H. Wee and K. Y. Lee, "Overview of the development of CO-tolerant anode electrocatalysts for proton-exchange membrane fuel cells," *Journal of Power Sources*, vol. 157(1), 128-135, 2006.
13. M. Steinberg and H. C. Cheng, "Modern and prospective technologies for hydrogen production from fossil fuels," *International Journal of Hydrogen Energy*, vol. 14(11), 797-820, 1989.
14. K. McHugh, S. Eisele, and J. Nestell, "Hydrogen production methods," MPR Associates Inc, 41, 2005.
15. J. J. Krummenacher, K. N. West, and L. D. Schmidt, "Catalytic partial oxidation of higher hydrocarbons at millisecond contact times: decane, hexadecane, and diesel fuel," *Journal of Catalysis*, vol. 215(2), 332-343, 2003.
16. M. Krumpelt, T. R. Krause, J. D. Carter, J. P. Kopasz, and S. Ahmed, "Fuel processing for fuel cell systems in transportation and portable power applications," *Catalysis today*, vol. 77(1), 3-16, 2002.
17. M. Krumpelt, "Fuel processing session summary," In Proceedings of the Joint DOE/ONR Fuel Cell Workshop, Baltimore (pp. 6-8), October, 1999.
18. R. J. Bellows, "Technical challenges for hydrocarbon fuel reforming," In Proceedings of the joint DOE/ONR Fuel Cell workshop, Baltimore (pp. 6-8), October, 1999.

19. F. Joensen and J. R. Rostrup-Nielsen, "Conversion of hydrocarbons and alcohols for fuel cells," *Journal of power sources,* vol. 105(2), 195-201, 2002.
20. S. K. Saraswat and K. K. Pant, "Ni–Cu–Zn/MCM-22 catalysts for simultaneous production of hydrogen and multiwall carbon nanotubes via thermo-catalytic decomposition of methane," *International Journal of Hydrogen Energy,* vol. 36(21), 13352-13360, 2011.
21. H. T. Jang and W. S. Cha, "Hydrogen production by the thermocatalytic decomposition of methane in a fluidized bed reactor," *Korean Journal of Chemical Engineering,* vol. 24(2), 374-377, 2007.
22. J. Lane and P. Spath "Technoeconomic analysis of the thermocatalytic decomposition of natural gas (No. NREL/TP-510-31351)," National Renewable Energy Lab., Golden, CO (US), 2001.
23. J. Dufour, D. P. Serrano, J. L. Galvez, J. Moreno, and C. Garcia, "Life cycle assessment of processes for hydrogen production. Environmental feasibility and reduction of greenhouse gases emissions," *International Journal of Hydrogen Energy*, vol. 34(3), 1370-1376, 2009.
24. G. Italiano, C. Espro, F. Arena, F. Frusteri, and A. Parmaliana, "Catalytic decomposition of natural gas for COx-free hydrogen production in a structured multilayer reactor," *Applied Catalysis A: General,* vol. 357(1), 58-65, 2009.
25. M. Appl, *Ammonia: principles and industrial practice*: Weinheim, Germany: Wiley-VCH, 1999.
26. G. J. Leigh, *Haber-Bosch and other industrial processes:* Springer Netherlands, 2004.
27. R. Schlögl, *Ammonia synthesis*: Wiley-VCH Verlag GmbH & Co. KGaA, 2008.
28. S. Giddey, S. P. S. Badwal, and A. Kulkarni, "Review of electrochemical ammonia production technologies and materials," *International Journal of Hydrogen Energy,* vol. 38(34), 14576-14594, 2013.
29. N. Z. Muradov and T. N. Veziroğlu, "From hydrocarbon to hydrogen–carbon to hydrogen economy," *International Journal of Hydrogen Energy*, vol. 30(3), 225-237, 2005.
30. R. H. Baughman, A. A. Zakhidov, and W. A. De Heer, "Carbon nanotubes--the route toward applications," *Science,* vol. 297(5582), 787-792, 2002.
31. B. Gaudernack and S. Lynum, "Hydrogen from natural gas without release of CO_2 to the atmosphere," *International journal of hydrogen energy,* vol. 23(12), 1087-1093, 1998.
32. Hawthorne C. Carbon fiber future, (11/12/2016), Available: www.metropolismag.com/html/content%200203/1b
33. N. S. Lee, D. S. Chung, I. T. Han, J. H. Kang, Y. S. Choi, H. Y. Kim, and J. E. Jung, "Application of carbon nanotubes to field emission displays," *Diamond and Related Materials,* vol. 10(2), 265-270, 2001.
34. A. Bachtold, P. Hadley, T. Nakanishi, and C. Dekker, "Logic circuits with carbon nanotube transistors," *Science,* vol. 294(5545), 1317-1320, 2001.
35. F. Legrain, J. Sottmann, K. Kotsis, S. Gorantla, S. Sartori, and S. Manzhos, "Amorphous (Glassy) carbon, a promising material for sodium ion battery anodes: a combined first-principles and experimental study," *The Journal of Physical Chemistry C,* vol. 119(24), 13496-13501, 2015.
36. M. Noh, Y. Kwon, H. Lee, J. Cho, Y. Kim, and M. G. Kim, "Amorphous carbon-coated tin anode material for lithium secondary battery," *Chemistry of Materials,* vol. 17(8), 1926-1929, 2005.
37. K. P. De Jong and J. W. Geus, "Carbon nanofibers: catalytic synthesis and applications," *Catalysis Reviews,* vol. 42(4), 481-510, 2000.

38. B. Glaser, J. Lehmann, and W. Zech, "Ameliorating physical and chemical properties of highly weathered soils in the tropics with charcoal-a review," *Biology and Fertility of Soils*, vol. 35(4), 219-230, 2002.
39. P. Somasundaran, *Encyclopedia of surface and colloid science (Vol. 2):* CRC press, 2006.
40. J. Rostrup-Nielsen, "Hydrogen generation by catalysis," *Encyclopedia of Catalysis*, 2003.
41. S. Majhi, P. Mohanty, H. Wang, and K. K. Pant, "Direct conversion of natural gas to higher hydrocarbons: A review," *Journal of Energy Chemistry*, vol. 22(4), 543-554, 2013.
42. (10/10/2016), Available: http://cbe.rutgers.edu/pdf/brochure.pdf
43. L. Jin, H. Si, J. Zhang, P. Lin, Z. Hu, B. Qiu, and H. Hu, "Preparation of activated carbon supported Fe–Al_2O_3 catalyst and its application for hydrogen production by catalytic methane decomposition," *International Journal of Hydrogen Energy*, vol. 38(25), 10373-10380, 2013.
44. B. Zapata, M. A. Valenzuela, J. Palacios, and E. Torres-Garcia, "Effect of Ca, Ce or K oxide addition on the activity of Ni/SiO_2 catalysts for the methane decomposition reaction," *International Journal of Hydrogen Energy*, vol. 35(21), 12091-12097, 2010.
45. P. Jana, A. Víctor, J. M. Coronado, and D. P. Serrano, "Cobalt based catalysts prepared by Pechini method for CO_2-free hydrogen production by methane decomposition," *International Journal of Hydrogen Energy*, vol. 35(19), 10285-10294, 2010.
46. A. Roine, *HSC Chemistry 5.11*: Outokumpu Research Oy, Pori, Finland, 76, 2002.
47. A. Venugopal, S. N. Kumar, J. Ashok, D. H. Prasad, V. D. Kumari, K. B. S. Prasad, and M. Subrahmanyam, "Hydrogen production by catalytic decomposition of methane over Ni/SiO_2," *International Journal of Hydrogen Energy*, vol. 32(12), 1782-1788, 2007.
48. S. Takenaka, M. Serizawa, and K. Otsuka, "Formation of filamentous carbons over supported Fe catalysts through methane decomposition," *Journal of Catalysis*, vol. 222(2), 520-531, 2004.
49. M. A. Ermakova and D. Y. Ermakov, "Ni/SiO_2 and Fe/SiO_2 catalysts for production of hydrogen and filamentous carbon via methane decomposition," *Catalysis Today*, vol. 77(3), 225-235, 2002.
50. A. C. Dupuis, "The catalyst in the CCVD of carbon nanotubes-a review," *Progress in Materials Science*, vol. 50(8), 929-961, 2005.
51. K. Otsuka, H. Ogihara, and S. Takenaka, "Decomposition of methane over Ni catalysts supported on carbon fibers formed from different hydrocarbons," *Carbon*, vol. 41(2), 223-233, 2003.
52. T. V. Choudhary, C. Sivadinarayana, C. C. Chusuei, A. Klinghoffer, and D. W. Goodman, "Hydrogen production via catalytic decomposition of methane," *Journal of Catalysis*, vol. 199(1), 9-18, 2001.
53. A. Chambers, T. Nemes, N. M. Rodriguez, and R. T. K. Baker, "Catalytic behavior of graphite nanofiber supported nickel particles, comparison with other support media," *The Journal of Physical Chemistry B*, vol. 102(12), 2251-2258, 1998.
54. D. Chen, K. O. Christensen, E. Ochoa-Fernández, Z. Yu, B. Tøtdal, N. Latorre, and A. Holmen, "Synthesis of carbon nanofibers: effects of Ni crystal size during methane decomposition," *Journal of Catalysis*, vol. 229(1), 82-96, 2005.
55. A. Hornés, P. Bera, M. Fernández-García, A. Guerrero-Ruiz, and, A. Martínez-Arias, "Catalytic and redox properties of bimetallic Cu–Ni systems combined with CeO_2 or Gd-

doped CeO_2 for methane oxidation and decomposition," *Applied Catalysis B: Environmental*, vol. 111, 96-105, 2012.
56. A. C. Lua, and H. Y. Wang, "Decomposition of methane over unsupported porous nickel and alloy catalyst," *Applied Catalysis B: Environmental*, vol. 132, 469-478, 2013.
57. N. Shah, D. Panjala, and G. P. Huffman, "Hydrogen production by catalytic decomposition of methane," *Energy & Fuels*, vol. 15(6), 1528-1534, 2001.
58. I. Suelves, M. J. Lázaro, R. Moliner, Y. Echegoyen, and J. M. Palacios, "Characterization of NiAl and NiCuAl catalysts prepared by different methods for hydrogen production by thermocatalytic decomposition of methane," *Catalysis Today*, vol. 116(3), 271-280, 2006.
59. A. F. Cunha, J. J. M. Órfão, and J. L. Figueiredo, "Methane decomposition on Fe–Cu Raney-type catalysts," *Fuel Processing Technology*, vol. 90(10), 1234-1240, 2009.
60. N. Shah, S. Pattanaik, F. E. Huggins, D. Panjala, and G. P. Huffman, "XAFS and Mössbauer spectroscopy characterization of supported binary catalysts for non-oxidative dehydrogenation of methane," *Fuel Processing Technology*, vol. 83(1), 163-173, 2003.
61. A. Punnoose, N. Shah, G. P. Huffman, and M. S. Seehra, "X-ray diffraction and electron magnetic resonance studies of $M/Fe/Al_2O_3$ (M= Ni, Mo and Pd) catalysts for CH_4 to H_2 conversion," *Fuel Processing Technology*, vol. 83(1), 263-273, 2003.
62. J. Chen, Y. Li, Z. Li, and X. Zhang, "Production of COx-free hydrogen and nanocarbon by direct decomposition of undiluted methane on Ni–Cu–alumina catalysts," *Applied Catalysis A: General*, vol. 269(1), 179-186, 2004.
63. A. J. Carrillo, D. Sastre, L. Zazo, D. P. Serrano, J. M. Coronado, and P. Pizarro, "Hydrogen production by methane decomposition over MnOx/YSZ catalysts," *International Journal of Hydrogen Energy*, vol. 41(42), 19382-19389, 2016.
64. L. B. Avdeeva, T. V. Reshetenko, Z. R. Ismagilov, and V. A. Likholobov, "Iron-containing catalysts of methane decomposition: accumulation of filamentous carbon," *Applied Catalysis A: General*, vol. 228(1), 53-63, 2002.
65. S. K. Saraswat, B. Sinha, K. K. Pant, and R. B. Gupta, "Kinetic Study and Modeling of Homogeneous Thermocatalytic Decomposition of Methane over a Ni–Cu–Zn/Al2O3 Catalyst for the Production of Hydrogen and Bamboo-Shaped Carbon Nanotubes," *Industrial & Engineering Chemistry Research*, vol. 55(45), 11672-11680, 2016.
66. A. Malaika and M. Kozłowski, "Influence of ethylene on carbon-catalysed decomposition of methane," *International Journal of Hydrogen Energy*, vol. 34(6), 2600-2605, 2009.
67. A. Dufour, A. Celzard, V. Fierro, E. Martin, F. Broust, and A. Zoulalian, "Catalytic decomposition of methane over a wood char concurrently activated by a pyrolysis gas," *Applied Catalysis A: General*, vol. 346(1), 164-173, 2008.
68. N. Muradov, "Catalysis of methane decomposition over elemental carbon," *Catalysis Communications*, vol. 2(3), 89-94, 2001.
69. N. Muradov, F. Smith, and T. Ali, "Catalytic activity of carbons for methane decomposition reaction," *Catalysis Today*, vol. 102, 225-233, 2005.
70. M. H. Kim, E. K. Lee, J. H. Jun, S. J. Kong, G. Y. Han, B. K. Lee, and K. J. Yoon, "Hydrogen production by catalytic decomposition of methane over activated carbons: kinetic study," *International Journal of Hydrogen Energy*, vol. 29(2), 187-193, 2004.
71. J. S. Prasad, V. Dhand, V. Himabindu, Y. Anjaneyulu, P. K. Jain, and B. Padya, "Production of hydrogen and carbon nanofibers through the decomposition of methane

over activated carbon supported Pd catalysts," *International Journal of Hydrogen Energy*, vol. 35(20), 10977-10983, 2010.
72. J. Zhang, L. Jin, Y. Li, and H. Hu, "Ni doped carbons for hydrogen production by catalytic methane decomposition," *International Journal of Hydrogen Energy*, vol. 38(10), 3937-3947, 2013.
73. J. Zhang, L. Jin, Y. Li, H. Si, B. Qiu, and H. Hu, "Hierarchical porous carbon catalyst for simultaneous preparation of hydrogen and fibrous carbon by catalytic methane decomposition," *International Journal of Hydrogen Energy*, vol. 38(21), 8732-8740, 2013.
74. D. W. Breck, *Zeolite molecular sieves: structure, chemistry and use:* Krieger, 1984.
75. G. T. Kokotailo, S. L. Lawton, D. H. Olson, and W. M. Meier, "Structure of synthetic zeolite ZSM-5," *Nature*, vol. 272(5652), 437-438, 1978.
76. L. Wang, L. Tao, M. Xie, G. Xu, J. Huang, and Y. Xu, "Dehydrogenation and aromatization of methane under non-oxidizing conditions" *Catalysis Letters*, vol. 21(1-2), 35-41, 1993.
77. S. Nahreen, S. Praserthdam, S. Perez Beltran, P. B. Balbuena, S. Adhikari, and R. B. Gupta, "Catalytic Upgrading of Methane to Higher Hydrocarbon in a Nonoxidative Chemical Conversion," *Energy & Fuels*, vol. 30(4), 2584-2593, 2016.
78. P. L. Tan, Y. L. Leung, S. Y. Lai, and C. T. Au, "The effect of calcination temperature on the catalytic performance of 2 wt.% Mo/HZSM-5 in methane aromatization," *Applied Catalysis A: General*, vol. 228(1), 115-125, 2002.
79. T. V. Choudhary, C. Sivadinarayana, C. C. Chusuei, A. Klinghoffer, and D. W. Goodman, "Hydrogen production via catalytic decomposition of methane," *Journal of Catalysis*, vol. 199(1), 9-18, 2001.
80. S. Abanades and G. Flamant, "Production of hydrogen by thermal methane splitting in a nozzle-type laboratory-scale solar reactor," *International Journal of Hydrogen Energy*, vol. 30(8), 843-853, 2005.
81. R. Moliner, I. Suelves, M. J. Lázaro, and O. Moreno, "Thermocatalytic decomposition of methane over activated carbons: influence of textural properties and surface chemistry," *International Journal of Hydrogen Energy*, vol. 30(3), 293-300, 2005.
82. I. Suelves, J. L. Pinilla, M. J. Lázaro, and R. Moliner, "Carbonaceous materials as catalysts for decomposition of methane," *Chemical Engineering Journal*, vol. 140(1), 432-438, 2008.
83. F. Liu, L. Chen, L. Yang, Z. Fan, H. Nikolic, L. Richburg, and K. Liu, "Application of chemical looping process for continuous high purity hydrogen production by methane thermocatalytic decomposition," *International Journal of Hydrogen Energy*, vol. 41(8), 4592-4602, 2016.
84. H. F. Abbas, and W. W. Daud, "Hydrogen production by thermocatalytic decomposition of methane using a fixed bed activated carbon in a pilot scale unit: apparent kinetic, deactivation and diffusional limitation studies," *International Journal of Hydrogen Energy*, vol. 35(22), 12268-12276, 2010.
85. K. K. Lee, G. Y. Han, K. J. Yoon, and B. K. Lee, "Thermocatalytic hydrogen production from the methane in a fluidized bed with activated carbon catalyst," *Catalysis Today*, vol. 93, 81-86, 2004.
86. J. L. Figueiredo, "Progress in Catalyst Deactivation," *Proceedings of the NATO Advanced Study Institute on Catalyst Deactivation*, Algarve, Portugal, vol. 54, Springer Science & Business Media, May 18–29, 1981.

87. A. Arcoya, X. L. Seoane, N. S. Figoli, and P. C. L'Argentiere, "Relationship between sulfur resistance and electronic state of the metal on supported palladium catalysts," *Applied Catalysis*, vol. 62(1), 35-45, 1990.
88. C. K. Ryu, M. W. Ryoo, I. S. Ryu, and S. K. Kang, "Catalytic combustion of methane over supported bimetallic Pd catalysts: Effects of Ru or Rh addition," *Catalysis Today*, vol. 47(1), 141-147, 1999.
89. J. N. Stanley, K. Worthington, F. Heinroth, A. F. Masters, and T. Maschmeyer, "Reversible bimetallic Pt-Ru alloy hydrogenation catalystswith improved sulfur tolerance," Chemeca 2011: Engineering a Better World: Sydney Hilton Hotel, NSW, Australia, 18-21 September 2011, 593, 2011.
90. S. Yasyerli, S. Filizgok, H. Arbag, N. Yasyerli, and G. Dogu, "Ru incorporated Ni–MCM-41 mesoporous catalysts for dry reforming of methane: Effects of Mg addition, feed composition and temperature," *International Journal of Hydrogen Energy*, vol. 36(8), 4863-4874, 2011.
91. X. Wang, W. Yue, M. He, M. Liu, J. Zhang, and Z. Liu, "Bimetallic catalysts for the efficient growth of SWNTs on surfaces" *Chemistry of Materials*, vol. 16(5), 799-805, 2004.
92. S. Link, S. Arvelakis, M. Hupa, P. Yrjas, I. Külaots, and A. Paist, "Reactivity of the biomass chars originating from reed, Douglas fir, and pine," *Energy & Fuels*, vol. 24(12), 6533-6539, 2010.
93. S. S. Liaw, Z. Wang, P. Ndegwa, C. Frear, S. Ha, C. Z. Li, and M. Garcia-Perez, "Effect of pyrolysis temperature on the yield and properties of bio-oils obtained from the auger pyrolysis of Douglas Fir wood," *Journal of Analytical and Applied Pyrolysis*, vol. 93, 52-62, 2012.
94. S. S. Liaw, S. Zhou, H. Wu, and M. Garcia-Perez, "Effect of pretreatment temperature on the yield and properties of bio-oils obtained from the auger pyrolysis of Douglas fir wood," *Fuel*, 103, 672-682, 2013.
95. (10/10/2017) Available: https://www.azonano.com/article.aspx?ArticleID=2885
96. S. Meyer, B. Glaser, and P. Quicker, "Technical, economical, and climate-related aspects of biochar production technologies: a literature review," *Environmental Science & Technology*, vol. 45(22), 9473-9483, 2011.
97. D. A. Laird, R. C. Brown, J. E. Amonette, and J. Lehmann, "Review of the pyrolysis platform for coproducing bio-oil and biochar," *Biofuels, Bioproducts and Biorefining*, vol. 3(5), 547-562, 2009.
98. A. V. Bridgwater, D. Meier, and D. Radlein, "An overview of fast pyrolysis of biomass," *Organic Geochemistry*, vol. 30(12), 1479-1493, 1999.
99. K. Qian, A. Kumar, H. Zhang, D. Bellmer, and R. Huhnke, "Recent advances in utilization of biochar," *Renewable and Sustainable Energy Reviews*, vol. 42, 1055-1064, 2015.
100. R. Azargohar and A. K. Dalai, "The direct oxidation of hydrogen sulphide over activated carbons prepared from lignite coal and biochar," *The Canadian Journal of Chemical Engineering*, vol. 89(4), 844-853, 2011.
101. Z. Bai, H. Chen, W. Li, and B. Li, "Hydrogen production by methane decomposition over coal char," *International Journal of Hydrogen Energy*, vol. 31(7), 899-905, 2006.
102. H. F. Abbas and W. W. Daud, "Thermocatalytic decomposition of methane using palm shell based activated carbon: kinetic and deactivation studies," *Fuel Processing Technology*, vol. 90(9), 1167-1174, 2009.

103. T. Otowa, R. Tanibata, and M. Itoh, "Production and adsorption characteristics of MAXSORB: high-surface-area active carbon," Gas Separation & Purification, vol. 7(4), 241-245, 1993.
104. D. Lozano-Castello, J. M. Calo, D. Cazorla-Amoros, and A. Linares-Solano, "Carbon activation with KOH as explored by temperature programmed techniques, and the effects of hydrogen," Carbon, vol. 45(13), 2529-2536, 2007.
105. E. Raymundo-Pinero, P. Azais, T. Cacciaguerra, D. Cazorla-Amorós, A. Linares-Solano, and F. Béguin, "KOH and NaOH activation mechanisms of multiwalled carbon nanotubes with different structural organization," Carbon, vol. 43(4), 786-795, 2005.
106. W. Qiao, S. H. Yoon, and I. Mochida, "KOH activation of needle coke to develop activated carbons for high-performance EDLC," Energy & Fuels, vol. 20(4), 1680-1684, 2006.
107. H. Wang, Q. Gao, and J. Hu, "High hydrogen storage capacity of porous carbons prepared by using activated carbon," Journal of the American Chemical Society, vol. 131(20), 7016-7022, 2009.
108. J. Romanos, M. Beckner, T. Rash, L. Firlej, B. Kuchta, P. Yu, and P. Pfeifer, "Nanospace engineering of KOH activated carbon," Nanotechnology, vol. 23(1), 015401, 2011.
109. Konieczny, A., Mondal, K., Wiltowski, T., & Dydo, P. (2008). Catalyst development for thermocatalytic decomposition of methane to hydrogen. *International Journal of Hydrogen Energy*, *33*(1), 264-272.
110. Reshetenko, T. V., Avdeeva, L. B., Ismagilov, Z. R., Chuvilin, A. L., & Fenelonov, V. B. (2005). Catalytic filamentous carbons-supported Ni for low-temperature methane decomposition. *Catalysis Today*, *102*, 115-120.
111. Bai, Z., Chen, H., Li, B., & Li, W. (2007). Methane decomposition over Ni loaded activated carbon for hydrogen production and the formation of filamentous carbon. *International journal of hydrogen energy*, *32*(1), 32-37.
112. Cunha, A. F., Orfão, J. M., & Figueiredo, J. L. (2009). Methane decomposition on Ni–Cu alloyed Raney-type catalysts. *International Journal of hydrogen energy*, *34*(11), 4763-4772.
113. Figueiredo, J. L., Órfão, J. J. M., & Cunha, A. F. (2010). Hydrogen production via methane decomposition on Raney-type catalysts. *International Journal of Hydrogen Energy*, *35*(18), 9795-9800.

CHAPTER THREE: EXPERIMENTAL AND CHARACTERIZATION METHODS

3.1 Catalysts for Methane Decomposition

Name of six different catalysts used in this study are represented in Table 3.1.

Table 3.1: Name of catalysts

Catalysts Description	Name of Catalysts
Commercial ZSM-5 (SiO_2/Al_2O_3 ratio:23:1)	ZSM-5
3 wt % Ru doped in commercial ZSM-5 (SiO_2/Al_2O_3 ratio:23)	Ru-ZSM-5
Activated Carbon (Commercial)	AC
3 wt % Ru doped in commercial activated carbon	Ru-AC
Activated Biochar (from Douglas fir biomass)	AB
Biochar with heat-treatment	HB

3.1.1 Commercial Catalysts

Among six catalysts, ZSM-5 and AC were bought from Alfa Aesar. ZSM-5 (Zeolite Scony Mobil-5) has SiO_2/Al_2O_3 ratio 23:1, (stock no. 45879, Lot # T16B032). Molecular weight of activated carbon (AC) is 12.01 and melting point is 3550 ^oC (stock no. 242241-250G, Lot# MKBW724BV).

3.1.2 Ru-doped Catalysts

Ru was doped on ZSM-5 and AC by wet impregnation method. Ruthenium (III) nitrosyl nitrate solution ($Ru(NO)NO_3$) was used as Ru precursor solution. This Ru-solution was bought from Alfa Aesar and had 1.5 w/v % Ru (stock no. 12530, Lot# S17B028). The solution had density 1.07 kg/m^3 and molecular weight 317.09. Since chloride ions are hard to eliminate entirely in pre-treatment process [1], nitrate solution was chosen over chloride solution.

The required amount of Ru precursor solution was manually mixed with ZSM-5 and AC following the incipient wet impregnation method in several steps. Initially, the total amount of precursor solution required for the wet impregnation process was calculated based on the concentration of the precursor solution and the desired doping percentage. Then, the precursor solution was slowly added to the support material until the mixture became sticky. This quantity of solution indicated the amount of solution could be added in one single steps. The total amount of required precursor solution was divided by the amount of precursor solution that made support sticky gave the number of mixing steps [2]. In between every step, the mixture of ruthenium precursor solution and support material (ZSM-5 or AC) was dried for 12 h in the presence of air in a Thermolyene furnace. After drying step, the Ru-ZSM-5 catalyst was calcined at 500 ^oC for 5 h in the presence of air in a Thermolyene furnace [3]. In the case of Ru-AC, the catalyst was calcined in a fixed bed reactor at 500 ^oC for 5 h in the presence of nitrogen to get the inert environment. Figure 3.1 and Figure 3.2 represent Ru-ZSM-5 and Ru-AC catalyst's appearance after every preparation steps, respectively.

Figure 3.1: Ru-ZSM-5 catalyst after different steps

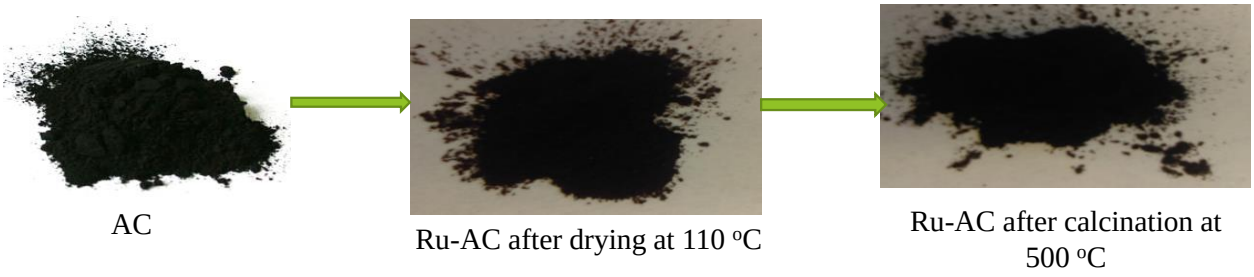

Figure 3.2: Ru-AC catalyst after different preparation steps

3.1.3 Biochar Catalysts

Douglas fir biomass (0.8 mm crumbles from chips) was used in this study. Biomass was obtained from Forest Concepts, LLC. (Auburn, Washington). Biomass sample was stored in cold room at 4 °C until used in this study. Fast pyrolysis process was used to produce biochar. Two different treatments (heat treatment and activation) were done to obtain HB and AB. Figure 3.3 represents biomass used in this study.

Figure 3.3: Douglas fir biomass

Biochar Production Process

Douglas fir biomass was dried at 50 ^{o}C for 24 h to get moisture content less than 10 %. A bubbling fluidized bed reactor was used for fast pyrolysis. Figure 3.4 represents fluidized bed reactor set-up for fast pyrolysis. The reactor set-up used in the current study was similar to some of our previous gasification and pyrolysis studies [4-8]. Briefly, the reactor set-up has a biomass hopper connected with a twin screw auger and an injection screw, a bubbling fluidized bed reactor which is connected with a high temperature filter (HTF) (filter temperature is maintained at 350 ^{o}C), two series condenser which is cooled by a circulating condenser (cooling agent is a mixture of ethylene glycol and water which is maintained below 3 ^{o}C), an electrostatic precipitator (ESP) (20 kV is supplied in top attached rod), bio-oil collector, and a NOVA gas analyzer (Note: All the units are connected in series, respectively). The fluidized bed reactor consists of main reactor and freeboard. The main reactor has 2 in (50 mm) diameter and 22.75 in (580 mm) height, and freeboard has 4 in (100 mm) diameter and 8 in (200 mm) height.

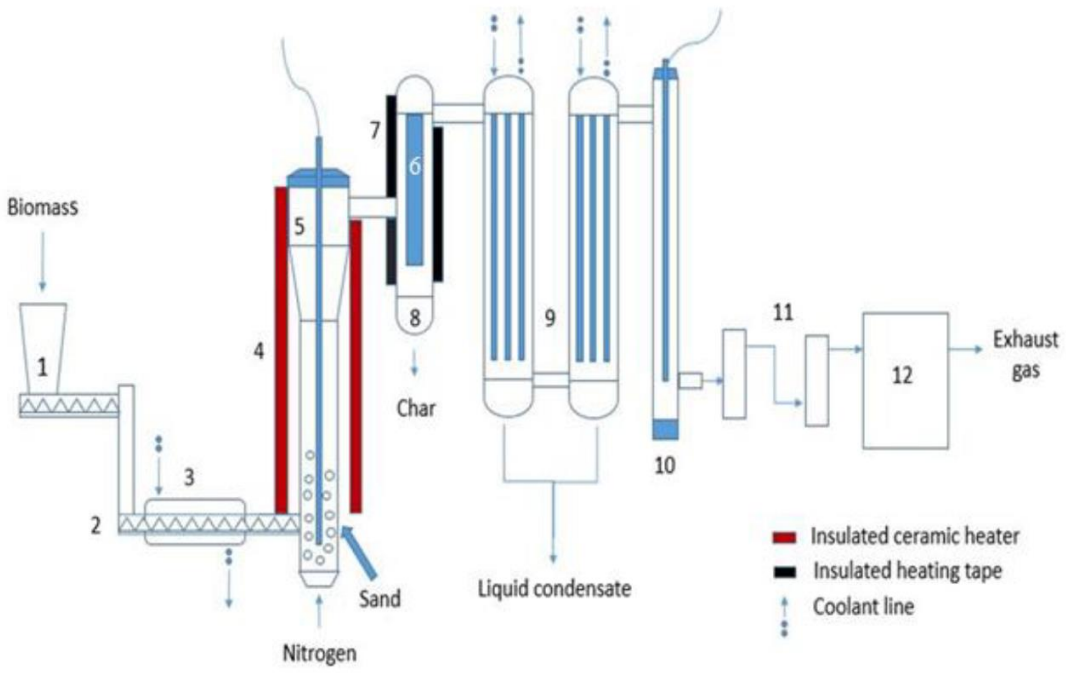

Figure 3.4: Fast pyrolysis reactor system [5]: 1) Hopper, 2) Screw auger, 3) Heat exchanger, 4) Heater, 5) Fluidized bed reactor, 6) High temperature filter, 7) High temperature filter heater, 8) Char Collector, 9) Condenser, 10) ESP, 11) Gas absorber, 12) NOVA gas analyzer

Silica sand (7062-06, Macron Fine Chemicals) was used as bed material in a fluidized bed reactor. 1000 g silica sand was placed in the reactor. The reactor was heated to 500 ^{o}C with a 20 ^{o}C/min heating rate. At the same time, chiller was started and was set at 3 ^{o}C. 12 LPM air was passed through the reactor system to fluidize bed material and to ensure the uniform heating. 500 g Douglas fir biomass was placed into the biomass hopper. After that, the hopper was sealed. When the bed material and middle part of the reactor reached at 500 ^{o}C, the air was turned off, and 12 LPM nitrogen was passed through the whole reactor system to get the inert environment for fast pyrolysis. The inert atmosphere was ensured by NOVA gas analyzer. When oxygen concentration was low down to ≤ 0.1 %, biomass was feed into the main reactor through auger feeder (feed rate 1.5 g/min). O_2, H_2, CH_4, CO and CO_2 contents of product gases were monitored continuously to

ensure inert environment and successful pyrolysis. The clear drop tube between hopper and feeder was monitored continuously to ensure all the biomass was fed into the reactor. When all the biomass was fed into the reactor, the feeder was turned off. However, the heater was kept on for about 10 min to ensure complete pyrolysis of biomass. After 10 min, the heater was turned off, but nitrogen was passed through the system for an additional 30 min to exhaust all the pyrolysis gases. After 30 min, the whole system was shut down. Char from HTF was collected when the reactor system cooled down to the room temperature. The collected biochars were stored in a cold room at 4 ^{o}C until use. Figure 3.5 represents biochar produced from the fast pyrolysis process.

Figure 3.5: Biochar

Heat-treated Biochar Catalyst

A fixed bed reactor was used to perform the heat-treatment of biochar. Figure 3.6 represents the experimental set-up for carrying out the heat-treatment process. Fixed bed reactor has a diameter of 1 in (25 mm) and length about 11 in (279.4 mm). The reactor is connected to a nitrogen cylinder by the bottom feed line. The product line is connected to a condenser which is cooled down by ice. The outlet from the condenser is passed through a water trap and finally exhausted to vent.

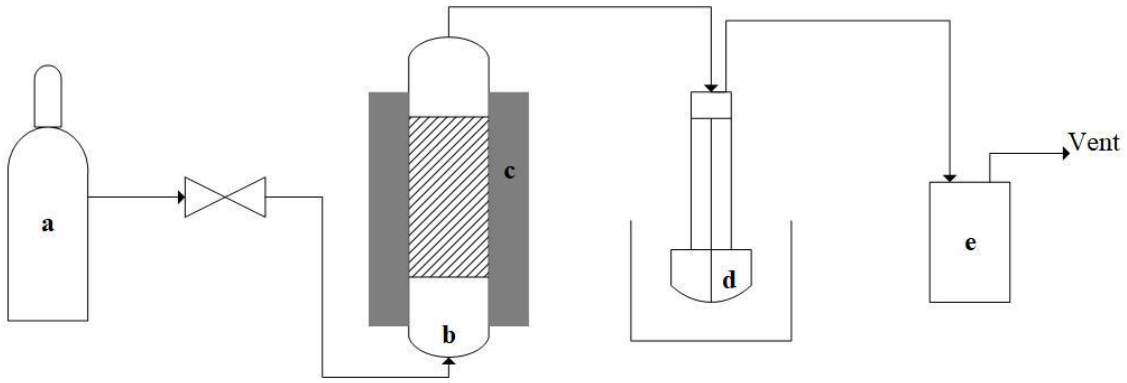

Figure 3.6: Biochar heat-treatment set-up: a) nitrogen cylinder, b) fixed bed reactor, c) furnace, d) condenser, e) water trap

For this process, about 25 g biochar was placed in the fixed bed reactor, and then a small quartz wool and 316 stainless steel mesh were placed on the bottom of the reactor. Nitrogen at 0.3 LPM was passed through the reactor system continuously to get the inert environment for heat-treatment. Bubbling in water trap ensured nitrogen gas flow through the reactor system. The reactor was heated to 800 ^{o}C with a 5 ^{o}C/min heating rate. The heat-treatment was done for 2 h once the temperature reached 800 °C. After two hours, the furnace was turned off. Nitrogen flow was reduced to 0.1 LPM and kept on until the reactor cooled down to room temperature. Heat-treated biochar (Figure 3.7) was ball milled with a Retsch ball miller (model PM 100) at 400 rpm for 2 h to get uniform particle size and also increase the surface area.

Figure 3.7: Heat-treated biochar (HB)

Activated Biochar (AB) Catalyst

KOH was used to activate the biochar. Reagent grade KOH was bought from VWR and used in this study. Biochar from fast pyrolysis was dried at 105 ^{o}C for 12 h. The required amount of KOH pellets (3 g KOH for 1 g biomass) were mixed with water (3 mL water for 1 g KOH) in a glass biker. For better mixing, the solution was stirred with a magnetic stirrer for 30 min. Dried biochar was added into KOH solution on a weight basis. The mixture was stirred with a magnetic stirrer for 2 h to ensure uniform mixing. Then, the solution was dried at 105 ^{o}C for 12 h in a corrosion resistant crucible. The mixture was not dried completely because complete drying causes the KOH to stay at the top of dried mixture. The dried mixture was crushed by hand crusher (pestle and mortar) for homogeneity. The crushed mixture was placed in a fixed bed reactor which was used for heat-treatment (Figure 3.6). 0.3 LPM nitrogen was passed through the reactor system for 30 min to get the inert environment for heat-treatment. Then the reactor was heated initially to 400 ^{o}C with a 5 ^{o}C/min heating rate. Once the reactor reached at 400 ^{o}C, nitrogen flow was reduced to 0.05 LPM. The reactor was kept at 400 ^{o}C for 1 h. After heat-treatment at 400 ^{o}C, the mixture was heated to 800 ^{o}C and kept that temperature for 2 h. Finally, the furnace was turned off, and 0.1

LPM nitrogen was passed through the reactor system until it cooled down to room temperature. Heat treated mixture was washed continuously with 0.1 M HCl and DI water until pH was closer to 7.0. Neutralized activated biochar was dried at 105 ^{o}C for 12 h. Finally, dried activated biochar was ball milled with a Retsch ball miller (model PM 100) (400 rpm for 2 h) to get higher surface area. Biochar activation process train is represented in Figure 3.8.

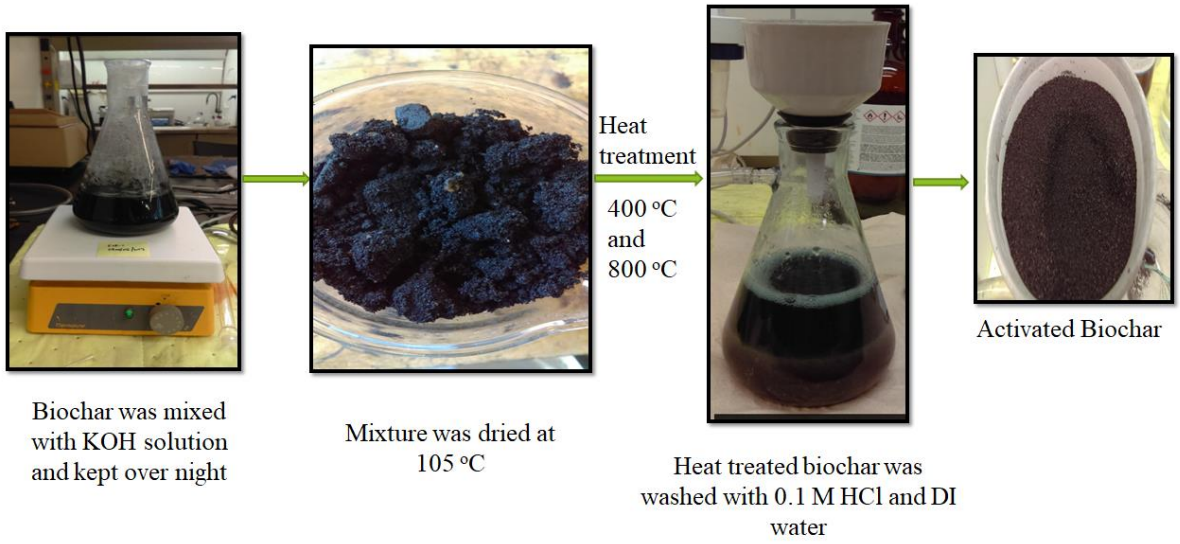

Figure 3.8: Biochar activation procedure

3.2 Catalyst Characterizations

Following analysis were performed to characterize the catalysts.

1. Moisture analysis
2. Elemental analysis
3. BET analysis
4. XRD analysis
5. TPR analysis
6. Chemisorption analysis

7. SEM and EDS
8. TGA analysis

3.2.1 Moisture Analysis

Moisture analysis of biomass was performed before fast pyrolysis process to check the moisture content. Mettler Toledo moisture analyzer (Model: MJ33) was used in this analysis. About 0.7 g sample was taken in an aluminum pan and placed in the moisture analyzer. The temperature inside the machine was increased to 105 ^{o}C to calculate weight loss of samples. Moisture content (MC) of the samples in percent was obtained directly from the machine based on the mass loss. Machine follows equation 1 to calculate moisture content.

$$MC(\%) = \frac{W_a - W_d}{W_a} \times 100 \quad \text{.....(1)}$$

Where, W_a= Weight of samples before drying

W_d = Weight of samples after drying

3.2.2 Elemental Analysis

Elemental analysis was performed to evaluate the carbon (C), nitrogen (N), hydrogen (H) and sulfur (S) content on biomass, biochar and biochar catalysts (AB and heat-treated biochar). Oxygen (O) content in the catalyst samples were then estimated by difference ([O %] = 100-sum ([C %] + [H %] + [N %] + [S %]). Ultimate analysis was performed using Elementar Vario Micro Cube CHNS analyzer.

3.2.3 XRD (Powder X-ray Diffraction) Analysis

XRD was performed to evaluate the surface species of catalysts and structure of catalysts (amorphous or crystalline). This analysis helped to find the type of Ru phase present in the Ru-doped catalyst (Ru-ZSM-5 and Ru-AC) after the calcination step. It also gave an idea about how the surface species and structure changes with different types of pre-treatment for biochar catalysts (AB and HB). XRD patterns for different catalysts were obtained by XRD analyzer (Bruker D2 Phaser Advance Diffractometer with LynxEye detector). Powder catalyst samples were placed in a sample holder with a very fine straight top surface. Then, sample holder was placed inside the machine. Patterns were achieved from 10^o to 80^o angle with an incremental step of 0.05^o and scanning time every 1 s.

3.2.4 TPR (Temperature Programmed Reduction) Analysis

After calcination, metals in catalyst are present in their oxides form. To get active metal phase on catalysts, the *in-situ* reduction was performed before every experiments. Reduction temperature was varied from the catalyst to catalyst. TPR analysis uses hydrogen to determine the reduction temperature of catalysts. In case of carbon catalysts, different impurities (from ash content) are present on catalysts surface, and the reduction is required to obtain better performance. TPR analysis was done with TPR analyzer (Quantachrome, ASIQC0YV200-4). 0.17 g Ru-ZSM-5 catalyst sample was placed in a quartz tube. Then quartz tube was placed on the machine for analysis. For Ru-AC, 0.08 g catalyst sample was used and for biochar catalysts, (AB and HB) 0.05 g catalyst sample was used. The sample was first heated to 100 ^oC with 50 ml/min N_2 flow for 1 h. Then, the sample was cooled down to room temperature. After that, temperature was increased

to 900 ^{o}C with a heating rate 5 ^{o}C/min. At that time, carrier gas was changed to (5% H_2 in N_2) with a flow rate of 50 ml/min. H_2 consumption pattern was recorded by a computer.

3.2.5 Chemisorption Analysis

ZSM-5 and activated carbon were doped with 3% Ru. Chemisorption analysis was done on Ru-doped catalysts to determine the percentage of metal dispersed on the catalyst surface and active metal surface area. Chemisorption analysis was done on Quantachrome, ASIQC0YV200-4. All the catalyst samples were dried at 105 ^{o}C for 12 h before analysis. Around 0.17 g of Ru-ZSM-5 and 0.12 g of Ru-AC samples were used for chemisorption analysis. The sample of catalysts was placed on a quartz tube for analysis. The sample was first heated to 105 ^{o}C with a heating rate 20 ^{o}C/min in the presence of helium. This temperature was maintained for 30 min. Then purging gas was changed to hydrogen and sample was heated to 400 ^{o}C with a heating rate 20 ^{o}C/min. The hydrogen gas flowed for 120 min, and the system was evacuated for 120 min.

3.2.6 Surface Area, Pore Volume and Average Pore Diameter Analysis

The surface area of catalysts plays a vital role in the reaction rate. The higher surface area gives more place to accommodate methane molecules and gives stability to resist against deactivation for a longer period. Surface area and average pore size were calculated from BET (Brunauer Emmett Teller) analysis. Brunauer Emmett Teller method calculates surface area, pore volume and pore diameter from nitrogen adsorption-desorption isotherm. For pore size distribution, two different methods were used. DFT (Density Functional Theory) method works well with materials those have a microporous structure, and BJH (Barrett Joyner Halenda) works well when mesopores and macropores are present. DFT method does not give any results if

macropores are present in the material. Since Ru-ZSM-5 and ZSM-5 have a mesoporous structure with macropores, the BJH method was used for pore size distribution analysis. Similarly, Ru-AC, AC, and AB have a microporous structure with mesopores and the DFT method was used for pore size distribution analysis. About 50 mg of Ru-ZSM-5 and ZSM-5 samples were taken into a quartz tube for degassing. Degassing profile for Ru-ZSM-5 and ZSM-5 samples are given in Table 3.2. About 20-15 mg of carbon catalysts (Ru-AC, AC, AB, HB) were taken for the analysis. Degassing profile for carbon catalysts is given in Table 3.3.

Table 3.2: Degassing profile for ZSM-5 and Ru-ZSM-5 catalysts

Temperature (ºC)	Heating Rate (ºC/min)	Soaking Time (min)
80	2	30
120	2	30
250	2	600

Table 3.3: Degassing profile for carbon catalysts (Ru-AC, AC, AB, HB)

Temperature (ºC)	Heating Rate (ºC/min)	Soaking Time (min)
80	2	30
120	2	30
300	2	720
300	2	720

After degassing, the sample was weighed again and placed in adsorption chamber with liquid nitrogen and nitrogen gas was passed through the sample cell to get Langmuir adsorption isotherm.

3.2.7 SEM (Scanning Electron Microscope) and EDS (Energy Dispersive X-ray Spectroscopy)

SEM was used to get the microscopic image of different catalysts. Zeiss, EVO 50, UK SEM analyzer was used in this experiment. Before taking SEM images, the samples were coated with gold (Au) to make samples conductive. Backscatter mode was used for Ru-ZSM-5 catalyst to distinguish between Ru and ZSM-5 phase. In case of Ru-AC, secondary electron mode was used. Carbon is a small molecule, and EDS detector could not capture backscatter electrons of carbon. EDS was used to determine the composition of catalysts.

After reaction, spent catalysts were analyzed by SEM to identify the nature of the carbon produced in reaction. Spent catalysts were coated with gold (Au) and placed in SEM vacuum chamber for capturing image.

3.2.8 TGA (Thermogravimetric Analysis)

TGA was performed to determine ash content on biomass, biochar, activated biochar, heat-treated biochar. 10-15 mg sample was placed on an aluminum pan. Then, the sample was placed in a weighing pan for analysis. The temperature profile for analysis is represented in Table 3.4. At first, the sample was heated up to 105 ^{o}C at a heating rate of 10 ^{o}C/min and maintained at that temperature for 30 min. After that, the sample was heated up to 575 ^{o}C with a heating rate 10 ^{o}C/min and kept that temperature for 120 min. Air of 20 ml/min was flown through the sample during the analysis.

Table 3.4: Temperature profile for TGA analysis

Step	Hold Temperature (ºC)	Heating Rate (ºC/min)	Time(min)
First	105	10	30
Second	575	10	120

3.3 Experimental Set-up and Procedure

A fixed bed reactor made of Inconel was used for the reaction. Inconel shows better stability than stainless steel in high-temperature applications. For this reason, Inconel was chosen for reactor material. Material composition for Inconel 600 is represented in Table 3.5. The reactor has ½ in (12.7mm) outer diameter, 3/8 in (9.53mm) inside diameter and 21 in (533.5mm) length.

Table 3.5: Material composition of reactor [8]

Component	Ni	Cr	Fe	Mn	Cu	Si	C	S
Percent (%)	72	14-17	6-10	1	0.5	0.5	0.15	0.015

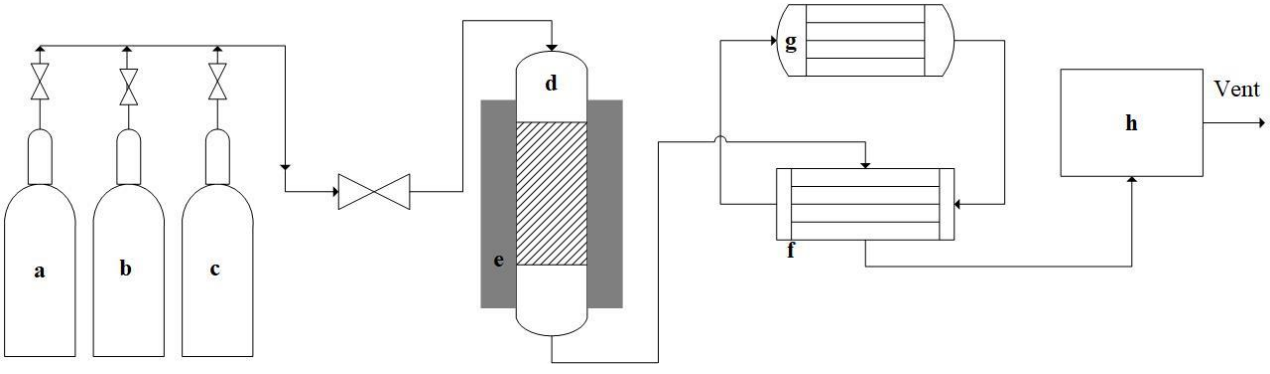

Figure 3.9: Schematic diagram of experimental set-up: a) nitrogen gas cylinder, b) hydrogen gas cylinder, c) methane gas cylinder, d) fixed bed reactor, e) electric heater, f) heat exchanger, g) chiller, h) micro-GC

Figure 3.9 represents the schematic diagram of the experimental set-up. An automatic reactor system was used for the reaction. Delta V operator system controled the reactor temperature and reactants flow rate. A fixed bed reactor (top-feed) was connected with feed gases cylinder. An electric heater was integrated with the reactor to increase the temperature of the reactor to the desired temperature. Reactor's product line was connected with a heat-exchanger which was cooled down by a circulating chiller (cooling agent ethylene glycol and water). Then, the product line was passed through a micro GC to analyze the gaseous products.

About 4.5 g ZSM-5 or Ru-ZSM-5 was mixed with 3 g silica sand (1-3 mm fused lamp, melting point 1680 ^{o}C) and placed in the reactor. The reactor temperature was increased to 500 ^{o}C for *in-situ* reduction. Nitrogen (5 mL/min) was passed through the system while increasing temperature. Once the reactor reached in 500 ^{o}C, nitrogen flow was stopped and 10 ml/min H_2 was passed through the catalyst bed for 5 h. Then the reactor temperature was increased to 800 ^{o}C for reaction.

About 4.5 g AC or Ru-AC mixed with 3 g silica sand (1-3mm fused lamp, melting point 1680 ^{o}C) were placed in the reactor. The reactor temperature was increased to 500 ^{o}C for calcination. Nitrogen (5 mL/min) was passed through the system while raising the temperature. The reactor temperature was maintained at 500 ^{o}C for 5 h in the presence of nitrogen for calcination. After calcination, the reactor temperature was increased to 600 ^{o}C for the *in-situ* reduction. Once the reactor was in 600 ^{o}C, nitrogen flow was stopped and 10 ml/min H_2 was passed through the catalyst bed for 5 h. After reduction, the reactor temperature was set to the desired temperature for reaction.

About 2.0 g AB and HB mixed with 1.3 g silica sand (1-3 mm fused lamp, melting point 1680 ^{o}C) were placed in the reactor. The reactor temperature was increased to 700 ^{o}C for *in-situ* reduction. Nitrogen (5 ml/min) was passed through the system while increasing temperature. Once the reactor was in 700 ^{o}C, nitrogen was stopped and 10 ml/min H_2 was passed through the catalyst bed for 30 min. After reduction, the reactor temperature was set to a desired temperature for the reaction.

A leak test was done with nitrogen to ensure the inert environment before increasing the reactor temperature. 0.1 and 0.4 WHSV flow rate with 50% N_2 and 50% CH_4 were passed after the reactor reached the desired temperature. Product gas was analyzed in every 30 min. The composition of reactor feed gas was measured at the beginning of the reaction.

3.4 Product Characterization

3.4.1 Micro GC

Micro GC (Agilent 3000A) was used to analyze gaseous product composition. Carrier gases (He, and Ar) product gases pass through the GC column. The light gases can pass the column quickly, but heavy gases collude with the wall of the column and sometimes adsorb in the wall filled with chemicals. Heat is given to desorb heavy gas from the wall and to pass through the column. Therefore, light gases will come first at the graph, and heavy gas will come according to their weight. Micro-GC used in this thesis was equipped with four capillary columns which could identify hydrogen, saturated, unsaturated hydrocarbon (C_1-C_5 and C_{6+} grouped peaks), and fixed gases (N_2, O_2, CO, CO_2). Column A (Molsieve, 10 m ×320 µm ×12 µm) used Ar as a carrier gas. Column B (PLOTU, 8 m ×320 µm ×30 µm), column C (Alumina, 10 m ×320 µm ×8 µm), and column D (OV1, 14 m ×150 µm ×20 µm) used He as a carrier gas. The method used in this study

is represented in Table 3.6. Ultra-pure CH_4, N_2, and H_2 gases were mixed in different ratio, and those mixed gases were used to calibrate GC.

Table 3.6: GC method used in this study

	Column A	Column B	Column C	Column D
Injection Time (ms)	25	25	25	40
Backflash (s)	10	6	5	-
Sample Inlet Temperature (^oC)	80	80	80	80
Injector Temperature (^oC)	80	80	80	80
Column Temperature (^oC)	100	80	135	90
Column Pressure (psi)	32	32	32	35
Post Run Pressure (psi)	32	32	32	35

3.4.2 TEM (Transmission Electron Microscope)

Product carbon (ZSM-5 and Ru-ZSM-5) were analyzed in TEM (Zeiss EM10) using 80 kV to determine product carbon identity (nanotube or nanofiber or amorphous). In the same way, spent catalyst (Ru-AC, AC, AB, and HB) were analyzed by TEM (JEOL 200CX) using 100 kV. SEM only scan the surface of the sample and display the surface of the sample. TEM uses electron beam that transmits the samples. Transmitted electrons capture in the detector and give the image which can identify the nature of carbon product.

3.5 Conversion Calculation

Feed gas composition was recorded at the beginning of the reaction, and product gas composition was collected every 30 min. Since feed gas composition was measured and the product line from the reactor to GC machine is long, the first 2 h of product gas composition was not analyzed. Feed gases flow rates were controlled by Delta V operating system. The following calculation procedure was used.

Total feed flow was recorded from Delta V operating system. Feed gases compositions were measured by GC in the beginning of the reaction. For example, the total inlet flow was V_1, and N_2 and CH_4 gases compositions were S_{N2in} and S_{CH4in}, respectively. Product gases compositions were S_{H2}, S_{N2out}, and S_{CH4out} for H_2, N_2, and CH_4, respectively.

From N_2 balances,

$$V_1 \times S_{N2in} = V_2 \times S_{N2out}$$

$$\therefore V_2 = \frac{V_1 \times S_{N2in}}{S_{N2out}} \text{ ml/min}$$

where, V_2 = Total product flow rate

Now, $Methane\ flow\ in = V_1 \times S_{CH4in}$

$$Methane\ flow\ out = V_2 \times S_{CH4out}$$

$$\%\ Conversion = \frac{Methane\ flow\ in - Methane\ flow\ out}{Methane\ flow\ in} \times 100\ \%$$

$$= \frac{V_1 \times S_{CH4in} - V_2 \times S_{CH4out}}{V_1 \times S_{CH4in}}$$

$$= \frac{V_1 \times S_{CH4in} - \frac{V_1 \times S_{N2in}}{S_{N2out}} \times S_{CH4out}}{V_1 \times S_{CH4in}}$$

$$= \frac{V_1 \times S_{CH4in} \times S_{N2out} - V_1 \times S_{N2in} \times S_{CH4out}}{V_1 \times S_{CH4in} \times S_{N2out}}$$

$$= \frac{S_{CH4in} \times S_{N2out} - S_{N2in} \times S_{CH4out}}{S_{CH4in} \times S_{N2out}}$$

and,

H_2 flow out = $V_2 \times S_{H2}$ ml/min

So, H_2 production = $\frac{V_2 \times S_{H2}}{(1000 \times 22.4)} \times 1000$ mmol/min

3.6 References

1. M. M. Koranne, D. W. Goodman, and G. W. Zajac, “Direct conversion of methane to higher hydrocarbons via an oxygen free, low-temperature route,” *Catalysis letters*, vol. *30*(1), 219-234, 1994.
2. G. L. Bezemer, J. H. Bitter, H. P. Kuipers, H. Oosterbeek, J. E. Holewijn, X. Xu, and K. P. de Jong, “Cobalt particle size effects in the Fischer−Tropsch reaction studied with carbon nanofiber supported catalysts,” *Journal of the American Chemical Society*, vol. 128(12), 3956-3964, 2006.
3. S. Nahreen, S. Praserthdam, S. Perez Beltran, P. B. Balbuena, S. Adhikari, and R. B. Gupta, “Catalytic upgrading of methane to higher hydrocarbon in a nonoxidative chemical conversion,” *Energy & Fuels*, vol. 30(4), 2584-2593, 2016.
4. N. Sadhwani, S. Adhikari, and M. R. Eden, “Biomass gasification using carbon dioxide: effect of temperature, CO2/C ratio, and the study of reactions influencing the process,” *Industrial & Engineering Chemistry Research*, vol. 55(10), 2883-2891, 2016.
5. N. Abdoulmoumine, A. Kulkarni, and S. Adhikari, “Effects of temperature and equivalence ratio on pine syngas primary gases and contaminants in a bench-scale fluidized bed gasifier,” *Industrial & Engineering Chemistry Research*, vol. 53(14), 5767-5777, 2014.
6. A. Kulkarni, R. Baker, N. Abdoulmomine, S. Adhikari, and S. Bhavnani, “Experimental study of torrefied pine as a gasification fuel using a bubbling fluidized bed gasifier,” *Renewable Energy*, vol. 93, 460-468, 2016.
7. S. Thangalazhy-Gopakumar, S. Adhikari, H. Ravindran, R. B. Gupta, O. Fasina, M. Tu, and S. D. Fernando, “Physiochemical properties of bio-oil produced at various temperatures from pine wood using an auger reactor,” *Bioresource Technology*, vol. 101(21), 8389-8395, 2010.
8. (10/20/2017). Special metals. Available,http://www.specialmetals.com/assets/smc/documents/alloys/inconel/inconel-alloy600.pdf

CHAPTER FOUR: RESULTS AND DISCUSSION

4.1 Catalysts Characterizations

4.1.1 XRD (Powder X-ray Diffraction)

After calcination, the Ru-precursor solution makes bonds with Al_2O_3 and SiO_2 in the zeolite. In order to determine which of the Ru species is present on the catalyst surface, XRD was performed. XRD also gives an idea about the structure of the catalysts (amorphous and crystalline). Ru-ZSM-5 (3% Ru doped ZSM-5) and Ru-AC (3% Ru doped activated carbon) were used for XRD analysis. Figure 4.1 represents the XRD pattern for Ru-ZSM-5 and ZSM-5. Sharp peaks in the figure represent the crystalline structure of ZSM-5. Besides, there are three extra peaks for Ru-ZSM-5 at 28º, 35º and 54º. These three peaks were matched with the XRD library and also with the RuO_2 XRD pattern from the literature [1,2]. These peaks represent the presence of RuO_2 on the catalyst surface.

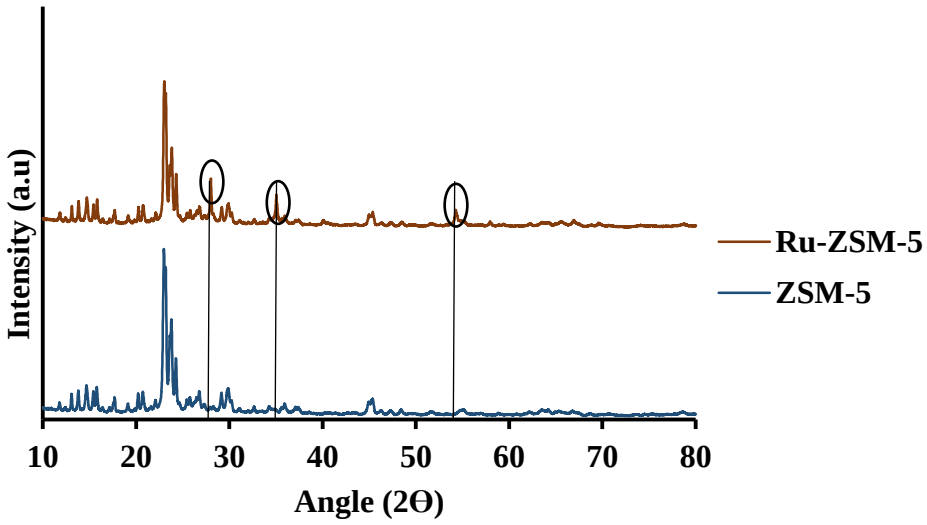

Figure 4.1: XRD pattern for Ru-ZSM-5 and ZSM-5

Figure 4.2 represents the XRD patterns of AC and Ru-AC. Broad peaks from 20° to 30° and 40° to 50° indicate the amorphous structure of AC and Ru-AC. Ru doping did not change the structure of the catalyst. It just reduced the intensity of the peak. Broad peaks of AC were matched with the XRD library and with the literature [3-5].

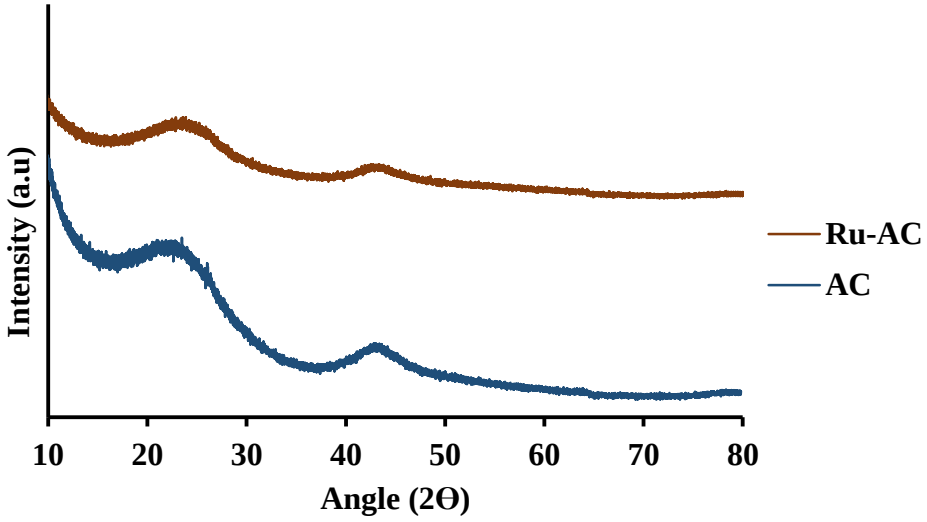

Figure 4.2: XRD pattern of AC and Ru-AC

Figure 4.3 represents the XRD pattern of biochar, HB (Heat-treated biochar), and AB (Activated biochar). In the XRD pattern for biochar, broad peaks from 20° to 28° and 35° to 50° ensure the amorphous structure. Sharp peaks at 21°, 26°, 50°, 60°, and 68° indicate the presence of quartz (SiO_2) on biochar. A similar pattern was observed for HB with more sharp peaks. Douglas fir biochar has alkali, alkaline earth metals and quartz (SiO_2) in its structure [6]. The volatile compounds present in biochar were responsible for the reduced height of the peaks. In the case of HB, heat treatment process eliminated all the volatile compounds. Therefore, extra sharp peaks at 36°, 39°, and 43° were observed. All of these peaks indicated the presence of quartz (SiO_2) [7]. On the other hand, a small wide peak from 24° to 26° and a broad peak from 40° to 50° indicated the

amorphous structure of AB [4,5]. Chemical activation (KOH) eliminated most of the quartz from AB. Therefore, no quartz peak was observed for AB.

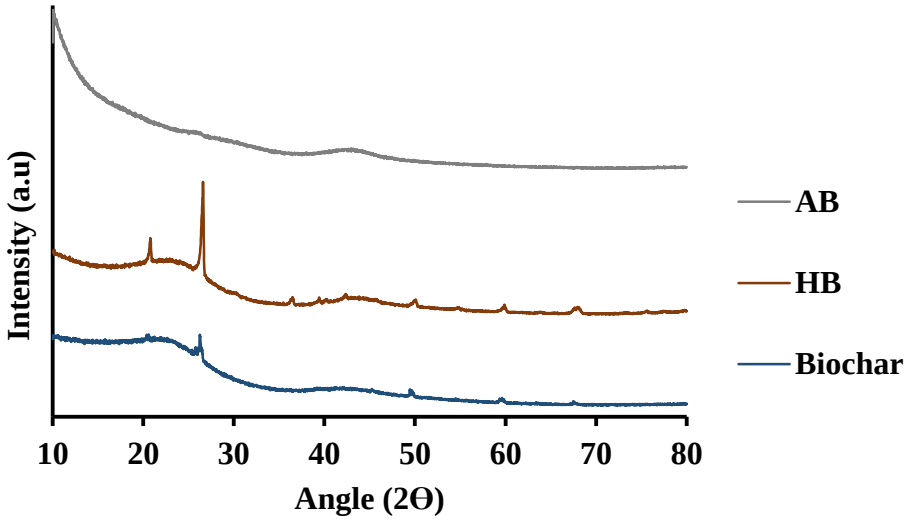

Figure 4.3: XRD pattern of Biochar, HB, AB

4.1.2 TPR (Temperature Programmed Reduction)

Since Ru-oxide was present (confirmed from the XRD results) on Ru-ZSM-5 and Ru-AC catalysts surface, the reduction was needed to be done before carrying out the methane decomposition reaction. To determine the reduction temperature, H_2 TPR was performed on calcine catalysts. Figure 4.4 represents TPR profile of different catalysts.

Figure 4.4 (a) represents the TPR profile of Ru-ZSM-5. There is a small hump at 130 ^oC, which represents the reduction temperature of RuO_4. The sharp peak at 189 ^oC represents the reduction temperature of RuO_2. The TPR profile of Ru-oxide was also matched with the literature [2,5]. The reduction was executed at 500 ^oC for Ru-ZSM-5.

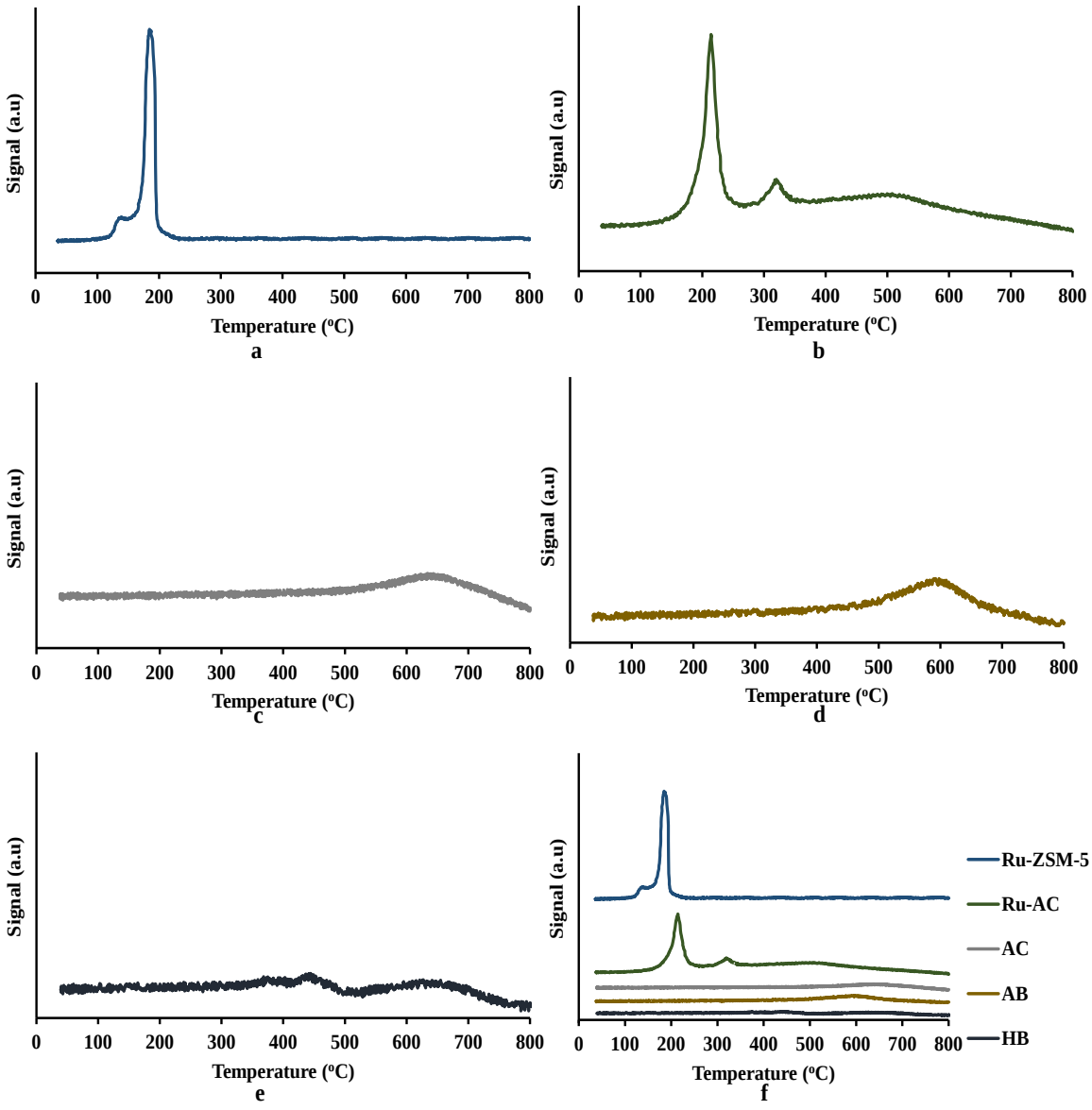

Figure 4.4: TPR profile of different catalysts: a) Ru-ZSM-5, b) Ru-AC, c) AC, d) AB, e) HB, f) combined TPR graph

Figure 4.4 (b) represents the TPR profile of Ru-AC. There is a big sharp peak at 214 °C and a small sharp peak at 327 °C. These two peaks represent the reduction temperature of RuO_4 and RuO_2 on AC, respectively. RuO_4 was reduced at 214 °C and became RuO_2. RuO_2 was reduced to Ru-metal at 327 °C. A broad peak at 520 °C represents the presence of impurities on support

AC or unknown Ru species [5]. To ensure this, TPR was performed on AC. The TPR profile of AC is represented in Figure 4.4 (c). The reduction was executed at 600 ^{o}C for Ru-AC and at 700 ^{o}C for AC. Biochar derived catalysts have ash content as impurities. TPR was performed on AB and HB to figure out the reduction temperature of those impurities. Figure 4.4 (d) represents the TPR profile of AB. Ash contents of AB were reduced at 600 ^{o}C. The TPR profile of HB (Figure 4.4 (e)) indicates that ash contents of HB were reduced at 380 ^{o}C, 450 ^{o}C, and 650 ^{o}C. The reduction was performed at 700 ^{o}C for both of the catalysts (AB and HB). However, carbon catalysts (AC, AB, and HB) showed very small hydrogen consumption (Figure 4.4 (f)).

4.1.3 Chemisorption

ZSM-5 and AC were doped with 3% Ru. The chemisorption was performed to determine the percent of metal dispersion on the catalyst's surface. Table 4.1 represents the chemisorption results for Ru-ZSM-5 and Ru-AC. Around 2.94% Ru was dispersed on ZSM-5 catalyst and active metal surface area (per gram of sample) was 1.07 m^2/g, whereas 3.16% Ru was dispersed on AC and the active metal surface area was 1.15 m^2/g.

Table 4.1: Results of chemisorption analysis

Name of catalysts	Percent of metal dispersion (%)	Active metal surface area (per gram of sample) (m^2/g)	Active metal surface area (per gram of metal) (m^2/g)	Average crystallite size (nm)
Ru-ZSM-5	2.94±0.08	1.07±0.03	10.69±0.31	44.64±1.31
Ru-AC	3.16±0.04	1.15±0.01	11.49±0.13	42.46±0.50

4.1.4 FTIR (Fourier Transform Infrared Spectroscopy)

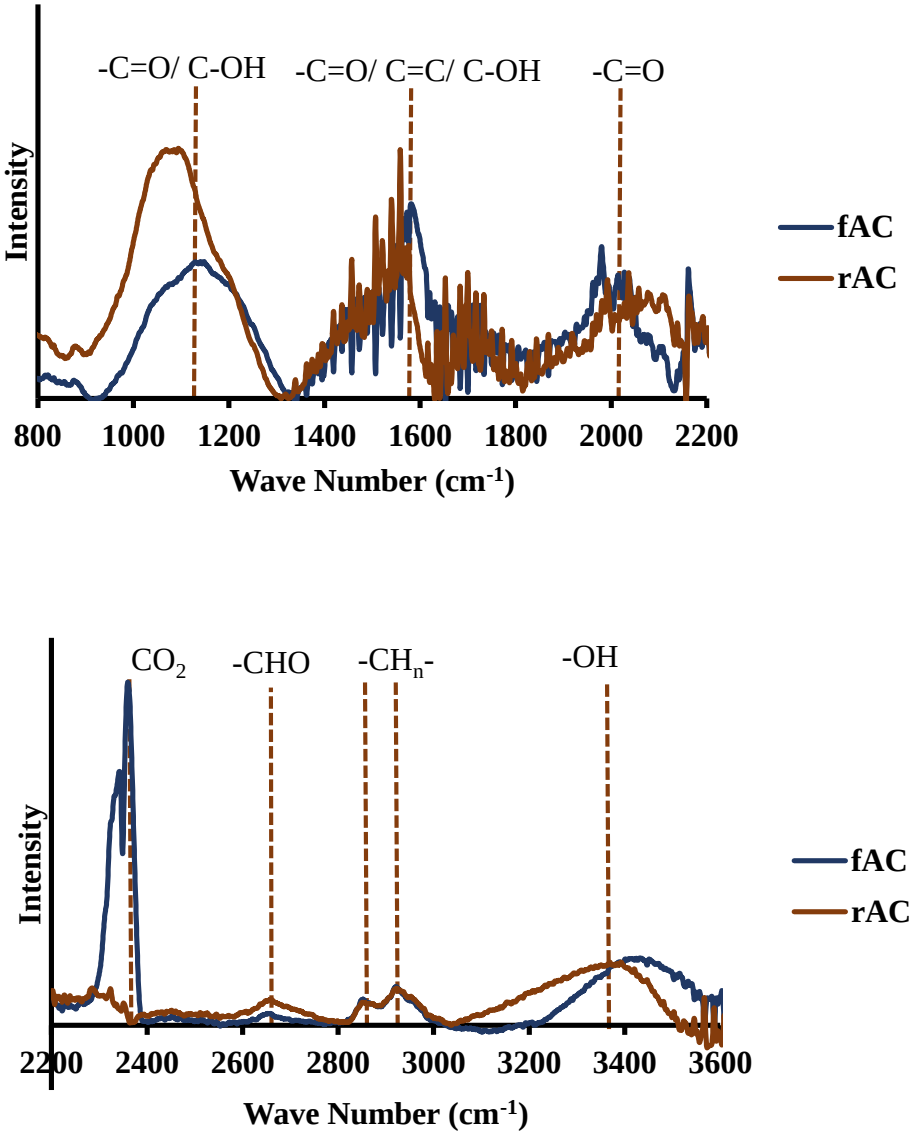

Figure 4.5: FTIR spectra of fresh AC (fAC) and AC reduced by hydrogen (rAC)

Results from FT-IR analysis is shown in Figure 4.5. Peaks at 1107 cm^{-1} (rAC) and 1155 cm^{-1} (fAC) indicated the presence of C=O or –CHOH (C-O stretching vibration in phenol or alcohol group) in AC [8]. Peaks at 1550 cm^{-1} (rAC) and 1590 cm^{-1} (fAC) indicated the presence of C-OH/ C=C/ C=O (aromatic structure or chelated carbonyl group) [8-10]. Peaks at 1983 cm^{-1} (fAC) and 2035 cm^{-1} (rAC) indicated the presence of –C=O or alkynes ($-C \equiv C-$) [8,10]. There

is an extra peak at 2361 cm^{-1} for fresh AC. This peak corresponds to CO_2 absorbed from the surroundings [10]. Small peak around 2680 cm^{-1} (for both spectra) designated for the presence of aldehydes (-CHO) [10]. Two consecutive peaks at 2845 cm^{-1} and 2939 cm^{-1} (for both spectra) indicated alkane stretching ($-CH_n-$) [8,10]. Finally, peaks around 3416 cm^{-1} (rAC) and 3430 cm^{-1} (fAC) designated for alcohols or phenol (-OH stretching mode of hexagonal group) presence [8,10]. FITR spectra for fresh and reduced AC are similar except the presence of CO_2 in fresh AC. Reduction did not eliminate different functional groups from AC.

4.1.5 Elemental Analysis

Elemental analysis was performed to determine carbon, nitrogen and hydrogen content of biomass derived catalysts and data are presented in Table 4.2. Ash content was obtained from TGA analysis. Weight differences of samples between initial weight and weight remaining at 575 ^oC were used to calculate the ash content. To calculate the effect of pre-treatment on biochar, elemental analysis was also performed on the biochar. Elemental analysis was also performed on Douglas fir biomass to find out the composition of nitrogen, carbon and hydrogen contents. Around 3.91 ± 0.28 %, ash content in AB indicated that chemical activation (KOH) could not eliminate all the alkali and alkaline earth metals. The ash content of HB (7.59 ± 0.27%) was higher than the ash content of biochar (4.77 ± 0.56). Heat-treatment eliminated volatile components and increased the percent of ash content in HB. Weight loss profiles of AB, HB, biochar, and biomass are presented in Figure 4.6. AC has the highest heat resistance ability. So 4.1% weight remaining after 575 ℃ might not be ash content.

Table 4.2: Elemental analysis of biomass, biochar, AB, and HB

Name	C(%)	H(%)	N(%)	S(%)	Ash(%)
AB	84.75±0.49	2.84±0.13	0.31±0.01	0.032±0.02	3.91±0.28
HB	81.95±0.42	2.38±0.01	0.32±0.01	ND	7.59±0.27
Biochar	84.15±1.11	3.76±0.04	0.12±0.00	ND	4.77±0.56
Biomass	50.14±0.42	7.79±0.05	0.02±0.01	ND	0.38±0.30
AC	90.11±0.33	1.65±0.13	0.31±0.12	0.01±0.00	4.10±0.39

*ND= not detectable

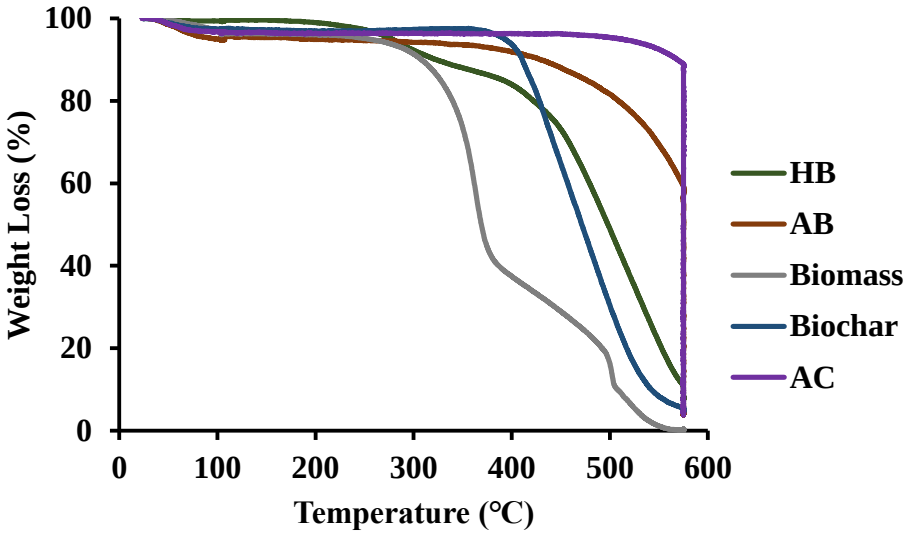

Figure 4.6: Weight loss profiles of AB, HB, biochar, AC, and biomass for ash content determination in the presence of air

4.1.6 Surface Area, Pore Volume, and Pore Size Distribution Analysis

Surface area plays an important role in catalysis. Higher surface area gives higher space for methane molecules to get adsorbed on the catalyst surface. Surface area, pore volume, and average pore size of six different catalysts were measured by using the Brunauer Emmett Teller (BET) analysis. Figure 4.7 represents N_2-adsorption/desorption profiles for different catalysts. ZSM-5 and Ru-ZSM-5 have high mesoporous structures. Both of the catalysts exhibited type IV isotherm (exhibited a hysteresis loop at higher relative pressure) as shown in Figure 4.7 (a) and (b). Initially, capillary condensation of N_2 molecules took place on the mesoporous structures of ZSM-5 and Ru-ZSM-5. At high relative pressure (P/P_o), N_2 desorption from the mesoporous structures became difficult. So, desorption of N_2 molecules followed different paths at high P/P_o and created a hysteresis loop [4]. AC and Ru-AC have micropores and mesopores in their structures. So, type IV isotherms were observed for both of the catalysts as well (Figure 4.7 (c) and (d)). AB displayed type I isotherm (Figure 4.7(e)) as it has high microporous structure.

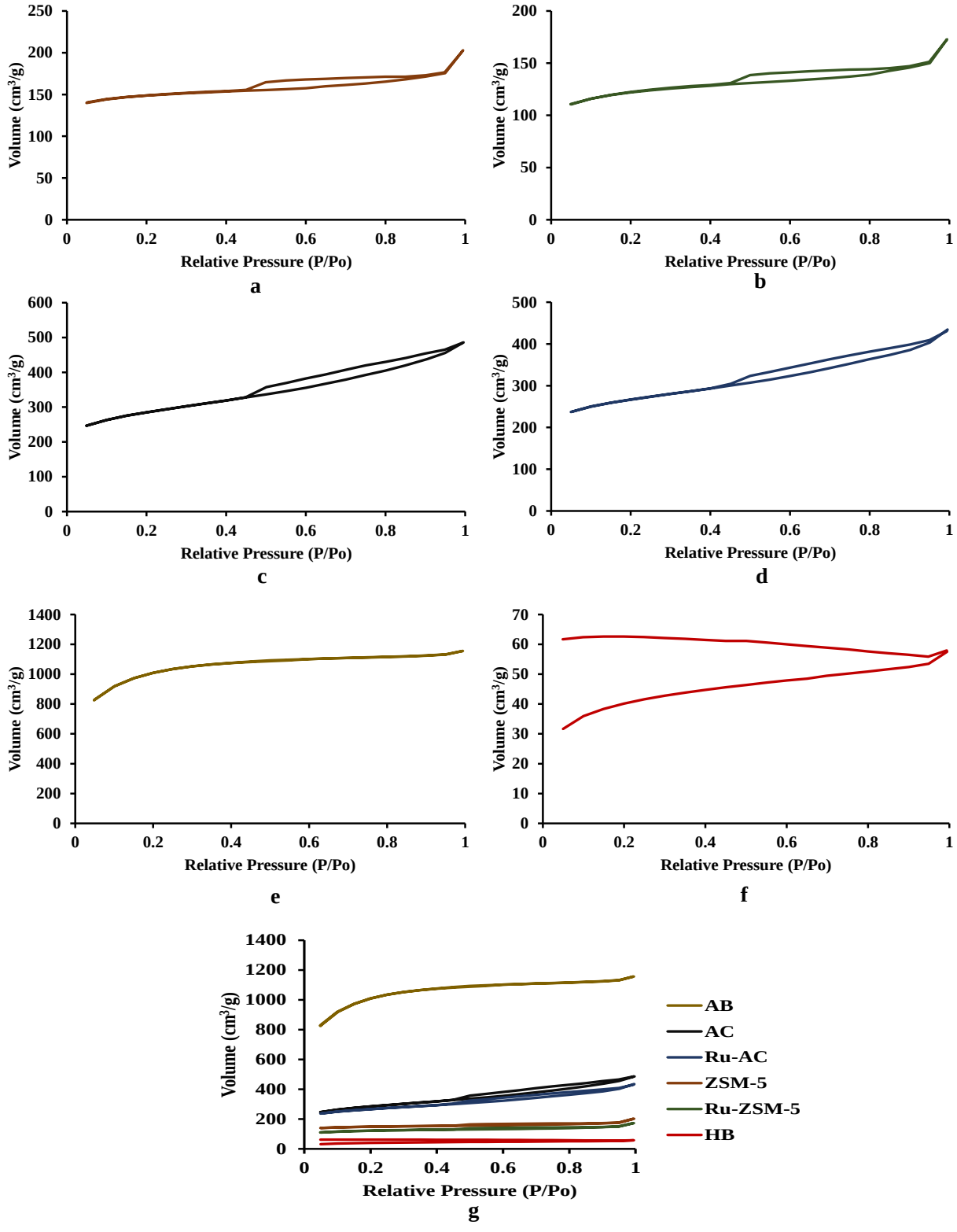

Figure 4.7:N2 adsorption/desorption isotherm of different catalysts: a) ZSM-5, b) Ru-ZSM-5, c) AC, d) Ru-AC, e) AB, f) HB, g) combine isotherms

Chemical treatment (KOH) created a microporous structure for AB. Figure 4.7(f) represents N_2- adsorption/desorption isotherm for HB. Adsorption/ desorption isotherm did not match with each other. This type of isotherm indicates that there is no defined pore structure. The reason behind this type of isotherm is that it was easy for N_2 molecules to adsorb on the HB surface at high P/P_o. At the same time, it was difficult for N_2 molecules to desorb from the HB surface as it does not have any well-defined pore structure. Therefore, N_2 desorption isotherm followed a different path from the adsorption isotherm. Normally, biochar shows this type of isotherm [11,12]. Heat-treatment did not make any changes in N_2 adsorption/desorption isotherm for HB.

Table 4.3 represents BET analysis results. Micro, meso, and macro pore volumes of different catalysts were calculated by DFT (Density Functional Theory), SF (Satio Foley), and DH (Dollimore Heal) methods. Micropore and mesopore volumes were subtracted from the total pore volume to calculate macropore volume. Typically, pore diameter less than 2 nm considers as micropore, from 2 nm to 50 nm considers as mesopore and greater than 50 nm considers as macropore [13]. ZSM-5 and Ru-ZSM-5 catalysts have mesopore and macropore (Figure 4.8). So, the DFT method did not give any results for zeolite catalysts. The SF method was used to calculate micropore volume for ZSM-5 and Ru-ZSM-5, as SF method only works for micropore. Mesopore and macropore volume of ZSM-5 and Ru-ZSM-5 were calculated by DH method, as DH method is famous for calculating mesopore and macropore volume. On the other hand, Ru-AC, AC, and AB have only micropore and mesopore (Figure 4.9). So, the DFT method was used for pore size distribution analysis. HB did not have any defined pore structure (Figure 4.7 (f)). Micropore and mesopore volume could not be calculated for this catalyst. Among the six catalysts, HB has the lowest surface area (109 ± 4.17 m^2/g), and AB has the highest surface area (3256 ± 42.40 m^2/g). Loading of Ru reduced the surface areas of ZSM-5 and AC. Ru-ZSM-5 has 297 ± 0.10 m^2/g surface

area whereas ZSM-5 has 363±11.3 m^2/g surface area. On the other hand, Ru-AC has 693±3.40 m^2/g surface area, and AC has 776±18.60 m^2/g surface area.

Table 4.3: Surface area, pore volume, and average pore size of different catalysts

Name of Catalysts	Surface Area (BET) (m^2g^{-1})	Pore Volume (cm^3 g^{-1})				Average Pore Size (nm)
		Micropore	Mesopore	Macropore	Total Pore Volume	
Ru-ZSM-5	297±0.10	0.19±0.00[a]	0.07±0.01[b]	0.04±0.01[b]	0.27±0.01[c]	3.65±0.01[c]
ZSM-5	363±11.30	0.23±0.02[a]	0.06±0.01[b]	0.04±0.01[b]	0.32±0.01[c]	3.56±0.01[c]
Ru-AC	693±3.40	0.32±0.01[d]	0.26±0.01[d]	--	0.65±0.03[c]	1.88±0.03[c]
AC	776±18.60	0.35±0.01[d]	0.34±0.01[d]	--	0.75±0.01[c]	1.89±0.02[c]
AB	3256±42.40	1.30±0.03[d]	0.29±0.03[d]	--	1.78±0.01[c]	1.10±0.01[c]
HB	109±4.17	--	--	--	0.09±0.00[c]	1.64±0.06[c]

a = Satio Foley method (SF), b = Dollimore Heal method (DH), c = Brunauer Emmett Teller (BET), d = Density Functional Theory method (DFT)

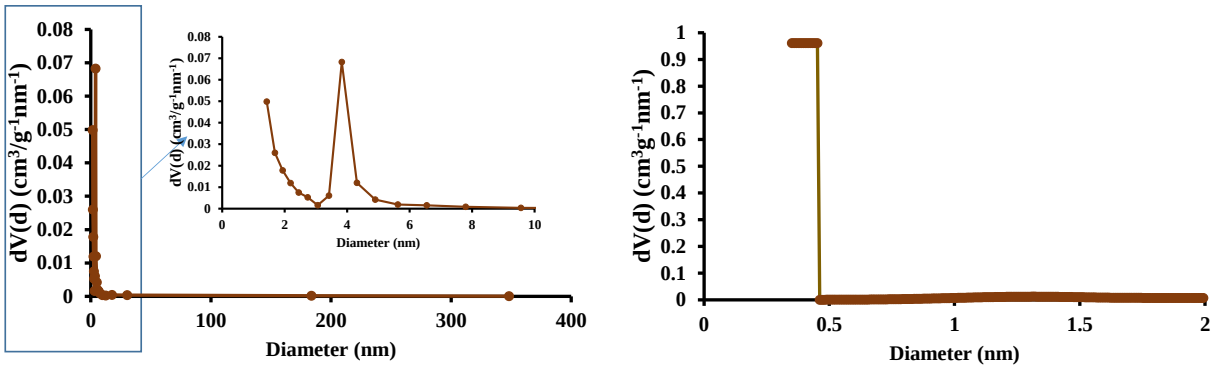

ZSM-5

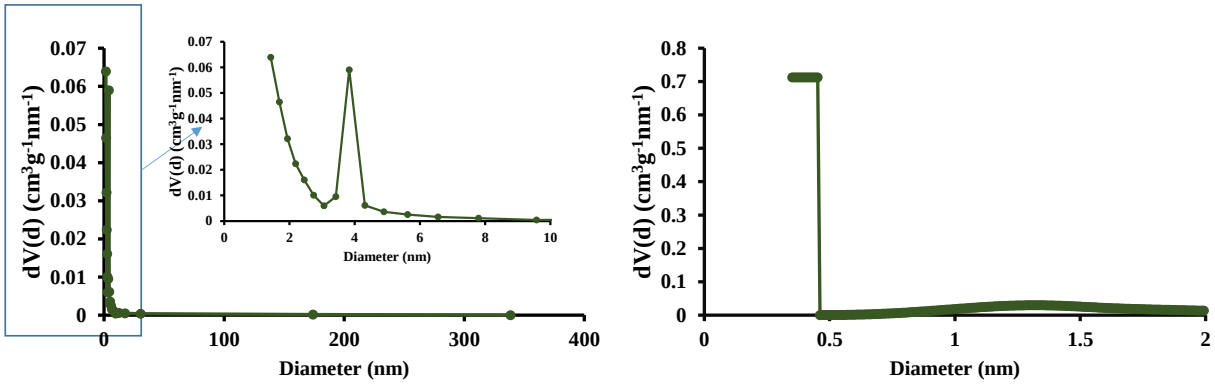

Ru-ZSM-5

Figure 4.8:Pore size distribution of ZSM-5 and Ru-ZSM-5

Figure 4.8 represents pore size distribution graph for ZSM-5 and Ru-ZSM-5. Most of the micropore centered at 0.45 nm for both ZSM-5 and Ru-ZSM-5. According to the DH method, highest amount of pore has 3.83 nm diameter in case of ZSM-5, whereas highest amount of pore has 1.43 nm diameter after doping with Ru. Since ruthenium nitrosyl nitrate diluted in nitric acid was used as Ru-precursor solution, the effect of nitric acid and Ru loading on pores increased the micropore volume and reduced mesopore volume.

Figure 4.9 represents pore size distribution graph for AC, Ru-AC, and AB. According to DFT method, highest amount of pore has 1.68 nm diameter for both AC and Ru-AC. In case of AB, around 82% pore is micropore and most of the pores were centered at 1.18 nm diameter.

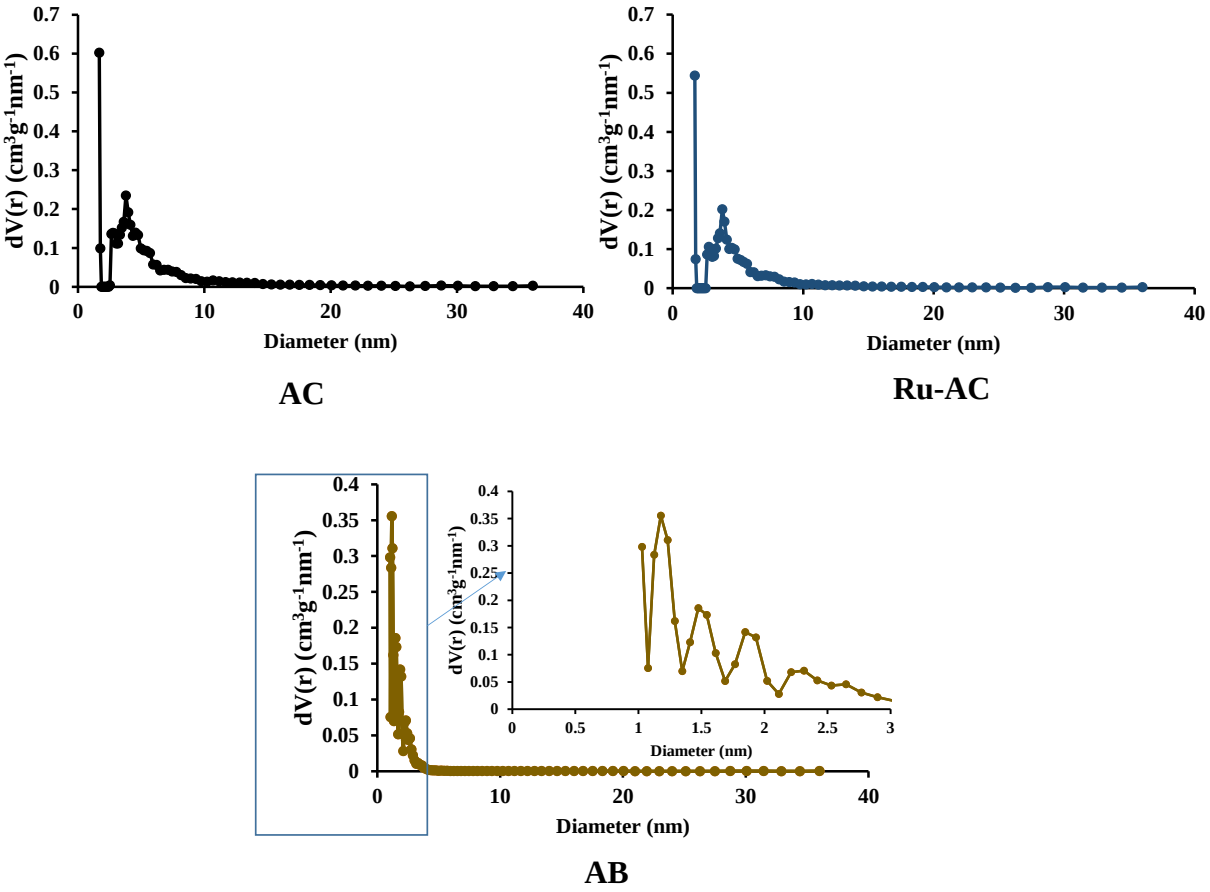

Figure 4.9: Pore size distribution of AC, Ru-AC, and AB

4.1.7 SEM and EDS (Scanning Electron Microscope and Energy Dispersion Spectroscopy)

Figure 4.10 represents fresh ZSM-5, and Figure 4.11 represents Ru-ZSM-5 catalysts. Both of the images were captured by using backscatter electrons. By comparing Figure 4.10 and 4.11, it is noticeable that white dots are uniformly distributed on Ru-ZSM-5. These white dots indicate Ru-metal uniformly distributed on ZSM-5. Normally, back scatter electrons are used to distinguish two phases in SEM image.

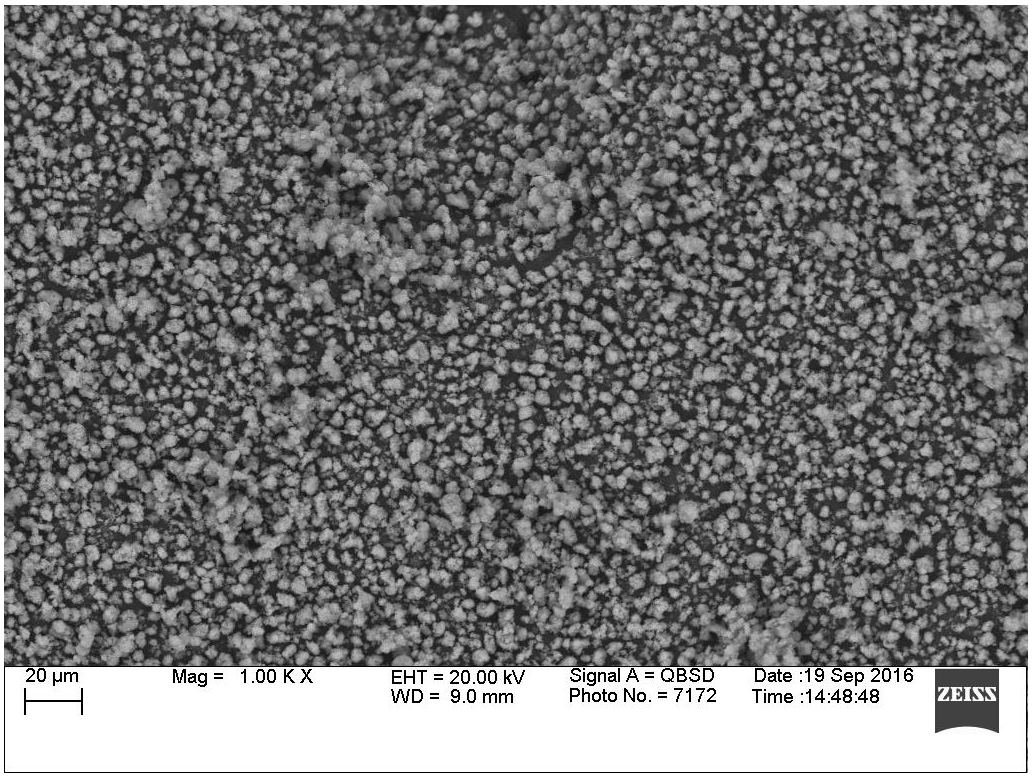

Figure 4.10: SEM image of fresh ZSM-5 catalyst

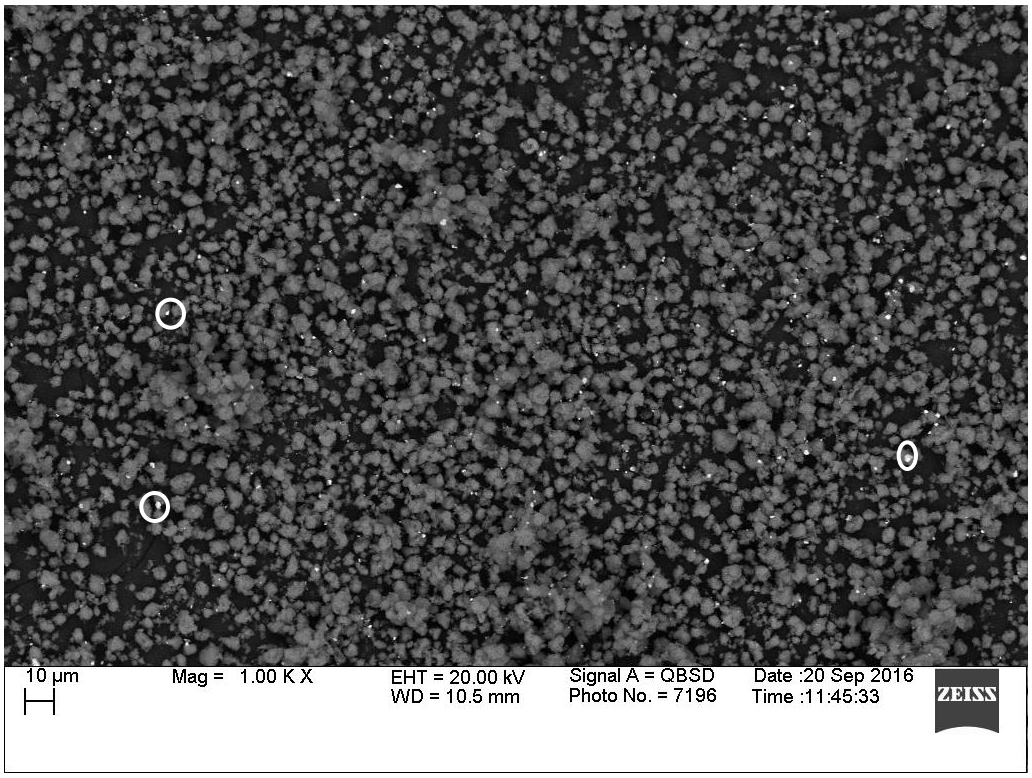

Figure 4.11: SEM image of fresh Ru-ZSM-5 catalyst

Figure 4.12 represents the SEM image of fresh AC catalyst, and Figure 4.13 represents the SEM image of fresh Ru-AC catalyst. A secondary electron detector was used to capture both of the images. Since carbon is a very small molecule, the energy released by backscatter electron cannot be captured on the detector. So, it was not possible to separate Ru and AC phases on SEM. Figure 4.14 and 4.15 represent SEM images of fresh AB and HB. There is no major difference between the SEM images of fresh AC, Ru-AC, AB, and HB. Particle sizes are bigger for AC and Ru-AC. Ball milling in catalyst preparation step reduced the particle size of AB and HB.

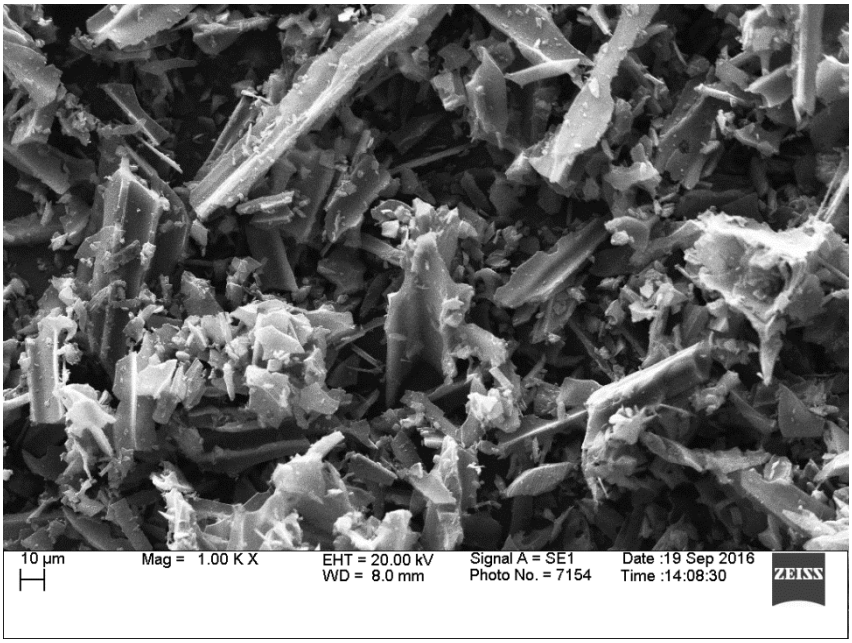

Figure 4.12: SEM image of fresh AC catalyst

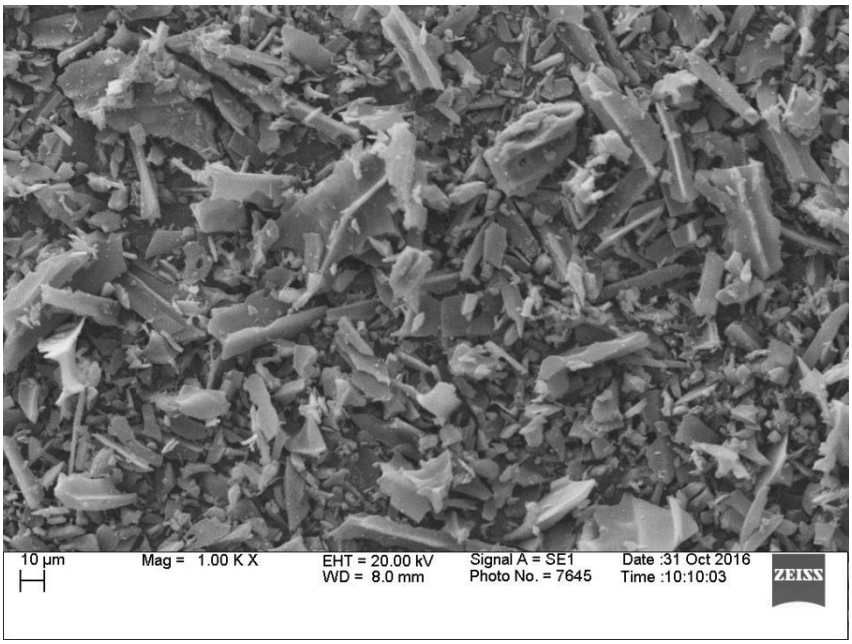

Figure 4.13: SEM image of fresh Ru-AC catalyst

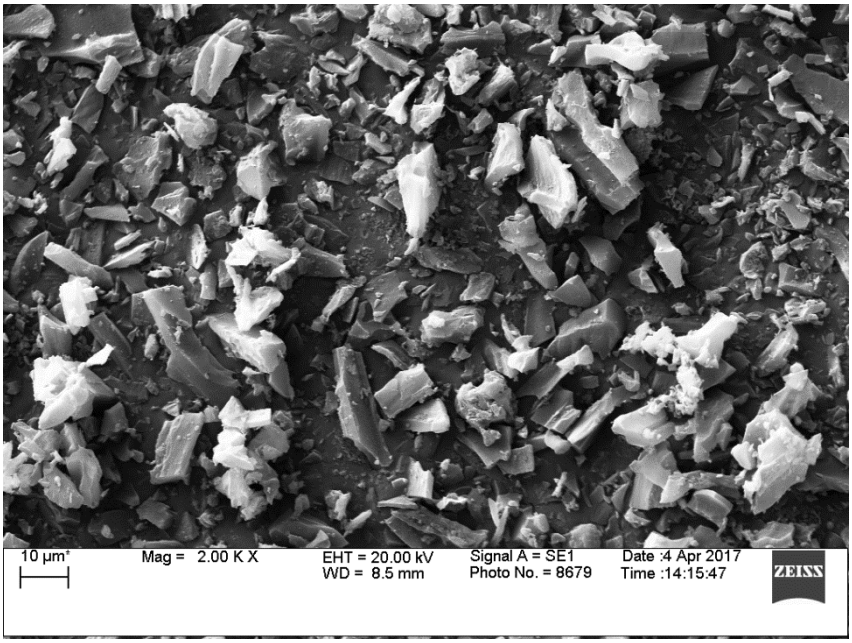

Figure 4.14: SEM image of fresh AB

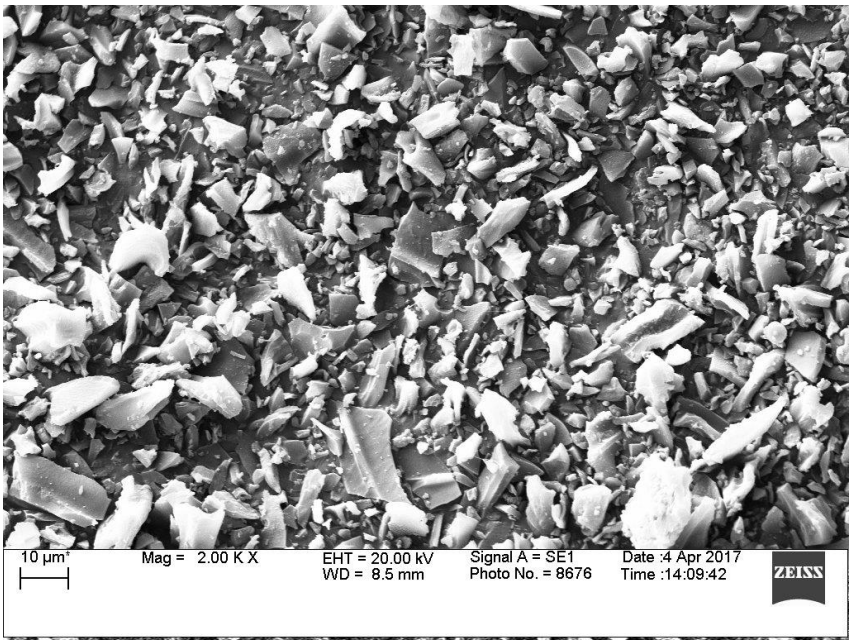

Figure 4.15: SEM image of fresh HB

EDS (Energy dispersion spectroscopy) analysis was performed to estimate the composition of different catalysts. Table 4.4 represents the composition of Ru-ZSM-5, and Table 4.5 represents

the composition of Ru-AC. Results from EDS analysis ensured that around 3% Ru was on both catalysts.

Table 4.4: EDS results for Ru-ZSM-5

Element	Weight%	Atomic%
O	58.09± 0.12	71.50± 0.10
Al	2.09±0.06	2.09±0.06
Si	36.05± 0.14	25.42± 0.12
Ru	3.01±0.02	0.59±0.01

Table 4.5: EDS results for Ru-AC

Element	Weight%	Atomic%
C	86.69±1.16	91.37±0.94
O	10.44±1.14	8.27±0.93
Ru	2.90±0.07	0.36±0.01

Table 4.8 and Table 4.9 represent EDS results for AB and HB. Small amounts of Si was present on AB. Similar results were observed for HB. Small amounts of K and Si were observed on the surface of HB.

Table 4.6: EDS results for ZSM-5

Element	Weight%	Atomic%
O	62.43±0.24	74.42±0.19
Al	2.85±0.15	2.02±0.10
Si	34.72±0.36	23.57±0.28

Table 4.7: EDS result for AC

Element	Weight%	Atomic%
C	91.87±0.52	93.77±0.40
O	8.13±0.52	6.23 ±0.40

Table 4.8: EDS results for AB

Element	Weight%	Atomic%
C	85.56±0.32	88.85±0.27
O	14.12 ±0.38	11.01 ±0.30
Si	0.33 ±0.06	0.15 ±0.03

Table 4.9: EDS results for HB

Element	Weight%	Atomic%
C	91.72±0.23	93.80±0.18
O	7.87±0.20	6.04±0.16
Si	0.43±0.19	0.08±0.02
K	0.24± 0.03	0.08± 0.01

4.2 Reaction Results

After characterization, the six catalysts were used to perform thermocatalytic decomposition of methane. Reactions were performed at two different flow rates of 0.1 WHSV and 0.4 WHSV (Weight hourly space velocity: total mass flow rate of reactants divided by total mass of catalyst in the reactor). All of the reactions were run for 8 h, and 50% N_2, 50% CH_4 were used as feedstock. Figure 4.16 represents the reaction results for different catalysts at 800 ^oC and 0.1 WHSV. Blank run indicates the reaction without any catalyst. Methane gas was flown at 800 ^oC in an empty reactor. Conversion with the blank run was around 2-3%. Normally, methane should not be converted at that temperature without any catalysts [14]. Since the reactor has Ni and Fe as reactor components, those might have caused a small conversion of methane. ZSM-5 gave 21% conversion after 8 h of reaction time. After being doped with Ru, ZSM-5 gave 40% conversion at the same time of reaction. Ru enhanced the catalytic activity of ZSM-5 by 20%. Ru metal particles give electron to zeolite surface sites. So zeolite channels confined with small particles are electron deficient. This electrophilic character enhance the activity of zeolite

supported catalyst [15]. Only AC gave 51% conversion after 8 h of reaction time, whereas Ru-AC gave 73% conversion at the same amount of reaction time. Methane conversion for AB was 69% after 8 h of reaction time. The high surface area and the presence of ash contents on the structure of AB were the reasons for this higher conversion. HB gave 41% conversion after the same time of reaction time. HB has a low surface area compared to Ru-ZSM-5 and ZSM-5. Irregularity, free valences, abnormality, and the presence of ash contents on the structure of HB played an important role to obtain a similar conversion as Ru-ZSM-5 and the higher conversion than ZSM-5.

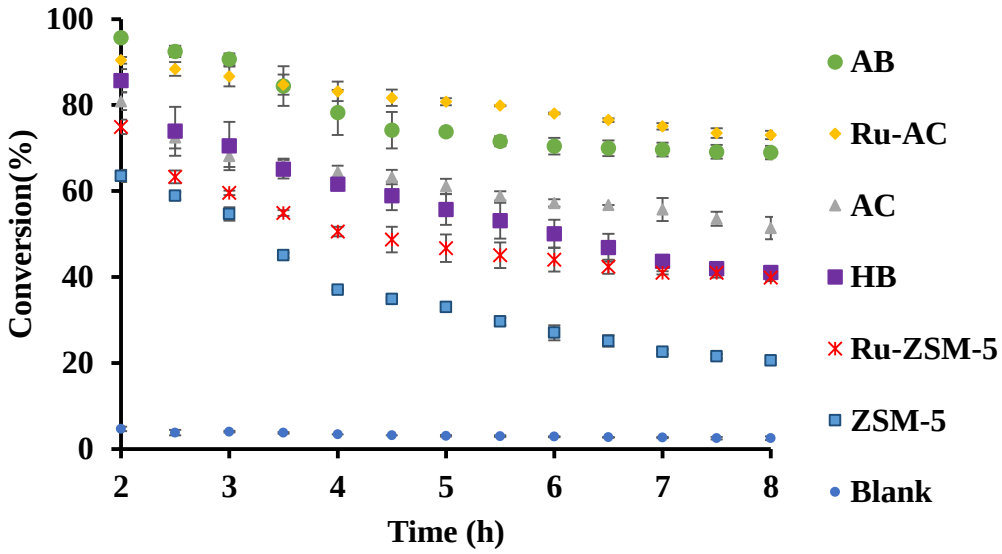

Figure 4.16: Catalytic effect of different catalysts on methane conversion at 800 ^{o}C and 0.1 WHSV

Figure 4.17 represents the total amount of hydrogen produced in the reaction. Hydrogen production graph followed the same sequence as the conversion graph. Initial hydrogen yields were low in every case. According to literature [16], most of the activated carbon has carbon-oxygen groups in structure. FTIR result of fresh AC (Figure 4.5) ensured the presence of different carbon-oxygen group on AC. FTIR spectra of hydrogen reduced AC also has similar pattern. Reduction process did not eliminate all the oxygen group from the structure of catalyst. Product

hydrogen might be consumed by these functional group in first few hours of reaction. Ru-ZSM-5 caused 0.14 mmol/min of hydrogen production, and ZSM-5 caused 0.07 mmol/min of hydrogen production after 8 h of reaction time. Ru-AC produced 0.26 mmol/min of hydrogen whereas AC produced 0.18mmol/min of hydrogen after 8 h of reaction time. AB caused 0.23 mmol/min of hydrogen production after 8 h of the reaction. In the case of HB, it was 0.14 mmol/min same as Ru-ZSM-5 after 8 h of the reaction. Hydrogen yields were above 90% for all of the catalysts at 800^{o}C and 0.1 WHSV.

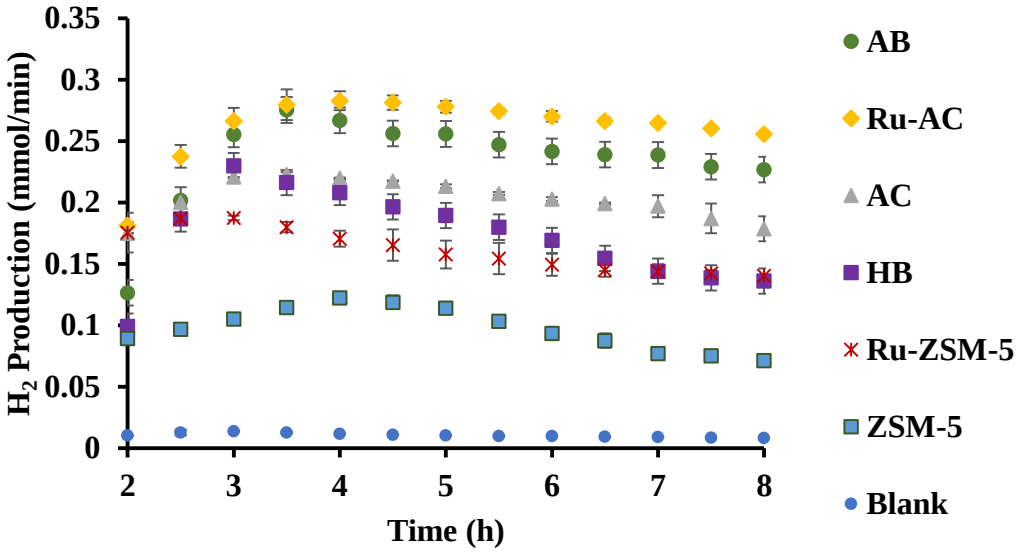

Figure 4.17: Catalytic effect of different catalysts on hydrogen production at 800 ^{o}C and 0.1 WHSV

Thermocatalytic decomposition of methane was performed at 0.4 WHSV and 800 ^{o}C on different catalysts. Figure 4.18 represents reaction results at 0.4 WHSV. ZSM-5 gave 10% conversion whereas Ru-ZSM-5 gave 26% conversion. AC exhibited 35% conversion whereas Ru-AC exhibited 61% conversion. Overall, Ru enhanced the catalytic activity of ZSM-5 and AC. In the case of biomass-derived catalysts, HB caused 29% methane conversion, and AB caused 59% methane conversion. All the conversions were considered after 8 h of the reaction.

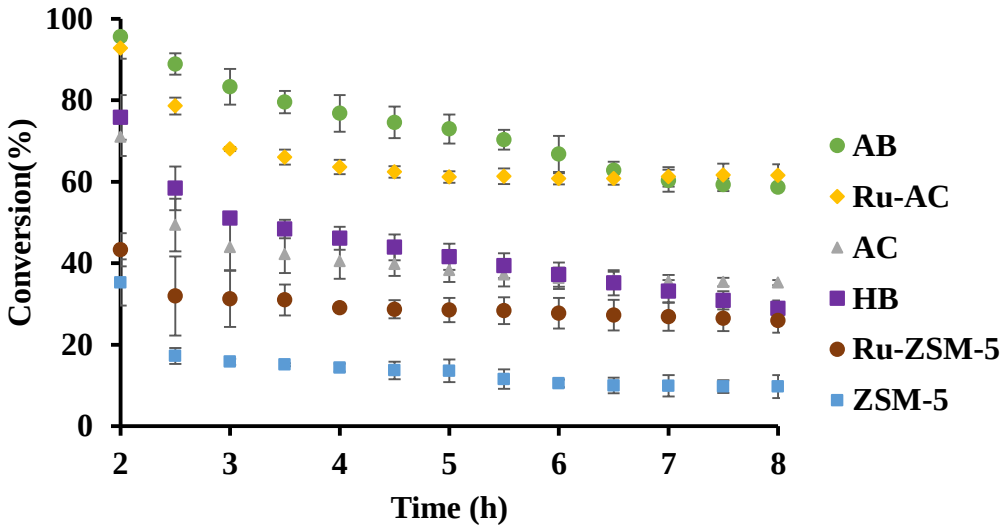

Figure 4.18: Catalytic effect of different catalysts on methane conversion at 800 ^{o}C and 0.4 WHSV

Figure 4.19 represents the total amount of hydrogen production in methane conversion at 800 ^{o}C and 0.4 WHSV. ZSM-5 caused 0.12 mmol/min of hydrogen production after 8 h of the reaction whereas Ru doping increased hydrogen production to 0.34 mmol/min after the same amount of reaction time. AC produced 0.45 mmol/min of hydrogen production, and Ru-AC produced 0.76 mmol/min of hydrogen after 8 h of the reaction. In the case of biochar derived catalysts, AB caused 0.73 mmol/min, and HB caused 0.37 mmol/min of hydrogen production after 8 h of the reaction. Hydrogen yields were around 90% for all of the catalysts.

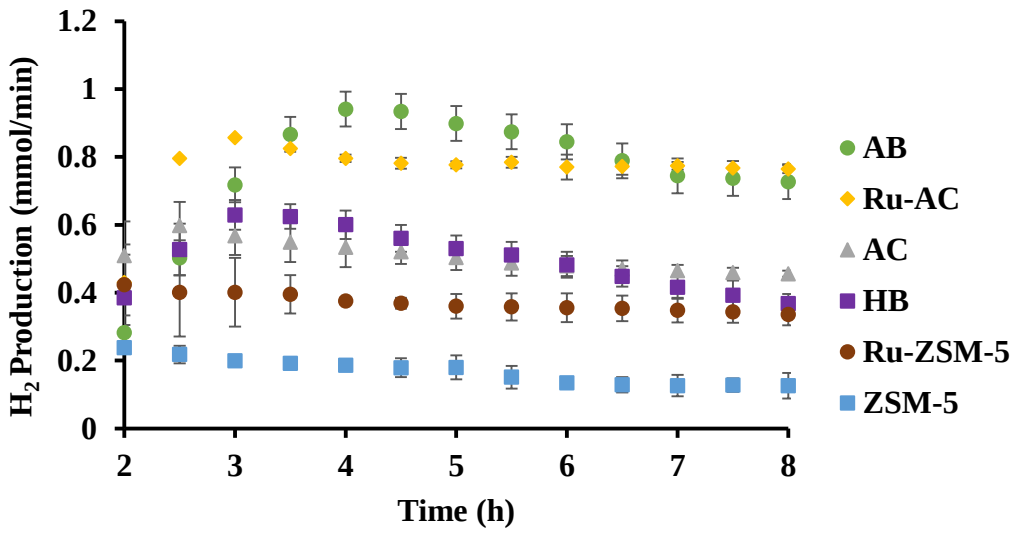

Figure 4.19: Catalytic effect of different catalysts on hydrogen production at 800 ^{o}C and 0.4 WHSV

Among six different catalysts, AB and Ru-AC exhibited the highest conversions after 8 h of reaction time. Therefore, these catalysts were tested to determine long-term catalytic behavior. Methane conversion reaction was run for 60 h. Figure 4.20 represents methane conversion reaction results on AB and Ru-AC for 60 h. Methane conversion was higher for Ru-AC than AB for the first 14 h. For Ru-AC, conversion was decreasing with time and after 60 h, conversion became 21%. For AB, conversion showed a decreasing trend for the first 10 h. Then conversion increased a little bit (from 58 to 60%). After that, the conversion curve was pretty stable and after 60 h, conversion was 51%.

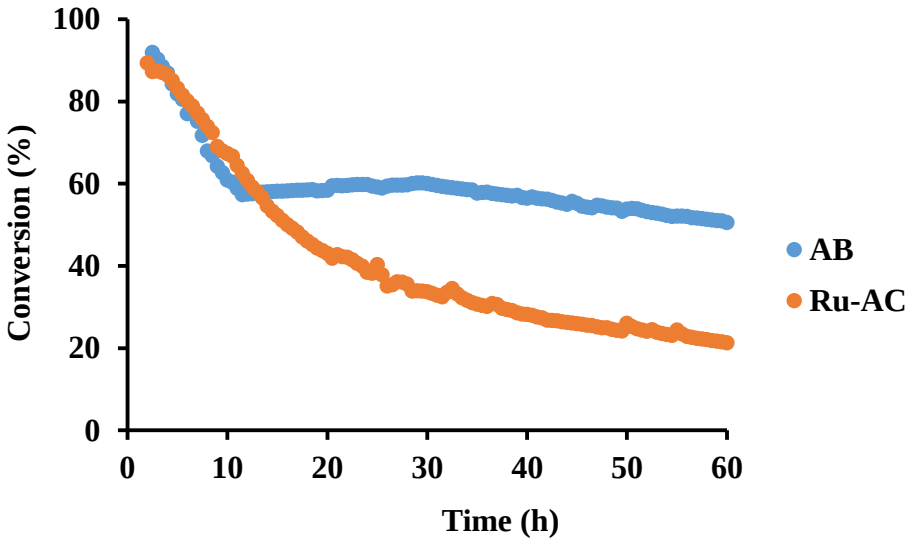

Figure 4.20: Catalytic behavior of Ru-AC and AB at 800 ^{o}C and 0.1 WHSV in 60 h reaction run

Metal-support interaction plays an important role in CNT growth as well as catalyst deactivation. If metal support interaction is weak, then metal particles detach from the support. Detach metal particles localize at the tip of the nanotubes. This type of phenomena causes separation of the metal particles from support and catalyst deactivates with time. For strong metal-support interaction, the metal particle does not separate from support and deactivation rate is slow [17].

Since Ru-AC catalyst was prepared by the wet impregnation method, weak metal–support interaction presented between Ru and AC. Production of nanotube (Figure 4.30) caused separation of Ru particles from AC. With time, Ru particles were covered by carbon. All these phenomena were responsible for deactivation in the long run. Ash contents are part of biochar structure. In case of AB, strong metal-support interaction presented between ash content and carbon. CNTs growth (Figure 4.31 to Figure 4.33) could not separate the metal particle from carbon support.

As a catalyst, Ru always exhibits good conversion but Ru-AC has a comparatively low surface area (693 m^2/g). AB has a large surface area (3256 m^2/g). This large surface area accommodated product carbon for the long reaction time. AB has 82% microporous structure. According to Krzyzynski et al. [18] higher surface area and higher pore volume give higher resistant to catalyst deactivation. Ashok et al. [19] and Dhunker et al. [20] concluded that methane decomposition mainly occur at micropores. According to Kim et al. [21] methane decomposition rate is higher for smaller particles and methane decomposition occur on outer shell of catalyst particles. For larger particles, pore mouth blocked by carbon deposition while inner area remain intact [21]. Shear stress develops on the catalyst in case of micropore. Shear stress directly depends on superficial velocity. This shear stress causes self-cleaning phenomena on the catalyst and increases conversion in the middle of reaction. The superficial velocity is high in case of AB. Shear stress cleaned the active pore of AB. So, the conversion was slightly increased in the middle of reaction (10 h). BET analysis results for spent catalysts also support this phenomena. After 8 h of reaction, surface area was reduced to 1893 m^2/g. Surface area reduction by 8 h of reaction was 170 m^2/g per h whereas surface area reduction by rest of 52 h of reaction was 22 m^2/g per h. After 60 h of reaction, AB still had higher surface area (746 m^2/g) than fresh Ru-AC (693 m^2/g). Moreover, product CNTs also has catalysis ability in methane conversion. Several researcher's used CNTs as catalyst for methane conversion [22-25]. Because of high superficial velocity, product CNTs were separated from main catalyst AB. Product carbon create new active sites for TCD by growing outside of catalyst pore [16]. Product CNTs took part in auto catalysis [26-27]. Combining all the phenomena, AB showed a stable conversion pattern in the long reaction run. Ru-AC has 50% micropore and 50% mesopore in its structure whereas mainly micropores were contributed for methane conversion [18-19]. Sometimes, mouth of larger pores block with product carbon without

using the inside surface area [21]. Superficial velocity was comparatively low for this catalyst. Though the small increase in conversion in several times were observed for Ru-AC. Since product carbon separated Ru from AC and covered it, effect of Ru addition diminished in the long run. Because of lower conversion, production of CNTs were also low and those CNTs were attached with catalyst pores (blocked active pore of catalyst). Therefore, auto catalysis reaction rate was comparatively low for Ru-AC.

Table 4.10: BET analysis results for fresh and spent AB catalyst

Name	Surface Area (BET) (m^2/g)	Pore Volume (cm^3/g) (DFT)		
		Micropore	Mesopore	Total pore
Fresh AB	3256	1.30	0.29	1.59
After 8 h	1893	0.74	0.22	0.96
After 60 h	746	0.29	0.10	0.39

4.3 Carbon Produced in Reaction

Carbon produced in the reactions were analyzed by SEM and TEM. Figure 4.21 represents the SEM image of the spent Ru-ZSM-5 catalyst after reaction at 800 ^oC. A big tube structure with lots of small tube structures were observed in this SEM image. Figure 4.22 represents the SEM image of carbon produced in the same reaction at higher magnification. Lots of nano-carbon structures were observed. Figure 4.23 represents the TEM image of carbon produced in the same reaction. This TEM image confirmed that carbon nano-tubes (CNTs) were produced by Ru-ZSM-5 catalyst. For the TEM image, produced carbon was separated from the catalyst and crushed to fine powder.

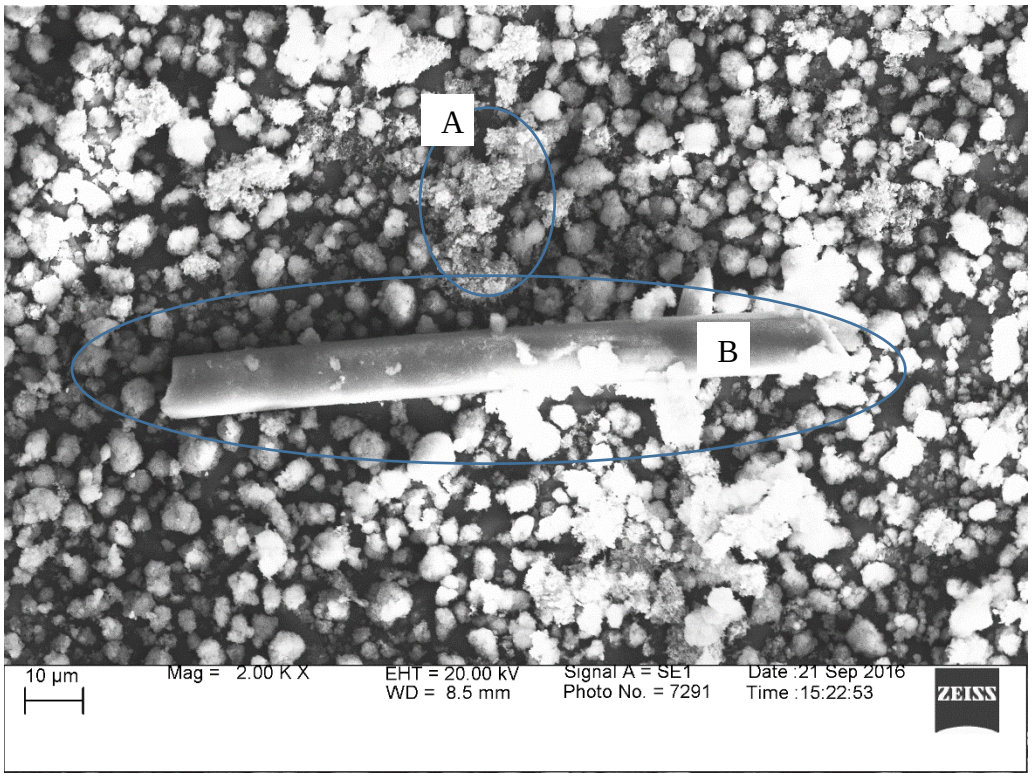

Figure 4.21: SEM image of spent Ru-ZSM-5 catalyst after reaction at 800 ^{o}C: A) Small tube structures, B) Big tube structure

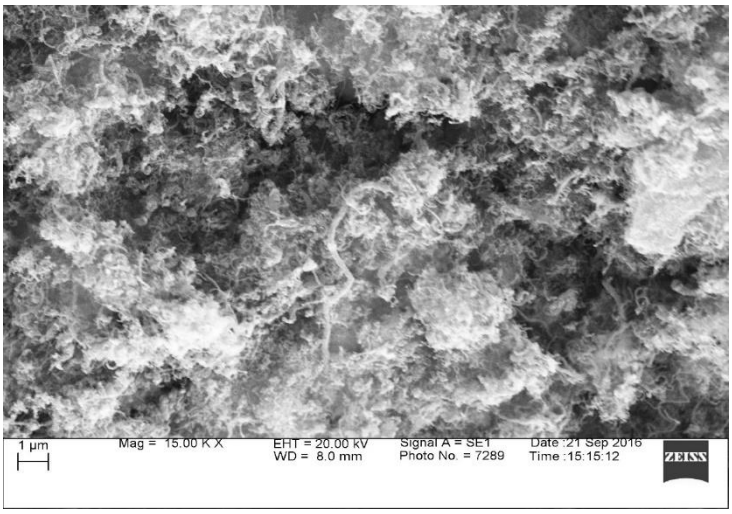

Figure 4.22: SEM image of spent Ru-ZSM-5 catalyst after reaction at 800 ^{o}C in higher magnification

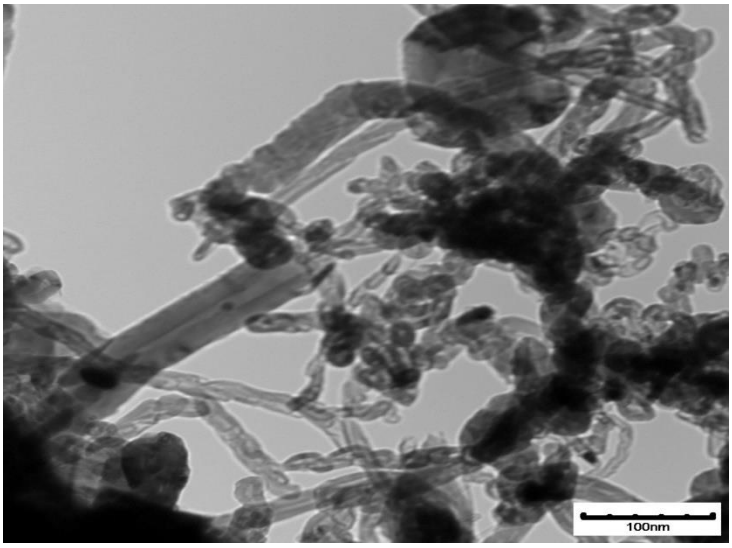

Figure 4.23: TEM image of carbon produced by Ru-ZSM-5 at 800 ^{o}C

The similar type result was also observed for ZSM-5 catalyst. Figure 4.24 and Figure 4.25 represents the SEM image of the spent ZSM-5 catalyst after reaction at 800 ^{o}C in low and high magnifications. Figure 4.26 represents the TEM image of carbon produced by ZSM-5 at 800 ^{o}C. After analyzing all these figures, it was confirmed that CNTs were produced with ZSM-5. In zeolite, metal ions are impregnated only in ion exchange positions of case systems and are accessible only for the small molecule, which has the diameter less than pore diameter and the only product with the small diameter less than pore diameter can exit pore channel of the catalyst. So, CNTs growth can be possible only on the outer surface metal particle of zeolites. That's why zeolite gives less conversion as well as less CNTs. Because catalyst surface is easily blocked with CNTs and become non-accessible within few hours of reactions [28-29].

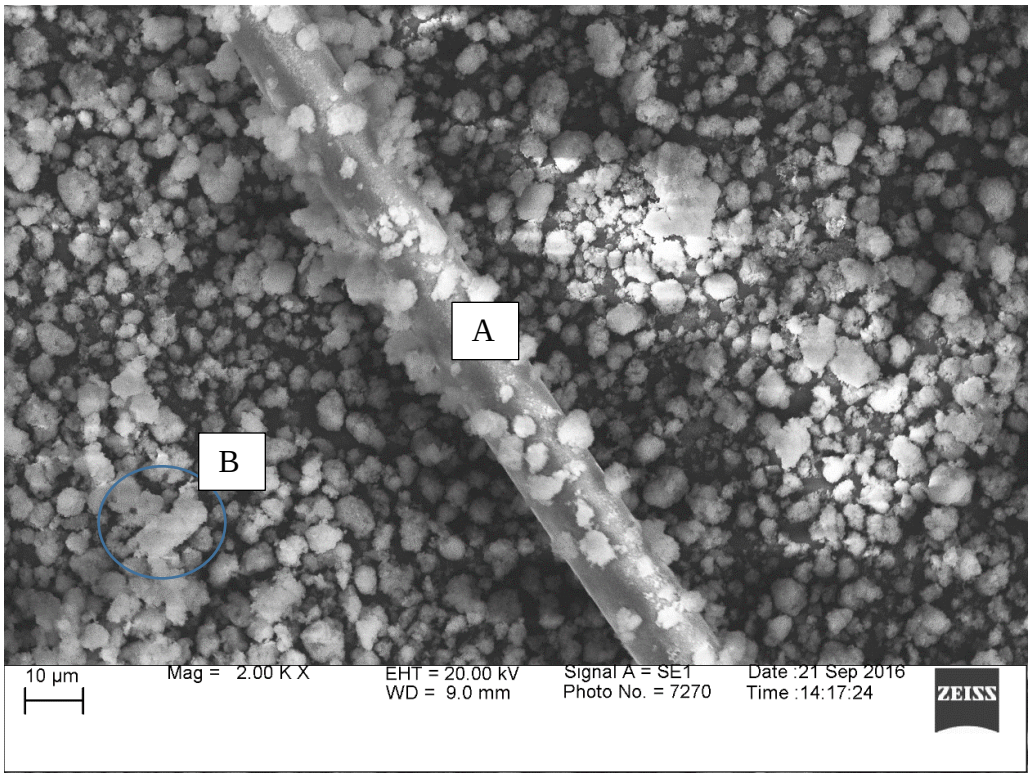

Figure 4.24: SEM image of spent ZSM-5 catalyst after reaction at 800 ^{o}C in lower magnification:

A) Big carbon structure, B) Small tube structures

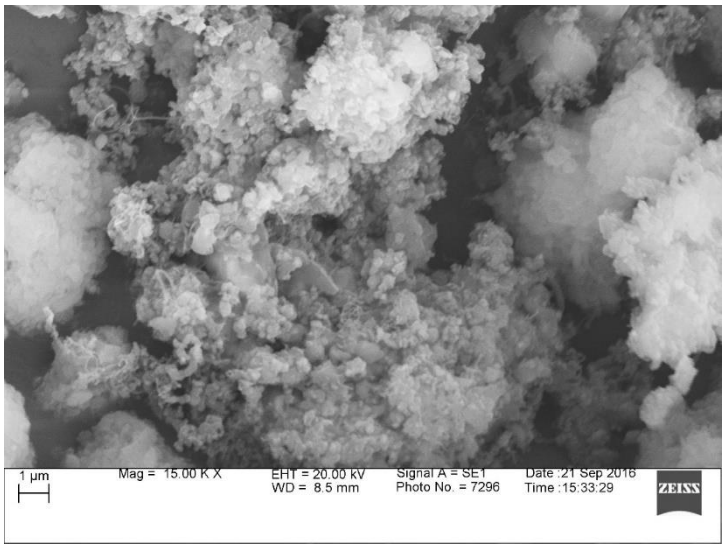

Figure 4.25: SEM image of spent ZSM-5 after reaction at 800 ^{o}C at higher magnification

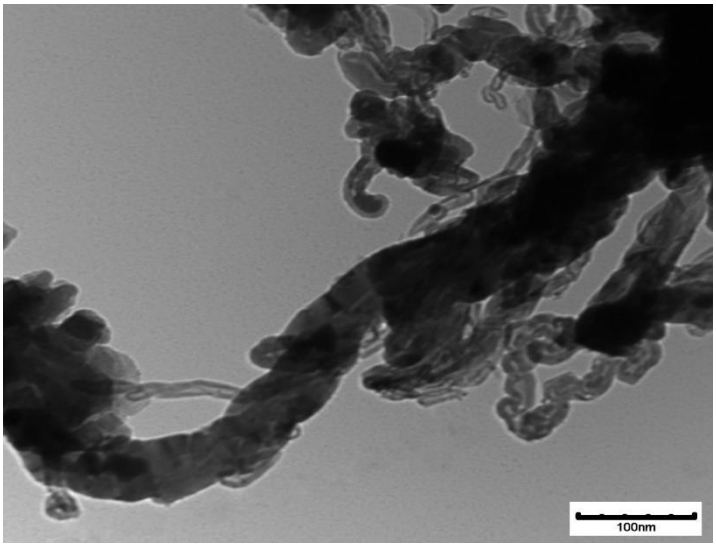

Figure 4.26: TEM image of carbon produced ZSM-5 at 800 ^{o}C

Figure 4.27 represents the SEM image of the spent AC and Figure 4.28 represents the SEM image of the spent Ru-AC after reaction at 800 ^{o}C. Figure 4.29 and Figure 4.30 represents the TEM image of the spent AC and Ru-AC after reaction at 800 ^{o}C. After analyzing all these images, it can be concluded that carbon produced by AC had a turbostratic structure whereas 3% Ru doping on AC caused CNT production. For TEM analysis, spent catalysts were crashed to fine powder.

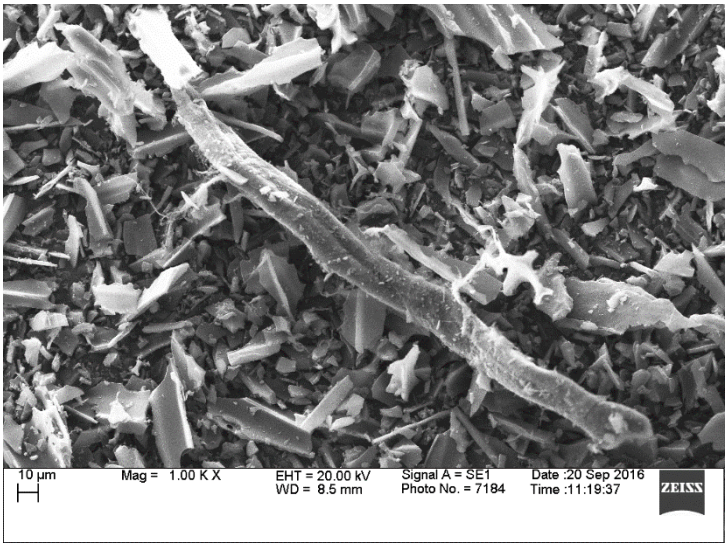

Figure 4.27: SEM image of spent AC after reaction at 800 ^{o}C

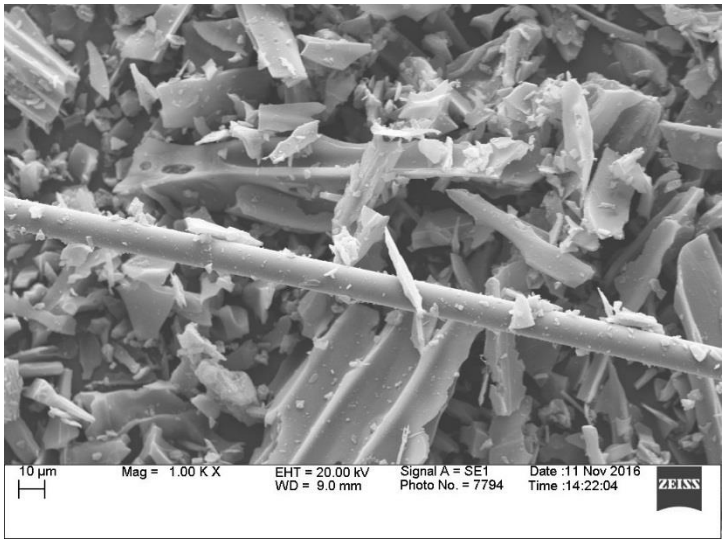

Figure 4.28: SEM image of spent Ru-AC after reaction at 800 ^{o}C

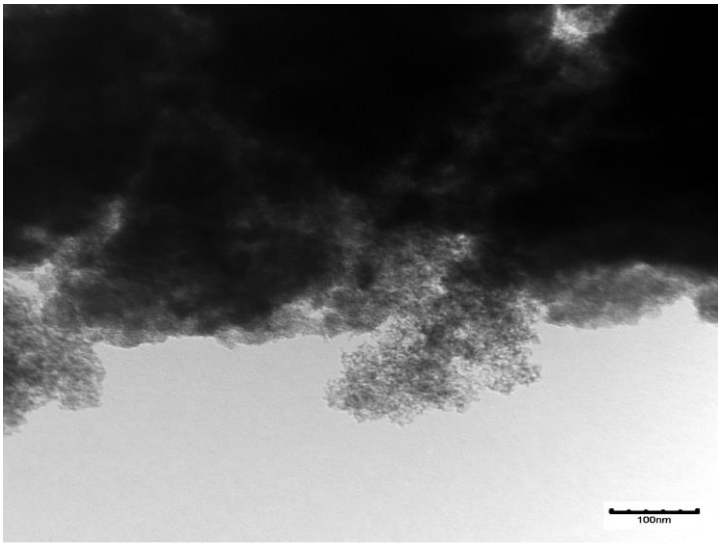

Figure 4.29: TEM image of spent AC after reaction at 800 ^{o}C

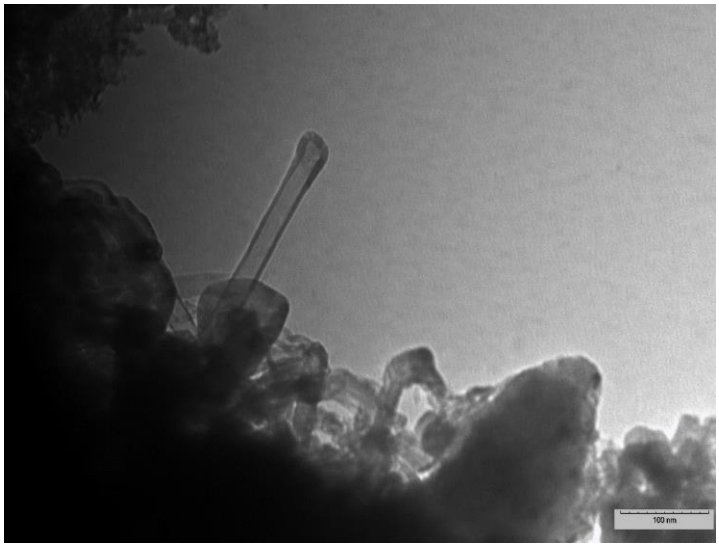

Figure 4.30: TEM image of spent Ru-AC after reaction at 800 ^{o}C

Figure 4.31 and 4.32 represent the SEM image of the spent AB after reaction at 800 ^{o}C in lower and higher magnifications. Figure 4.33 represents the TEM image of the spent AB after reaction at 800 ^{o}C. After analyzing these three images, it can be concluded that CNTs were produced by AB. The similar SEM image was observed for HB (Figure 4.34). But it was not

possible to observe any CNTs in the TEM image. Since similar SEM images were captured for Ru-ZSM-5, ZSM-5, and Ru-AC, it can be concluded that CNTs were produced by HB.

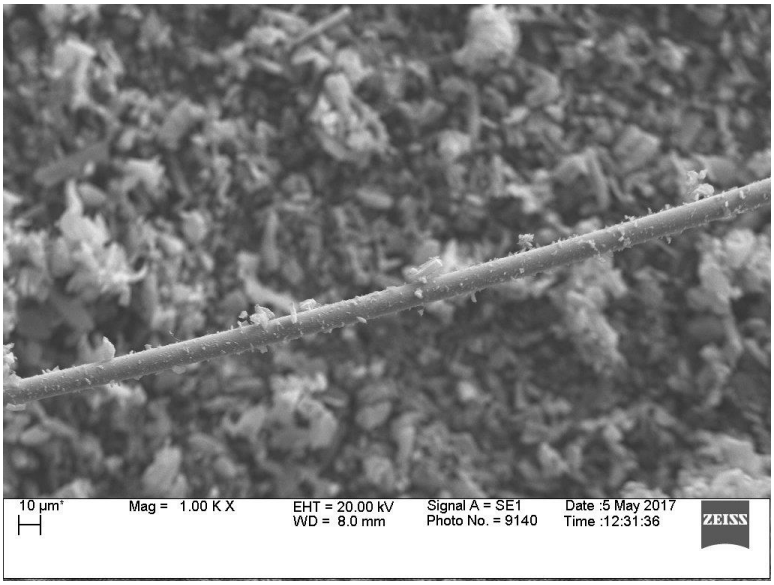

Figure 4.31: SEM image of spent AB after reaction at 800 ^{o}C in lower magnification

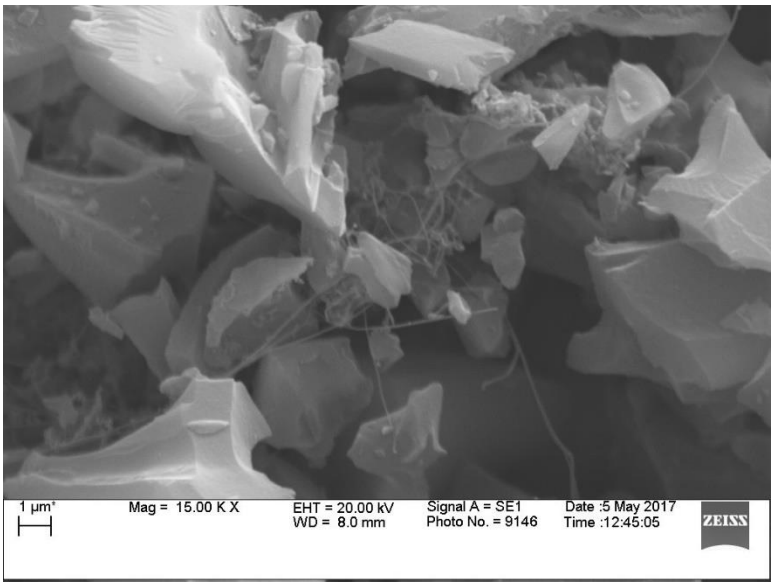

Figure 4.32: SEM image of spent AB after reaction at 800 ^{o}C in higher magnification

Figure 4.33: TEM image of spent AB after reaction at 800 ^{o}C

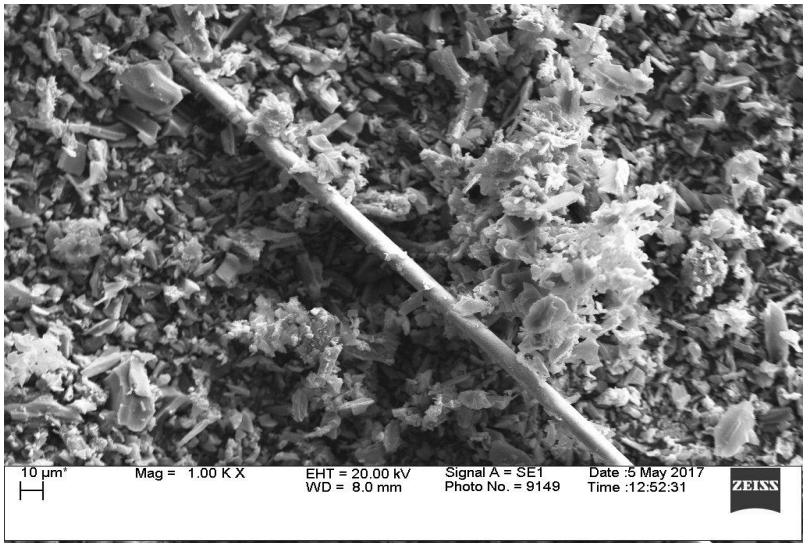

Figure 4.34: SEM image of spent HB after reaction at 800 ^{o}C

4.4 Temperature Effect on Different Catalysts

Thermocatalytic decomposition of methane (TCD) was performed on the best four catalysts (AC, Ru-AC, AB, and HB) at four different temperatures (800, 700, 600, and 500 ^{o}C) to determine how the temperature effect on these catalysts. Figure 4.35 represents reaction results at

700 ºC. There were drastic decreases in the conversion from 800 ºC to 700 ºC. Ru-AC exhibited the highest conversion (31%) among four catalysts. Though AB and Ru-AC exhibited almost the same conversion at 800 ºC, AB exhibited only 21% conversion at 700 ºC. AC and HB exhibited almost the same conversion 10% and 11.5%, respectively. All of the conversions were considered after 8 h of the reaction time.

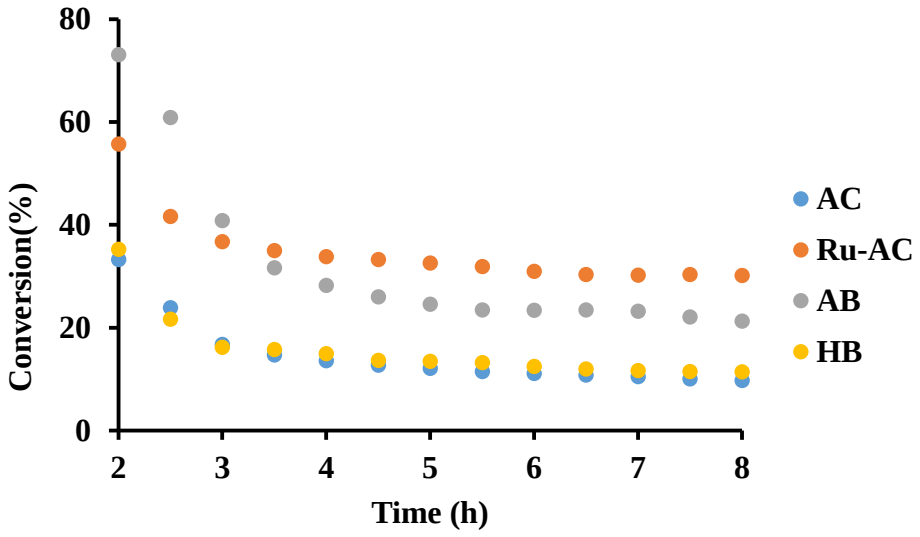

Figure 4.35: TCD reaction results of methane conversion at 700 ºC on different catalysts

Figure 4.36 represents the reaction results of methane conversion at 600 ºC on different catalysts. At 600 ºC, all of the catalysts exhibited similar conversions. There was no effect of surface area or Ru doping at this temperature. AC and HB conversions did not change from 700 ºC to 600 ºC. In both temperature conversions were around 10%. Figure 4.37 represents reaction results of methane conversion at 500 ºC on different catalysts. After 4 h, methane conversion for AC and HB became zero. For Ru-AC and AB, methane conversion decreased to 2-3% after 8 h of reaction time. Since all the catalysts were carbonaceous catalysts, they exhibited very poor activity at low temperatures.

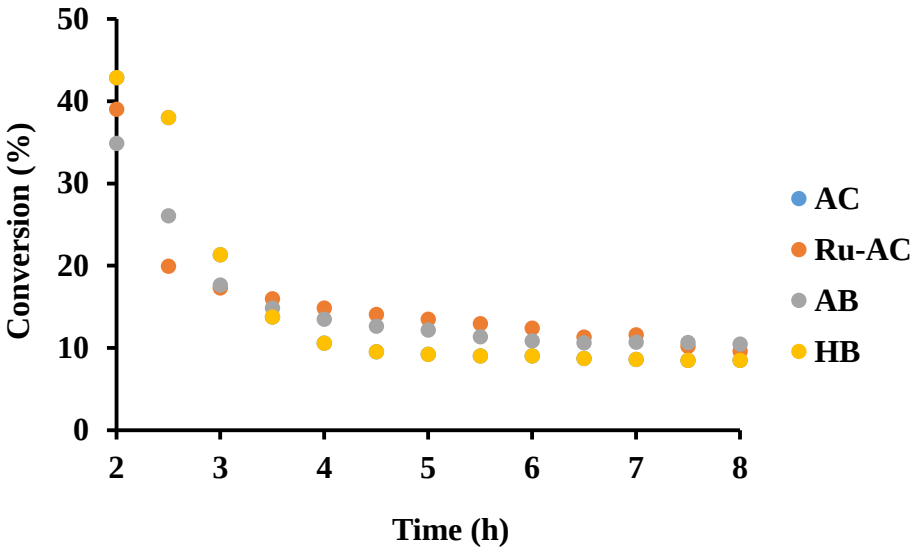

Figure 4.36: TCD reaction results of methane conversion at 600 ºC on different catalysts

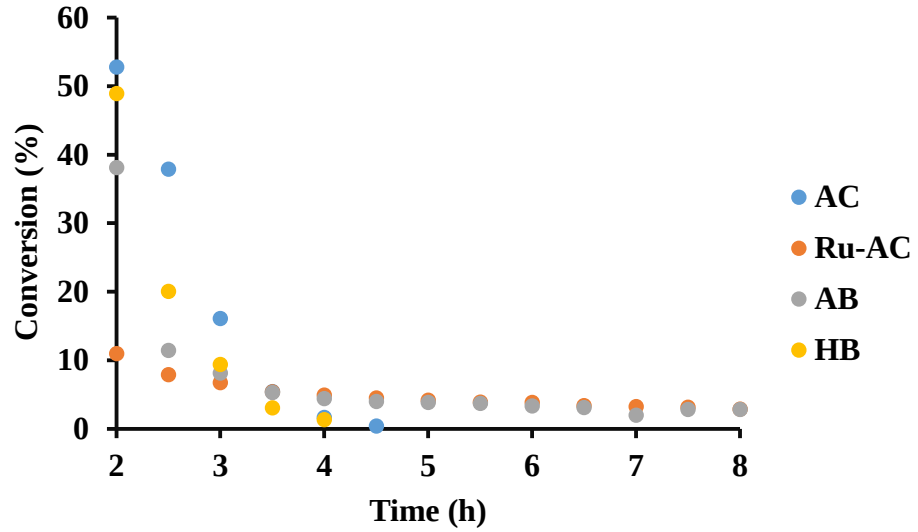

Figure 4.37: TCD reaction results of methane conversion at 500 ºC on different catalysts

4.5 References

1. S. Kaliaguine, A. Adnot, and G. Lemay, "A model for the quantitative analysis of ESCA intensity ratios for supported catalysts with partial surface segregation," *Journal of Physical Chemistry*, vol. *91*(11), 2886-2890, 1987.
2. S. Nahreen, S. Praserthdam, S. Perez Beltran, P. B. Balbuena, S. Adhikari, and R. B. Gupta, "Catalytic upgrading of methane to higher hydrocarbon in a nonoxidative chemical conversion," *Energy & Fuels*, vol. 30(4), 2584-2593, 2016.
3. D. P. Serrano, J. A. Botas, J. L. G. Fierro, R. Guil-López, P. Pizarro, and G. Gómez, "Hydrogen production by methane decomposition: origin of the catalytic activity of carbon materials," *Fuel*, vol. 89(6), 1241-1248, 2010.
4. L. Jin, H. Si, J. Zhang, P. Lin, Z. Hu, B. Qiu, and H. Hu, "Preparation of activated carbon supported Fe–Al_2O_3 catalyst and its application for hydrogen production by catalytic methane decomposition," *International Journal of Hydrogen Energy*, vol. 38(25), 10373-10380, 2013.
5. P. K. Vanama, A. Kumar, S. R. Ginjupalli, and V. C. Komandur, "Vapor-phase hydrogenolysis of glycerol over nanostructured Ru/MCM-41 catalysts," *Catalysis Today*, vol. 250, 226-238, 2015.
6. S. Link, S. Arvelakis, M. Hupa, P. Yrjas, I. Külaots, and A. Paist, "Reactivity of the biomass chars originating from reed, Douglas fir, and pine," *Energy & Fuels*, vol. 24(12), 6533-6539, 2010.
7. S. R. Teixeira, A. E. de Souza, A. F. V. Peña, R. G. de Lima, and Á. G. Miguel, "Use of charcoal and partially pirolysed biomaterial in fly ash to produce briquettes: sugarcane bagasse," *In Alternative Fuel.* InTech, 2011.
8. A. S. Alzaydien, "Physical, chemical and adsorptive characteristics of local oak sawdust based activated carbons," *Asian Journal of Scientific Research*, vol. 9(2), 45-56, 2016.
9. 9. S. B. Daffalla, H. Mukhtar, and M. S. Shaharun, "Characterization of Adsorbent Developed from Rice Husk," *Effect of Surface Functional Group on Phenol Adsorption Journal of Applied Sciences*, 50-58, 2010.
10. 10. N. Colthup, "Introduction to infrared and Raman spectroscopy," Elsevier, 2012.
11. X. Zhao, W. Ouyang, F. Hao, C. Lin, F. Wang, S. Han, and X. Geng, "Properties comparison of biochars from corn straw with different pretreatment and sorption behaviour of atrazine," *Bioresource Technology*, vol. 147, 338-344, 2013.
12. G. G. Choi, S. J. Oh, S. J. Lee, and J. S. Kim, "Production of bio-based phenolic resin and activated carbon from bio-oil and biochar derived from fast pyrolysis of palm kernel shells," *Bioresource Technology*, vol. 178, 99-107, 2015.
13. K. Sing, "The use of nitrogen adsorption for the characterisation of porous materials," *Colloids and Surfaces A: Physicochemical and Engineering Aspects*, vol. 187, 3-9, 2001.
14. U. P. M. Ashik, W. W. Daud, and H. F. Abbas, "Production of greenhouse gas free hydrogen by thermocatalytic decomposition of methane–a review," *Renewable and Sustainable Energy Reviews*, vol. 44, 221-256, 2015.
15. P. Somasundaran, "Encyclopedia of surface and colloid science," vol. 2, CRC press, 2006.
16. H. F. Abbas and W. W. Daud, "Hydrogen production by methane decomposition: a review," *International Journal of Hydrogen Energy*, vol. 35(3), 1160-1190, 2010

17. E. Lamouroux, P. Serp, and P. Kalck, “Catalytic routes towards single wall carbon nanotubes,” *Catalysis Reviews*, vol. *49*(3), 341-405, 2007.
18. S. Krzyżyński, and M. Kozłowski, “Activated carbons as catalysts for hydrogen production via methane decomposition,” *International Journal of Hydrogen Energy*, vol. 33(21), 6172-6177, 2008.
19. J. Ashok, M. Subrahmanyam, and A. Venugopal, “Development of methane decomposition catalysts for COx free hydrogen,” *Catalysis Surveys from Asia*, vol. 12(3), 229, 2008.
20. A. M. Dunker, and J. P. Ortmann, “Kinetic modeling of hydrogen production by thermal decomposition of methane,” *International Journal of Hydrogen Energy*, vol. 31(14), 1989-1998, 2006.
21. M. H. Kim, E. K. Lee, J. H. Jun, G. Y. Han, S. J. Kong, B. K. Lee, and K. J. Yoon, “Hydrogen production by catalytic decomposition of methane over activated carbons: deactivation study,” *Korean Journal of Chemical Engineering*, vol. 20(5), 835-839, 2003.
22. N. Muradov, F. Smith, and T. Ali, “Catalytic activity of carbons for methane decomposition reaction,” *Catalysis Today*, vol. 102, 225-233, 2005.
23. R. Guil-Lopez, J. A. Botas, J. L. G. Fierro, and D. P. Serrano, “Comparison of metal and carbon catalysts for hydrogen production by methane decomposition,” *Applied Catalysis A: General*, vol. 396(1), 40-51, 2011.
24. H. F. Abbas and W. W. Daud, “Hydrogen production by methane decomposition: a review,” *International Journal of Hydrogen Energy*, vol. 35(3), 1160-1190, 2010.
25. U. P. M. Ashik, W. W. Daud, and H. F. Abbas, “Production of greenhouse gas free hydrogen by thermocatalytic decomposition of methane–a review.” *Renewable and Sustainable Energy Reviews*, vol. 44, 221-256, 2015.
26. J. Zhang, L. Jin, Y. Li, and H. Hu, “Ni doped carbons for hydrogen production by catalytic methane decomposition,” *International Journal of Hydrogen Energy*, vol. 38(10), 3937-3947, 2013.
27. J. Zhang, L. Jin, Y. Li, H. Si, B. Qiu, and H. Hu, “Hierarchical porous carbon catalyst for simultaneous preparation of hydrogen and fibrous carbon by catalytic methane decomposition,” *International Journal of Hydrogen Energy*, vol. 38(21), 8732-8740, 2013.
28. K. Hernadi, A. Fonseca, J. B. Nagy, D. Bernaerts, and A. A. Lucas, “Fe-catalyzed carbon nanotube formation,” *Carbon*, vol. 34(10), 1249-1257, 1996.
29. K. Hernadi, A. Fonseca, J. B. Nagy, D. Bemaerts, A. Fudala, and A. A. Lucas, “Catalytic synthesis of carbon nanotubes using zeolite support,” *Zeolites*, vol. 17(5-6), 416-423, 1996.

CHAPTER FIVE: CONCLUSIONS AND FUTURE WORK

5.1 Conclusions

Thermocatalytic decomposition (TCD) of methane is the most economic and beneficial method for pure hydrogen production. The main objective of this study was to use the biomass-derived catalyst to thermocatalytic decomposition of methane. Six different catalysts were selected for thermocatalytic decomposition of methane in this study. Among these six catalysts, two catalysts (AB and HB) were prepared from Douglas fir biochar. Thermocatalytic decomposition of methane was investigated in a fixed bed reactor system. Two different feed flow rates (0.1 and 0.4 WHSV) were used at 800 ^{o}C to study the catalytic behaviors of six catalysts. In both flow rates, 3 wt% Ru doping on ZSM-5 and AC enhanced the catalytic activity of the catalysts, and Ru-AC exhibited the highest conversion after 8 h of reaction time among six catalysts. But Ru-AC catalyst deactivated continuously for 60 h reaction run whereas AB exhibited comparatively stable conversion up-to 60 h. The conversion was 21% for Ru-AC and 51% for AB after 60 h of reaction time at 800 ^{o}C. AB (activated biochar) has a huge surface area and high microporous structure. High microporous structure shows high resistance against deactivation. Moreover, it has different alkali and alkaline metal as ash contents (activation (in the lab) could not eradicate those metal) in its structure which cause CNTs production as by-product. HB (heat-treated biochar) has a lower surface area than Ru-ZSM-5 and ZSM-5. Irregularity, free valences, abnormality, and the presence of ash contents on the structure of HB played an important role to obtain a similar conversion as Ru-ZSM-5. Carbon nanotube produced with all the catalysts except AC. AC carbon has an amorphous structure which is the responsible for turbostratic carbon production. 3% Ru doping on

AC caused CNT production. Since biomass has alkali and alkaline metal oxides as ash content in its structure, use of biomass-derived catalysts eliminate the necessity of artificial expensive metal doping on carbon materials. Several researches were conducted on commercial activated carbon and coal char derived activated carbon. However, no researches were conducted on Douglas fir biomass derived activated carbon. This research's results showed that biomass derived activated carbon has a great potential to be used as a catalyst.

5.2 Future Work

Thermocatalytic decomposition of methane is still at research level. Catalyst deactivation is a major problem in this method. This research on the TCD of methane tried to use biomass-derived catalysts to maximize conversion. The information gained in this research can be used for future studies on the TCD of methane. The following topics can be used for future studies:

- Carbon produced in reactions were analyzed at 100 nm magnification by TEM. In several studies [1-5], researchers used 50 nm- 5nm magnifications for TEM analysis. At that high of magnification, metal particles were observed at the tip of CNTs. This phenomenon indicated that CNT growth started from metal particles, and this growth separated metal particles from the support and caused deactivation of catalysts. TEM analysis can be performed at a higher magnification to understand the reason behind catalyst deactivation.

- The reactor systems used in this thesis has a few limitations. The reactor's temperature could not be raised above 800 ^{o}C. Although carbon catalysts should work well above 700 ^{o}C, typically 850 ^{o}C and above have been used as reaction temperature for carbon catalysts [6]. The TCD of methane can be performed at higher temperatures such as 850 ^{o}C or above.

- The reactor system used in this thesis has another disadvantage. The product stream was cooled down by a heat-exchanger. But this heat can be used to pre-heat feed gas. That will make reactor system more energy efficient than the existing system [6].
- A fixed bed reactor system was used in this thesis. This type of reactor system is not industry friendly. According to Muradov et al. [7,8], a fluidized bed reactor is the most suitable reactor system for the TCD reaction, as in a fluidized bed reactor, it is easy to change catalysts in a continuous process. Therefore, a fluidized bed reactor system can be used to carry out the TCD of methane.
- From this thesis, it can be concluded that biomass-derived catalysts showed excellent conversions in the TCD of methane. Only Douglas fir biomass-derived catalysts were used in this study. Other available biomasses, like canola meal, rice husk, switchgrass can be used to perform the TCD reaction at higher temperatures.

5.3 References

1. S. Link, S. Arvelakis, M. Hupa, P. Yrjas, I. Külaots, and A. Paist, "Reactivity of the biomass chars originating from reed, Douglas fir, and pine," *Energy & Fuels*, vol. 24(12), 6533-6539, 2010.
2. J. Li and K. J. Smith, "Methane decomposition and catalyst regeneration in a cyclic mode over supported Co and Ni catalysts," *Applied Catalysis A: General*, vol. 349(1), 116-124, 2008.
3. D. Li, J. Chen, and Y. Li, "Evidence of composition deviation of metal particles of a Ni–Cu/Al 2 O 3 catalyst during methane decomposition to CO x-free hydrogen," *International Journal of Hydrogen Energy*, vol. 34(1), 299-307, 2009.
4. L. B. Avdeeva, T. V. Reshetenko, Z. R. Ismagilov, and V. A. Likholobov, "Iron-containing catalysts of methane decomposition: accumulation of filamentous carbon," *Applied Catalysis A: General*, 228(1), vol. 53-63, 2002.
5. S. Takenaka, Y. Shigeta, E. Tanabe, and K. Otsuka, "Methane decomposition into hydrogen and carbon nanofibers over supported Pd–Ni catalysts," *Journal of Catalysis*, vol. 220(2), 468-477, 2003.
6. U. P. M. Ashik, W. W. Daud, and H. F. Abbas, "Production of greenhouse gas free hydrogen by thermocatalytic decomposition of methane–a review," *Renewable and Sustainable Energy Reviews*, vol. 44, 221-256, 2015.
7. N. Muradov, "Thermocatalytic CO_2-free production of hydrogen from hydrocarbon fuels," *In Proceedings of the 2000 Hydrogen Program Review*, NREL/CP-570-28890, May, 2000.
8. N. Muradov, "Thermocatalytic CO2-free production of hydrogen from hydrocarbon fuels," *In Proceedings of the 2000 Hydrogen Program Review*, NREL/CP-570-28890, May, 2000.

APPENDIX-A: HYDROGEN YIELDS GRAPH

Yield of hydrogen was calculated by following equation,

$$\% \text{ Yield} = \frac{\text{Actual Yield}}{\text{Theoretical Yield}} \times 100\%$$

where, Actual Yield = Total moles of hydrogen production

And, Theoretical Yield = Total moles of methane molecule reacted × 2

Theoretically, 2 moles of hydrogen should be produced with every methane molecules conversion. For 800 ^{o}C, hydrogen yields were above 90% at 0.1 and 0.4 WHSV. But lower yields were observed at lower temperatures. Hydrogen yields graph for different temperatures are given below,

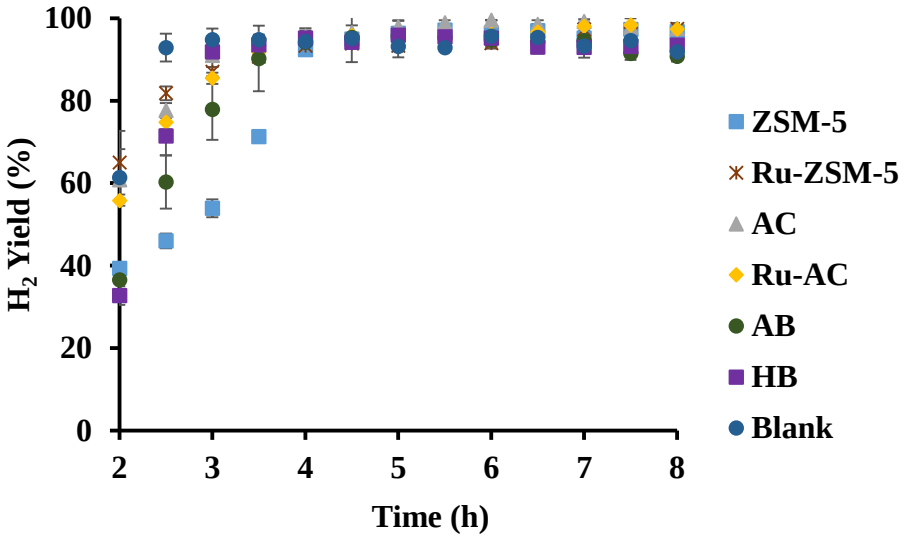

Figure A.A.1: Hydrogen yield graph with time at 800 ^{o}C and 0.1 WHSV

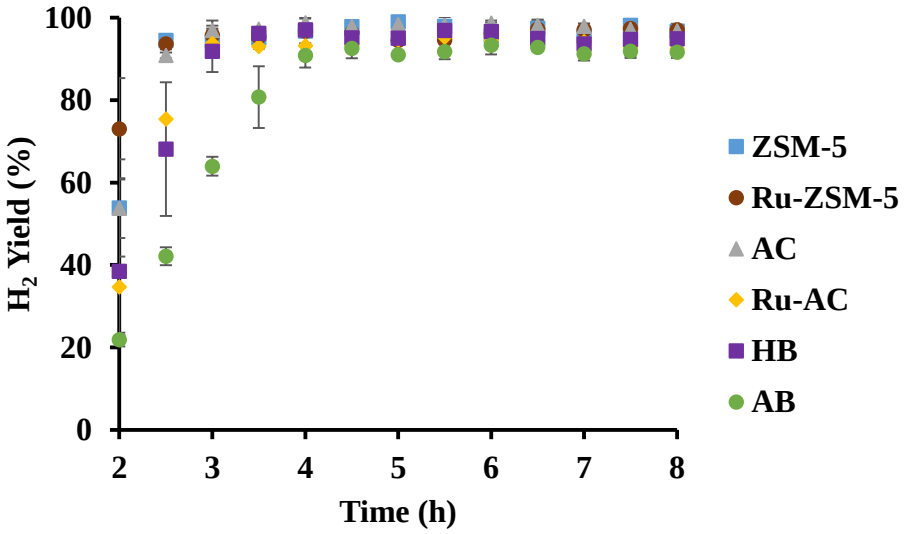

Figure A.A.2: Hydrogen yield graph with time at 800 ºC and 0.4 WHSV

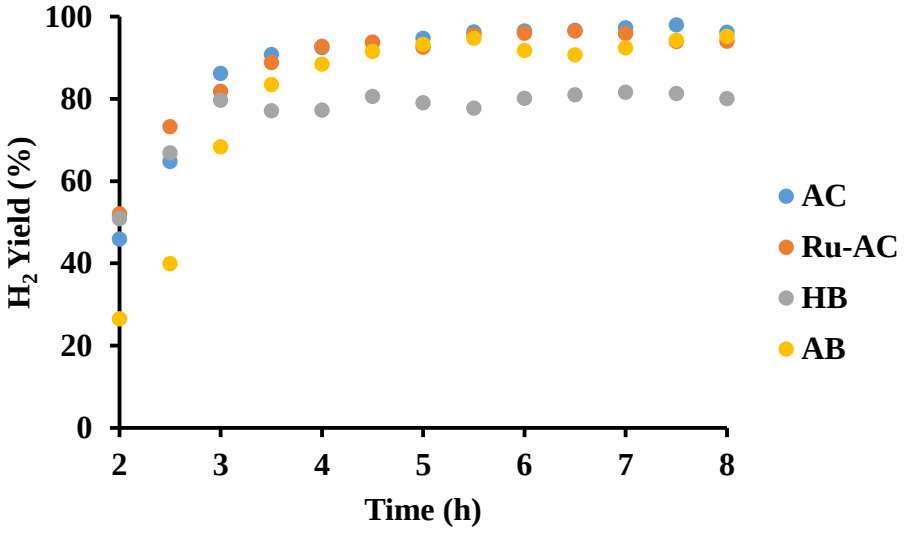

Figure A.A.3: Hydrogen yield graph with time at 700 ºC and 0.4 WHSV

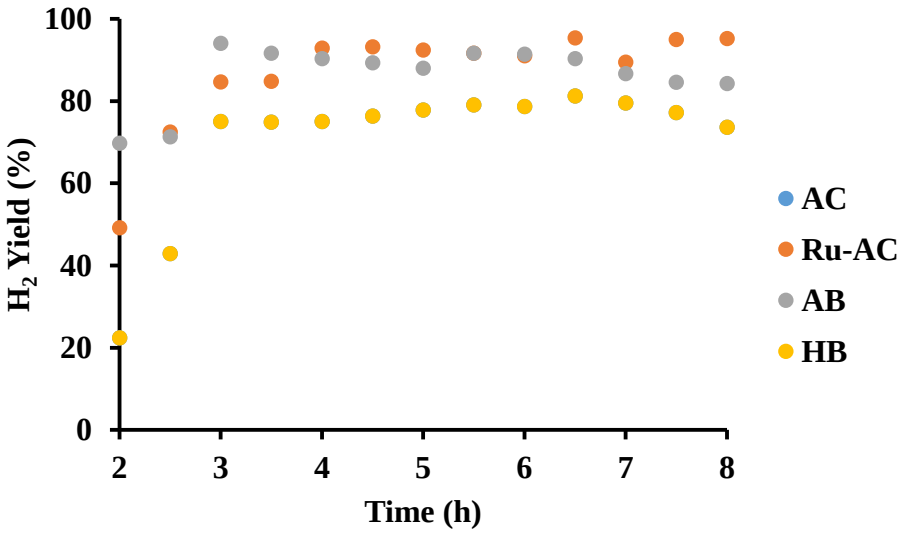

Figure A.A.4: Hydrogen yield graph with time at 600 ºC and 0.4 WHSV

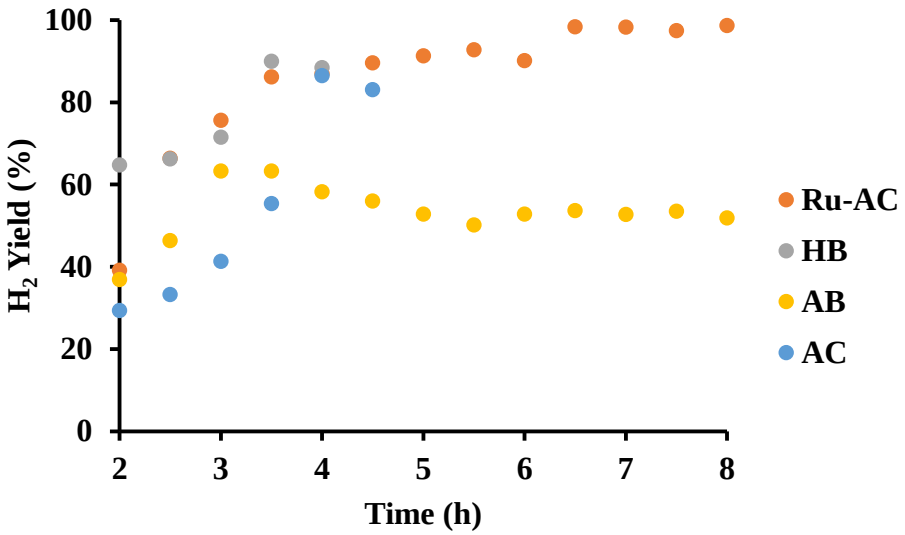

Figure A.A.5: Hydrogen yield graph with time at 500 ºC and 0.4 WHSV

APPENDIX-B: HYDROGEN DATA FOR 60 h

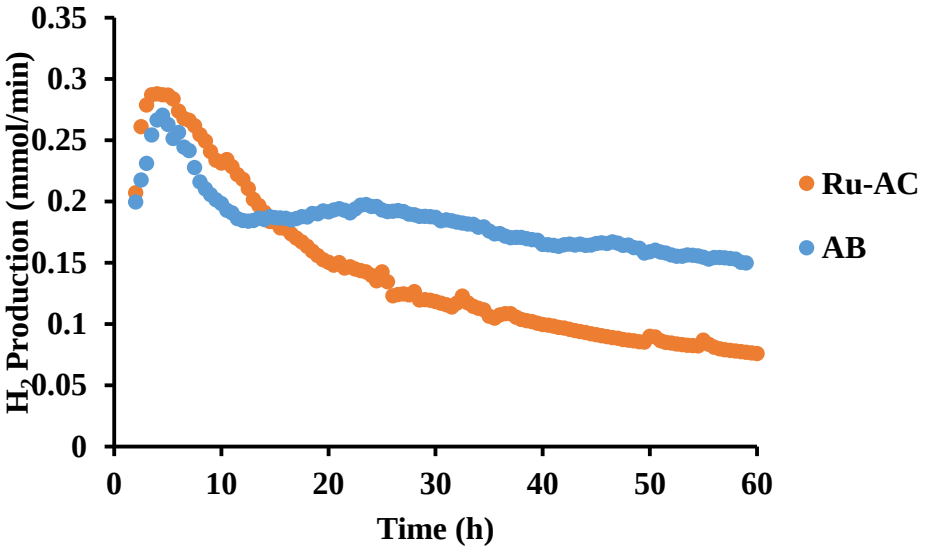

Figure A.B.1: Hydrogen production with time for 60 h reaction at 800 ^{o}C and 0.1 WHSV

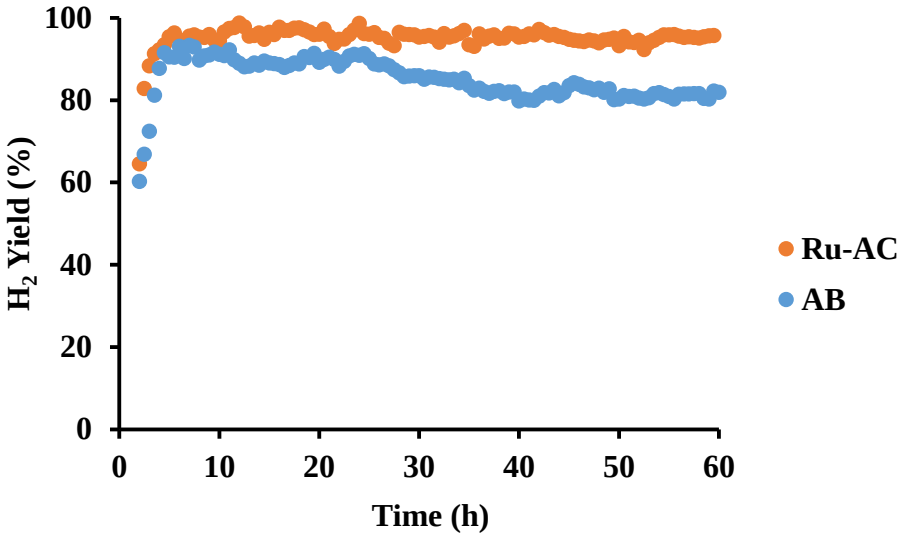

Figure A.B.2: Hydrogen yield for 60 h reaction with time at 800 ^{o}C and 0.1 WSHV

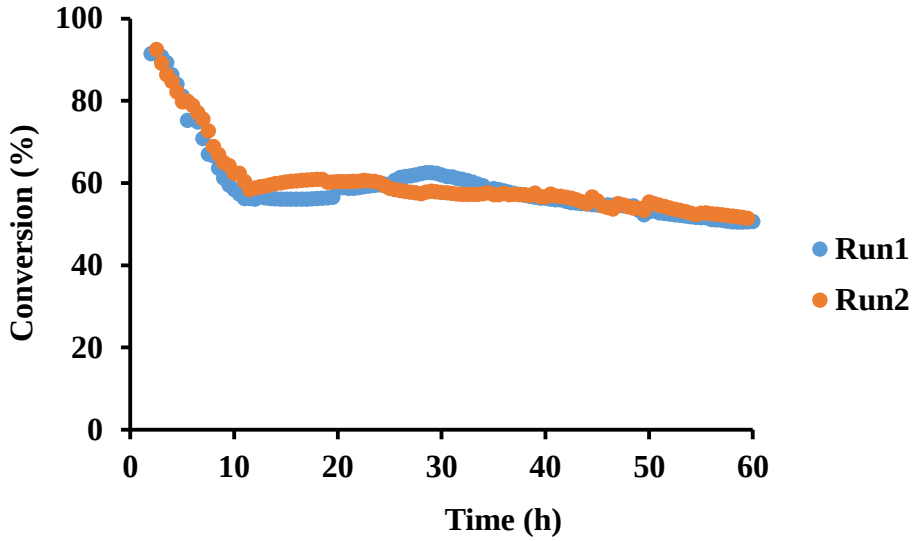

Figure A.B.3: Conversion Vs. time graph for two different run for AB at 800 ^{o}C and 0.1 WHSV

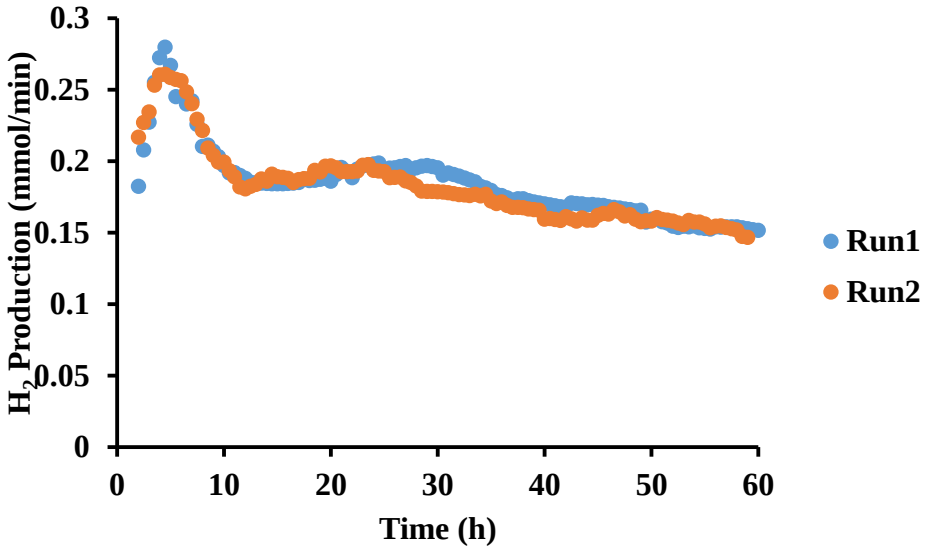

Figure A.B.4: Hydrogen production Vs. time graph for two different run for AB at 800 ^{o}C and 0.1 WHSV

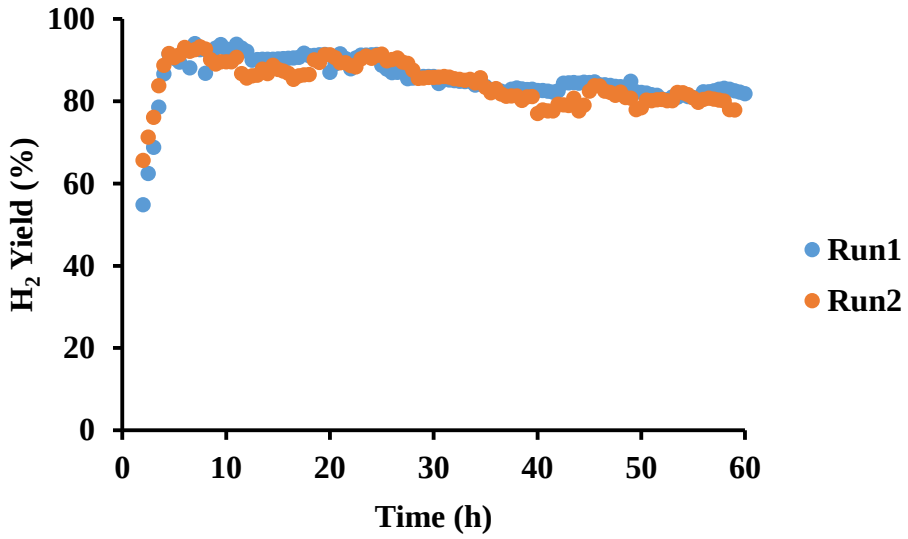

Figure A.B.5: Hydrogen yield Vs. time for two 60 h run at 800 ^{o}C and 0.1 WHSV

APPENDIX-C: MATERIAL LIST

Material Name	Brand	Stock No.	Lot No.
ZSM-5	Alfa Aesar	45879	T16B032
AC	SUPELCO	242241-250G	MKBW724BV
Ruthenium (III) nitrosyl nitrate solution	Alfa Aesar	12530	S17B028
Silica sand	Macron Fine Chemicals	7062-06	Batch No. 0000178045
KOH	VWR	EC No. 215-181-3 CAS No. 1310-58-3	0456C307